Targeting Fibrillar Structures Associated with Ocular Diseases

by

Mehdi Ghaffari Sharaf

A thesis submitted in partial fulfillment of the requirements for the degree of

Doctor of Philosophy
in Chemical Engineering

Department of Chemical and Materials Engineering

University of Alberta

Abstract

Impaired vision and blindness are serious global health problems that affect vast numbers of the population. The impact of ocular diseases is more severe in under-developed countries where, due to the lack of or limited access to vision care, many preventable or curable ocular diseases lead to vision loss and blindness. Exfoliation syndrome (XFS) and cataract are two ocular diseases that both strongly correlate with age and are associated with irreversible aggregation of proteins. These aggregates are mainly composed of fibrillar structures that cannot be removed through normal regulatory machinery that dictate ocular homeostasis. The exact pathomechanism of these diseases is unknown, and curative pharmacotherapy to prevent or eliminate protein fibrillation has not been achieved to date. The scope of this thesis rests on the thought that the effectiveness of future pharmacotherapy strategies for these diseases may be directly related to an ability to target these fibrillar aggregates. That said, the objectives of the study were as follows: to develop an *in vitro* model for cataract and to identify targeting peptides having specific binding ability to fibrillar aggregates of developed model, moreover to adopt an *ex vivo* strategy to identify targeting peptides having specific affinity to fibrillar aggregates associated with XFS and use identified peptides to investigate on development of a new therapeutic approach for XFS and exfoliation glaucoma (i.e. XFS

induced glaucoma).

The *in vitro* model of cataract was developed using recombinantly expressed human βB2-crystallin protein. Fibrillation of βB2-crystallin was conducted under acidic denaturing conditions at different temperatures. It was demonstrated that formed fibrillar aggregates follow common structural pattern of amyloid fibrils. The phage display method was used to screen a random cyclic peptide library against model fibrils *in vitro*. The binding ability of selected phage-displayed peptides was analyzed using enzyme-linked immunosorbent assay (ELISA). A disulfide-constrained cyclic heptapeptide (CKQFKDTTC) was identified with the highest binding affinity. The specific binding ability of identified peptides was confirmed *via* competitive inhibition assay.

A phage-displayed random peptide library was used to develop an *ex vivo* panning method over XFS materials on lens capsules excised from the XFS eyes. Two 12-mer peptides (LPSYNLHPHVPP, and IPLLNPGSMQLS) were identified over three rounds of biopanning. Further investigations using phage-displayed peptides and free peptides showed their specific targeting ability towards XFS materials. Fluorescently labeled phages displaying identified peptides showed specific binding to XFS materials on the surface of human lens capsule. Peptides were conjugated to magnetic particles through copper-catalyzed azide-alkyne cycloaddition reaction and chemical bonding was analyzed by different techniques including surface zeta potential measurement, Fourier-transform infrared spectroscopy (FTIR), and competitive labeling of magnetic particles. Upon interacting with XFS lens capsules in a solution containing aqueous humor, magnetic particle-peptide conjugates showed specific

binding to XFS materials. The behavior of the fibrillar materials upon binding to these magnetic particles was assessed using magnetic pins and rotating magnetic fields of various strengths. *Ex vivo* studies showed that the magnetic particle-peptide conjugates could generate enough mechanical force to remove large aggregates of exfoliation materials from the lens capsule when exposed to a low-frequency rotating magnetic field (5000 G, 20 Hz). Biocompatibility of magnetic particle-peptide conjugates was investigated using different methods including, MTT cell proliferation assay, live/dead cell viability assay, and DNA fragmentation analysis. Peptides in either free or conjugated form had no cytotoxicity effect. Electron microscopy was used to analyze possible internalization of magnetic particle-peptide conjugates into cultured trabecular meshwork cells, and it was shown that cellular uptake of aggregated particles could be limited. This is a novel, minimally invasive, therapeutic approach for the treatment of exfoliation glaucoma *via* the targeting and removal of exfoliation materials that could be applied to all tissues within the anterior segment of the eye.

Potential patient-to-patient structural polymorphism was investigated in fibrillar aggregates isolated from lens capsules of different XFS patients. Negative stain transmission electron microscopy was used to analyze the structural diversity of XFS fibrils. Fibrillar aggregates associated with XFS showed a wide range of fibril morphologies. It was speculated that this variation might arise from patient-specific fibril composition and/or formation mechanisms. These findings could open the door to further biophysical studies on XFS fibrils which might reveal more information about varying biological phenomena underlying that structural diversity.

Preface

Chapter 2 of the thesis has been published as "M. Ghaffari Sharaf, K. F. Damji, and L. D. Unsworth, "Recent advances in risk factors associated with ocular exfoliation syndrome," *Acta Ophthalmol.*, Nov. 2019". Published by John Wiley & Sons, Inc. All rights reserved. I was responsible for literature review and manuscript composition. L. D. Unsworth and K. F. Damji were the supervising authors and were involved with the editing of the manuscript.

Chapter 3 of the thesis has been published as "M. Ghaffari Sharaf, S. Cetinel, V. Semenchenko, K. F. Damji, L. D. Unsworth, and C. Montemagno, "Peptides for targeting βB2-crystallin fibrils.," *Exp. Eye Res.*, vol. 165, pp. 109–117, Dec. 2017." Published by Elsevier Ltd. All rights reserved. I was responsible for the fibrillation of crystallin protein, thioflavin-T assay, phage panning, ELISA, competitive inhibition assay, analysis, and manuscript composition. S. Cetinel was involved in phage display training and phage display results analysis. V. Semenchenko was involved in protein expression. L. D. Unsworth, K. F. Damji, and C. Montemagno were the supervising authors and were involved in the study design and manuscript composition.

Chapter 4 of the thesis was written in paper format. The paper is submitted and is under review. The authors of the paper include Mehdi Ghaffari Sharaf, Sara Amidian, Vineet Rathod, Andrew Crichton, Karim F. Damji, Holger Wille, and Larry D. Unsworth. I was responsible for sample collection, tissue processing, electron microscopy studies on tissue samples, analysis, and manuscript composition. Sara Amidian was responsible for electron microscopy studies on the isolated XFS materials, 2D class averages, image processing, and was involved in manuscript composition. Vineet Rathod was involved in electron microscopy studies on the isolated XFS materials and com-

position the methods section related to that. Andrew Crichton and Karim F. Damji were supervising author and were involved in providing human tissue samples. Holger Wille and Larry D. Unsworth were the supervising authors and were involved in the study design and manuscript composition.

Chapter 5 of the thesis was written in paper format. The paper is submitted and is under review. The authors of the paper include Mehdi Ghaffari Sharaf, Karim F. Damji, and Larry D. Unsworth. I was responsible for sample collection, protocol development for tissue processing, protocol development for *ex vivo* phage panning, phage labeling, *ex vivo* targeting evaluation studies, magnetic particle conjugation, characterization studies, designing the magnetic system along with further related studies, analysis, and manuscript composition. K. F. Damji was the supervising author and was involved in providing human tissue samples. L. D. Unsworth was the supervising author and was involved in the study design and manuscript composition.

To my parents, Mohammad Ali and Maryam
For being great role models and for all the sacrifices they have made.

To my best friend and loving wife, Mahshad
for her boundless love and support.

Acknowledgements

I am especially grateful to my supervisor, Dr. Larry Unsworth, for his guidance, continuous support, and encouragement. He provided me the freedom to pursue various ideas in my research and always gave me constructive and considerate feedback. He helped me to grow as a creative thinker and an independent scientist. I am incredibly grateful for his intellect and positive attitude that made the research a delightful journey for me.

I would also like to thank Dr. Karim Damji for his support and interest in this research project. He was a great collaborator to work and I am grateful for him and all the clinical staff in the operating room of the Royal Alexandra Hospital (Edmonton, AB, Canada) for their kind and welcoming cooperation during sample collection.

Many thanks to all the present and former labmates, for their kind help and for making the lab a friendly place to be.

Finally, I would like to express my deepest gratitude to my parents and my entire family, for their unwavering love and support, and, last but certainly not least, to my wife for her continued love and countless sacrifices.

Table of Contents

1 Introduction **1**
- 1.1 Eye diseases associated with fibrillar aggregates . . . 2
- 1.2 Overview of cataract and exfoliation syndrome . . . 3
  - 1.2.1 Cataract . . . 3
  - 1.2.2 Exfoliation syndrome . . . 3
  - 1.2.3 Exfoliation glaucoma . . . 4
  - 1.2.4 Fibrillar aggregates associated with cataract . . . 5
  - 1.2.5 Fibrillar aggregates associated with XFS . . . 6
- 1.3 Peptide-based therapeutics . . . 7
- 1.4 Phage display . . . 8
- 1.5 Nanotechnology-based approaches for targeting . . . 10
  - 1.5.1 Magnetic particles for biomedical applications . . . 10
- 1.6 Thesis statement . . . 12
  - 1.6.1 Significance of the study . . . 12
  - 1.6.2 Objective of the study . . . 13
- 1.7 Scope of the thesis . . . 14
- 1.8 References . . . 16

2 Recent advances in risk factors associated with ocular exfoliation syndrome **26**
- 2.1 Introduction . . . 29
- 2.2 Genetic factors: *LOXL1* . . . 32
- 2.3 Genetic factors: *CLU* . . . 35
- 2.4 Epigenetic factors . . . 37
  - 2.4.1 Epigenetic factors: lncRNA . . . 38
  - 2.4.2 Epigenetic factors: miRNA . . . 38
  - 2.4.3 Epigenetic factors: Novel Biomarkers . . . 40
- 2.5 Dysfunction of clearance of protein-aggregates: Autophagy . . . 41
- 2.6 Conclusions . . . 43
- 2.7 References . . . 45

3 Peptides for targeting βB2-crystallin fibrils **59**
- 3.1 Introduction . . . 62
- 3.2 Materials and methods . . . 65

3.2.1 Expression and purification of human βB2-crystallin protein . . . 65
3.2.2 Fibrillation of βB2-crystallin protein . . . 66
3.2.3 Thioflavin T (ThT) assay . . . 67
3.2.4 Electron microscopy . . . 67
3.2.5 X-ray fiber diffraction (XRFD) analysis of fibrillar aggregates . . . 68
3.2.6 Phage panning . . . 68
3.2.7 DNA sequencing of selected phage clones . . . 69
3.2.8 ELISA for phage binding assay . . . 70
3.2.9 Competitive inhibition assay . . . 71
3.3 Results and discussion . . . 72
3.3.1 Fibril formation: ThT assay . . . 72
3.3.2 Fibril formation: Electron microscopy studies . . . 72
3.3.3 X-ray fiber diffraction (XRFD) analysis of βB2-crystallin fibrils . . . 74
3.3.4 Identification of high binding peptides . . . 75
3.3.5 Identification of high binding peptides: ELISA assay . . . 76
3.3.6 Competitive Inhibition Assay . . . 78
3.4 Conclusions . . . 79
3.5 Acknowledgements . . . 80
3.6 References . . . 81

4 Structural polymorphisms in fibrillar aggregates associated with exfoliation syndrome 86
4.1 Introduction . . . 88
4.2 Materials and methods . . . 90
4.2.1 Sample collection . . . 90
4.2.2 Scanning electron microscopy (SEM) of lens capsule having XFS materials . . . 91
4.2.3 Transmission electron microscopy (TEM) of XFS deposits on lens capsule . . . 91
4.2.4 TEM of isolated XFS materials . . . 92
4.2.5 Two-dimensional (2D) class averages of the fibril segments 92
4.3 Results and discussion . . . 93
4.3.1 Identification of XFS materials on the lens capsule . . . 94
4.3.2 XFS materials liberated from the capsule . . . 98
4.4 Conclusions . . . 103
4.5 Acknowledgements . . . 105
4.6 References . . . 106

5 Towards preventing exfoliation glaucoma by targeting and removing fibrillar aggregates associated with exfoliation syndrome 111
5.1 Introduction . . . 114
5.2 Methods . . . 116
5.2.1 Patient sample collection . . . 116
5.2.2 Cell line . . . 117
5.2.3 Isolation of XFS materials-specific peptides . . . 117
5.2.4 Evaluation of the targeting ability of phage-displayed peptides . . . 118
Phage labeling . . . 118
Ex vivo evaluation of targeting ability of labeled phages 119
5.2.5 Magnetic bead-peptide conjugates . . . 120
5.2.6 Characterization of peptide-conjugated MPs . . . 120
5.2.7 *Ex vivo* evaluation of targeting ability of identified peptides 121
5.2.8 Evaluation of behavior of magnetized XFS materials under magnetic field . . . 121
Ex vivo evaluation using magnetic pin . . . 121
Ex vivo evaluation using rotating magnetic field . . . 122
5.2.9 Electron microscopy studies . . . 122
Scanning electron microscopy (SEM) . . . 122
Transmission electron microscopy (TEM) . . . 123
5.2.10 Morphology and phenotype of hTM cells . . . 123
5.2.11 Immunohistochemical study . . . 124
5.2.12 Biocompatibility studies . . . 124
MTT cytotoxicity assay . . . 124
Live/dead cell viability assay . . . 125
DNA fragmentation analysis . . . 125
5.3 Results and discussion . . . 126
5.3.1 *Ex vivo* phage display against XFS materials . . . 126
5.3.2 Evaluating the targeting ability of phage-displayed peptides . . . 126
5.3.3 Peptide-particle conjugation . . . 128
5.3.4 Targeting capability of MP-peptide conjugates . . . 130
5.3.5 Effect of magnetic field on the XFS materials . . . 131
Magnetic pin test . . . 131
Rotating magnetic field studies . . . 133
5.3.6 Cytotoxicity studies of MP-peptide conjugates . . . 137
Live/Dead cell viability assay performed on hTM monolayers . . . 138
MTT cell proliferation assay . . . 140
DNA fragmentation . . . 140
Cell uptake studies using electron microscopy . . . 141
5.4 Conclusions . . . 142

5.5 Acknowledgements 144
5.6 References 145

6 Concluding remarks and perspectives **149**
6.1 Major Conclusions 149
6.2 Future outlook 152
6.2.1 βB2-crystallin fibrils and cataract 152
6.2.2 Targeting of XFS fibrils 153
6.2.3 Structural diversity of XFS fibrils 154
6.3 References 155

References **157**
Chapter 1 157
Chapter 2 166
Chapter 3 180
Chapter 4 185
Chapter 5 189
Conclusions 193

Appendix **195**
Supplementary figures of chapter 3 195
TEM of βB2-crystallin fibrills 195
X-ray fiber diffraction (XRFD) pattern of βB2-crystallin fibrils 196
Supplementary figures of chapter 5 196
Peptide enrichment during *ex vivo* biopanning against exfoliated lens capsules 196
Immunohistochemical analyses of hTM cells 197
References 199

List of Tables

3.1 Identified peptides having highest affinity to βB2-crystallin fibrils 76

4.1 XFS samples used for TEM studies 90
4.2 Width measurement of fibrils from patients diagnosed with exfoliation syndrome 103

5.1 Live/dead assay performed on hTM monolayers treated with MP-peptide conjugates and free peptide solution 139
5.2 Live/dead assay performed on hTM monolayers incubated with MP-peptide conjugates and treated under 10 min rotating magnetic field 139

A1 Peptide enrichment during *ex vivo* biopanning against human lens capsules. 196

List of Figures

1.1 Schematic representation of the anterior chamber of the eye . 5
1.2 Schematic representation of the filamentous M13 bacteriophage (M13 phage) 10

3.1 Ribbon model structure of Human βB2-crystallin 65
3.2 Phage display process. Schematic representation of phage library screening against fibrillar aggregates of βB2-crystallin protein 70
3.3 ThT assay results. ThT assay of fibrillar aggregates formed from recombinantly expressed human βB2-crystallin protein in 10% (v/v) TFE, pH 2.0 at RT and 60 °C 73
3.4 Electron microscopy micrographs. Representative TEM images of recombinantly expressed βB2-crystallin protein 74
3.5 X-ray diffraction pattern analysis of βB2-crystallin fibrils . . . 75
3.6 ELISA result of phage binding to βB2-crystallin fibrils after three rounds of phage display 78
3.7 ELISA result of identified phage-displayed peptides from round 3 having highest affinity to βB2-crystallin fibrils 78
3.8 Competitive Inhibition Assay 79

4.1 Micrographs of the anterior surfaces of lens capsules excised from XFS patients 96
4.2 Micrographs of the cross-section of anterior lens capsules excised from XFS patients 97
4.3 Electron micrographs of XFS fibrils from the surface of lens capsule XFS-M1 99
4.4 Electron micrographs of XFS fibrils from the surface of lens capsule XFS-M2 100
4.5 Electron micrographs of XFS fibrils from the surface of lens capsule XFS-M3 101
4.6 Electron micrographs of XFS fibrils from the surface of lens capsule XFS-L 102
4.7 Electron micrographs of XFS fibrils from the surface of lens capsule XFS-H 103

5.1 *Ex vivo* panning of phage-displayed peptide library on exfoliative human lens capsule 119
5.2 Localization of labeled phage-displayed peptides on the human lens capsule having XFS materials. 128
5.3 Conjugation of peptides to MPs. 129
5.4 Competitive labeling of MPs with TAMRA dye. 130
5.5 Targeting of XFS materials on the surface of the human lens capsule with MP-peptide conjugates. 131
5.6 Effect of magnetic pins on the magnetized XFS materials. . . 133
5.7 Effect of rotating magnetic field on XFS materials. 136
5.8 Mean intensity measurements of XFS lens capsules incubated with MP-peptide conjugates. 137
5.9 Cell viability (live/dead) assay of hTM cells incubated with free peptide and MP-peptide constructs. 139
5.10 MTT colorimetric assay of viable hTM cells in the presence of XFS-specific peptides in free and conjugated form. 140
5.11 Electrophoretic analyses of the apoptotic chromosomal DNA fragmentation of hTM cells. 141
5.12 Electron micrographs of hTM cells incubated with MP-peptide conjugates. 142

A1 Transmission electron micrograph of βB2-crystallin incubated in 10% (v/v) TFE, pH 2.0 at 60 °C for 24 hr 195
A2 Diffraction pattern of βB2-crystallin fibrils formed in in 10% (v/v) TFE, pH 2.0 at 60 °C and RT 196
A3 Morphological analysis and immunofluorescence labeling of hTM Cells. 198

Acronyms

XFS Exfoliation syndrome

XFG Exfoliation glaucoma

IOP Intraocular pressure

POAG Primary open-angle glaucoma

OAG Open-angle glaucoma

LOXL1 Lysyl oxidase-like 1

SNP Single-nucleotide polymorphism

GWAS Genomewide association study

WHO World health organization

lncRNA Long non-coding RNA

miRNA MicroRNA

ATG Autophagy-related gene

MTOC Microtubule organizing center

TFE 2,2,2-trifluoroethanol

Hsp Heat-shock protein

ThT Thioavin-T

XRFD X-ray fibre diffraction

ELISA Enzyme-linked immunosorbent assay

TEM Transmission electron microscopy

SEM Scaning electron microscopy

PBS Phosphate-buffered saline

PBST Phosphate-buffered saline with Tween-20

TBS Tris-Buffered Saline

TBST Tris-Buffered Saline with Tween-20

BSA bovine serum albumin

TMB 3,3',5,5'-Tetramethylbenzidine

HMDS Hexamethyldisilazane

UA Uranyl acetate

PTA Phosphotungstic acid

MP Magnetic particle

BSS Balanced salt solution

THPTA Tris(3-hydroxypropyltriazolyl-methyl)amine

DAPI 4', 6-diamidino-2-phenylindole

EDTA Ethylenediaminetetraacetic acid

FTIR Fourier-transform infrared spectroscopy

TAMRA Carboxytetramethylrhodamine

G Gauss

hTM Human trabecular meshwork

EthD-1 Ethidium Homodimer-1

Chapter 1

Introduction

Vision impairment and age-related ocular diseases have a major impact on a large proportion of the population, drastically reducing their quality of life and adversely affecting both economic and educational opportunities [1]. It was estimated that ∼36 million people were blind, as defined as having the best-corrected visual acuity less than 3/60 in the better eye, in 2015. It is likely that both population growth and increased longevity will result in a world-wide total of ∼76 million people being blind by 2020 [2]. According to the World Health Organization (WHO), 1.3 billion people suffer from some form of vision impairment. From this, 80% is avoidable, however, due to lack of a definitive cure for some ocular diseases and solid barriers in underdeveloped and developing countries, vision problems are still a global burden [3–5]. Two age-related ocular diseases that are of particular importance are exfoliation syndrome (XFS) and cataract. XFS is the most common identifiable cause of glaucoma which is thought to affect 60-70 million world-wide with varying prevalence in different populations [6, 7].

Glaucoma leads to progressive degeneration of the optic nerve and gradual loss of retinal ganglion cell bodies in the retina [8]. This disease is the leading cause of irreversible blindness in the world and it has been estimated that by 2020 there will be nearly 80 million people diagnosed with glaucoma, an

increase of about 20 million cases since 2010. Eight million of these patients were blind and it is expected that the number will rise to over 11 million in 2020 [9]. The global burden of this disease is increasing and it has been estimated that its prevalence will reach nearly 112 million people in 2040 [10].

Age-related cataract is the leading cause of blindness, which according to the latest assessment reported by WHO in 2010, accounted for 51% of world blindness that represented about 20 million people, a number that due to the growth of populations is expected to grow [4, 11]. The only treatment for cataract is the surgical removal of the lens and replacement with an artificial lens, a procedure that is not easily available in many non-developed countries. Besides, despite being a highly successful surgery, there are several complications associated with this surgery [12, 13].

1.1 Eye diseases associated with fibrillar aggregates

Despite being age-related diseases of the eye, both XFS and cataract share another significant commonality, *viz.*, they are both characterized by the formation of insoluble fibrillar aggregates that are not removed through normal regulatory processes that dictate ocular homeostasis. Several electron microscopy studies have shown the fibrillar nature of XFS materials [14–16]. In the case of cataract, several *in vitro* studies have confirmed the presence of fibrillar aggregates in the studied models [17–19]. However, since the lens has a very high protein density (highest protein density in the body) it has not been possible to link the *in vitro* findings to *in vivo* biophysical data through electron microscopy studies. However, very recently, the presence of fibrillar aggregates in human cataractous lens has been confirmed with two-dimensional infrared spectroscopy [20].

1.2 Overview of cataract and exfoliation syndrome

1.2.1 Cataract

The lens is a highly organized multicellular syncytial and transparent tissue that focuses light onto the retina. Its transparency arises from the dense-packed order of organelle-free lens fiber cells which reduces the amount of light scattered by the normal human lens to less than 5% [21, 22]. Fiber cells are mainly composed of soluble crystallin proteins broadly categorized as α, β, and γ which exhibit a very high concentration in the lens ($\sim$320 mg.ml^{-1} in the soft human lens) [23]. Despite being highly concentrated, short-range and packed liquid-like organization of lens crystallin proteins minimizes light scattering. However, the formation of insoluble large protein aggregates will disturb this short-range order of crystallins causing lens opacification [22, 24].

1.2.2 Exfoliation syndrome

Exfoliation syndrome (XFS) is typically considered an age-related fibrillopathy that is characterized clinically through the observation of an accumulation of small 'dandruff-like' white precipitates that form within the anterior segment of the eye, particularly on the anterior lens capsule and pupillary border of the iris (Fig 1.1). Historically, this condition was referred to as pseudoexfoliation as suggested by Dvorak-Theobald in 1954 to distinguish it from true exfoliation [25]; the latter is a rare condition of the lens capsule initially described in glassblowers as a result of intense infrared radiation [26]. In XFS all anterior segment structures can be involved and, thus, the perturbation from ocular homeostasis can result in several clinical and surgical complications [27–30].

1.2.3 Exfoliation glaucoma

There is a continuous secretion of aqueous humor by ciliary epithelium into the posterior chamber that flows into the anterior chamber of the eye. This fluid, which is originally filtered from plasma, supplies nutrients to the nonvascularized tissues of the anterior chamber of the eye; most of its outflow is through trabecular meshwork/Schlemm's canal route [31]. This conventional egress route is a key regulator for homeostatic intraocular pressure (IOP) control [32], through which curvature of the cornea and thereby shape and refractive properties of the eye are maintained (Fig 1.1) [33]. However, any obstruction or dysfunction of trabecular meshwork cells may lead to elevated IOP, which is an important risk factor in the development and progression of glaucoma being the second leading cause of blindness worldwide according to the World Health Organization (WHO) [34].

Elevated IOP due to XFS-related trabecular blockage induces exfoliation glaucoma (XFG) which is the most common identifiable cause of open-angle glaucoma worldwide [35]. Primary open-angle glaucoma (POAG) and exfoliative glaucoma (XFG) are the most common types of open-angle glaucoma (OAG). Compared to POAG, XFG associates with higher mean IOP levels, higher rate of optic nerve damage and greater diurnal IOP fluctuations [36]. Although XFG is characteristically known as a high-IOP disease, other pressure-independent risk factors such as abnormalities of the elastic tissue of lamina cribrosa and impaired ocular and retrobulbar perfusion may play a role in further glaucomatous damage [37]. Apart from the risk of glaucoma development, exfoliation is a risk factor for many intraocular complications including zonular instability, lens dislocation, increased rates of cataract and complicated cataract surgery [38, 39].

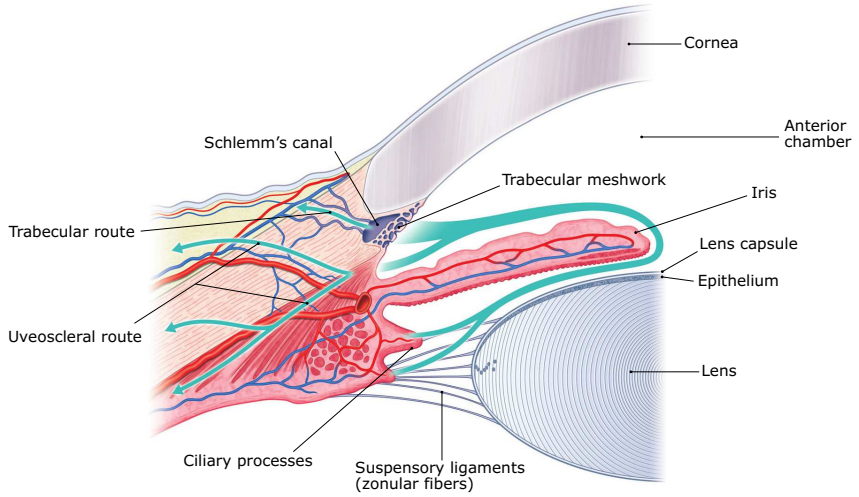

Figure 1.1: Schematic representation of the anterior chamber of the eye. Arrows indicate aqueous humor flow pathways. Aqueous humor is secreted from the ciliary processes, enters the posterior chamber, flows through the pupil into the anterior chamber, and leaves the eye *via* the trabecular and uveoscleral routes. (From *Adler's physiology of the eye*, Saunders; 11th ed., p. 275. Reproduced with permission from Elsevier).

1.2.4 Fibrillar aggregates associated with cataract

The human cataractous lens consists predominantly of aggregates of crystallin proteins. The most abundant crystallin in the mammalian lens is α-crystallin which shares similar sequences with ubiquitous small heat-shock proteins. Besides being a structural protein, α-crystallin is a potent molecular chaperone, that is responsible for preventing the uncontrolled aggregation of other lens crystallins and proteins, thereby maintaining lens transparency [40-42]. Both β- and γ-crystallins are structural proteins that share a similar secondary structure having four Greek key β-sheet motifs organized into two domains [43]. Despite the critical role of crystallin proteins in maintaining lens transparency and proper vision, there is no or very slow protein turnover in the lens nucleus, and only fiber cells in the cortex maintain limited levels of turnover mechanism and metabolic activity [44]. This implies the importance of the molecular regulatory system in maintaining the tertiary structure and solubility of crystallins in the lens for life-long transparency. However, these proteins, some of which as old as the individual, might undergo age-related irreversible

and covalent damages induced by different factors including proteolysis, oxidation, deamidation, glycation, truncation, heavy metals, and UV radiation resulting in the formation of misfolded and aggregation-prone structures in proteins. These post-translational modifications are non-enzymatic and therefore could non-specifically target all types of proteins including chaperons in the lens [23, 44]. Thus, during aging, chaperone proteins of the lens not only might be affected by those destabilizing changes but also could be overwhelmed by other aggregates contributing to the build-up of light scattering centers in the lens, which could lead to lens cloudiness and cataract development [44].

It has been speculated that the cataractous lens contains both amorphous and fibrillar protein aggregates and *in vitro* studies have shown that crystallin proteins form both fibrillar and amorphous aggregates in different denaturing conditions [17, 45, 46]. It has been recently shown that the cataractous human lens contains large quantities of amyloid structures and even mature lenses without signs of cataract showed the presence of amyloid β-sheet secondary structures, proving that fibrillation of lens proteins starts before cataract can be diagnosed [20].

1.2.5 Fibrillar aggregates associated with XFS

XFS materials are highly cross-linked glycoprotein-proteoglycan complexes composed of different proteins such as fibrillin family members, latent transforming growth factor binding proteins (LTBP), extracellular chaperone clusterin and cross-linking enzymes, such as lysyl oxidase-like 1 [47, 48]. Electron microscopy studies have shown that XFS materials consist of fibrils with varying diameters where thicker fibrils are formed through lateral aggregation of thinner protofilaments [49]. The origin of XFS materials has not been clearly identified yet, however, it is believed that several cell types including corneal endothelial cells, preequatorial lens epithelial cell, nonpigmented ciliary epithe-

lial cells, and trabecular endothelial cells appear to be involved in producing XFS material [50]. Further information regarding XFS, the composition of XFS materials and risk factors associated with this disease have been provided in the second chapter of this thesis.

Despite some success in elucidating pathomechanisms, curative pharmacotherapy for either of these diseases has not been achieved to date. Although the formation, composition, and characteristics of fibrillar structures related to XFS or cataract are largely unrelated, the ability to treat these diseases necessitates the ability to target them within the *in vivo* context; thus the effectiveness of pharmacotherapy strategies may be directly related to an ability to target these fibrillar structures. In terms of targeting biomolecules, phage display techniques are a powerful methodology in biomedicine for the identification of disease-related peptide structures that can be used to target a wide variety of materials, and, in fact, is a viable method for the identification of peptide fragments that act as targeting ligands.

1.3 Peptide-based therapeutics

In the past two decades, peptide-based therapeutics have played an important role in the modern pharmaceutical industry. It was estimated that annual global sales of peptide drugs would increase from nearly $28 billion in 2013 to over $70 billion in 2019 (insulin derivatives included). Although this is still a small fraction of the total global pharmaceutical sales, the peptide therapeutics market has been growing slightly faster than projected world-wide pharmaceuticals growth rate [51]. Targeting peptides are being generated against a broad range of molecular targets, which offer several advantages over molecular targeting ligands including lower manufacturing costs, ease of synthesis and chemical modification, better tissue or tumor penetration, low immunogenicity, higher activity per mass, favorable pharmacokinetics, acceptable stability

for long term storage at room temperature, higher binding affinity, and specificity due to their large binding interfaces with receptors and ability to simulate protein-protein interactions [52–54].

Methods of peptide ligand discovery rely on the screening of large libraries of peptides that are generated based upon either biological or synthetic approaches. There has been a growing interest in using biological library methods and among them, phage display technologies have been playing the leading role to date [51]. Phage display is a powerful technique that utilizes the innate ability of bacteriophage to express a plethora of random peptide sequences fused to the coat proteins that they use to bind to substrates. This technique has been widely used for mimotope selection and epitope mapping which are essential for immunotherapy, vaccine development, and diagnosis. Moreover, phage display is a promising tool for the identification of the active site and allosteric inhibitors of enzymes, receptor agonists and antagonists as well as protein-protein interaction studies [55].

1.4 Phage display

Bacteriophages or phages are viruses that infect bacterial cells. They are widely used as vectors in recombinant DNA technology. Bacteriophage vectors can accommodate segments of foreign DNA in the bacterial host and then replicate these foreign inserts along with their genetic material. The key feature of phage display expression vectors compared to conventional expression systems is that the foreign inserted DNA is expressed as an exogenous peptide or protein domain, thus providing a physical connection between expressed proteins and encoding gene (Fig. 1.2).

The coupling of phenotype to genotype and the subsequent selection of specific peptide binders was first reported by George P. Smith in 1985 [56]. By inserting a library of DNA with heterogeneous random sequences into phage

vectors one can produce a phage display library in which each recombinant phage vector is carrying a different sequence of foreign inserted DNA and therefore expressing a different peptide on its surface. Because of the unique characteristics of the phage display vectors, recombinant peptides can be replicated along with the proliferation of phages inside the bacterial hosts (∼200 phages per cell) [56]. Significant properties of bacteriophage vectors have made phage display a powerful, high-throughput, technique that is broadly used to screen for peptide sequences or small antibody fragments that bind to a selected target with high affinity (in micromolar to nanomolar range) among millions or even billions of candidates [57].

Due to their specific binding abilities, peptides are promising candidates for recognition of molecular aggregates and have already been employed for identifying peptides for binding Alzheimer's disease plaques [58, 59]. Moreover, the specific advantage of phage display being a high-throughput screening technique is that it does not rely on a *priori* knowledge of the materials that they are binding to. This is even more pertinent as the biochemical composition of the fibrillar structures involved in XFS is ill-defined. It is thought that the application of phage display techniques against divergent fibrillar structures involved in cataract and XFS will provide pharmacotherapeutic strategies, hitherto unavailable.

The most common bacteriophage used in phage display technology is filamentous M13 phage which is composed of a single-strand circular DNA and has five coat proteins (pIII, pVI, pII, pVIII). N-terminal domain of pIII protein plays the main role in attachment to the pilus of bacteria and start the infection (Fig. 1.2). Foreign DNA sequences are inserted into the reading frame of the coat protein gene [56]. Besides minimizing potential issues tied to phenotype, phage display technique offers several advantages over traditional screening techniques, considering its agility, ease of modifications, cost-effectiveness,

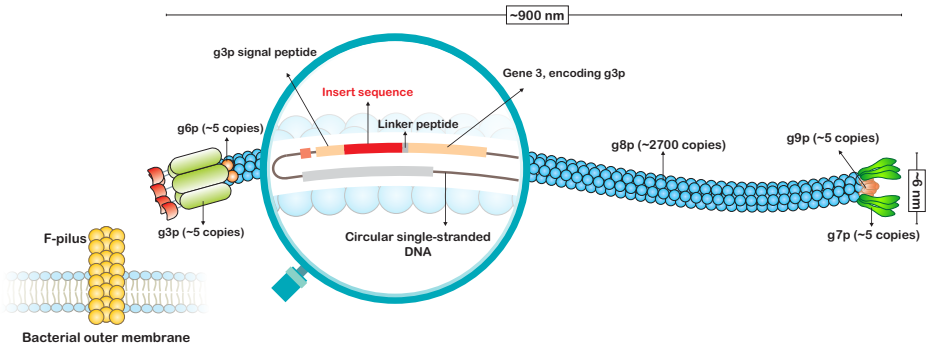

Figure 1.2: Schematic representation of the filamentous M13 bacteriophage (M13 phage). Gene 3 of phage encodes ∼5 copies of minor coat gene 3 proteins (g3p), which are responsible for docking of the phage to the tip of bacterial F-pilus (primary receptor) and infection process. Modified phages display five foreign peptides as N-terminal fusions to g3p coat protein [56, 61].

more importantly ability of high-throughput screening of peptide and peptide variants [60].

1.5 Nanotechnology-based approaches for targeting

Nanoparticle-based therapeutic systems are paving the way in cancer treatment, antimicrobial applications, gene delivery, drug delivery, and site-specific targeting. Moreover, molecular diagnostics has been greatly advanced by the advent of nanoparticles that permits highly sensitive and highly specific techniques [62, 63]. Among numerous studies on nanomaterials, a lot of literature has focused on magnetic particles because of their unique features (discussed in the next section).

1.5.1 Magnetic particles for biomedical applications

Magnetic mirco- and nanoparticles are widely used in biomedical and diagnostic applications. Besides a broad range of coatings and adaptable surface functionalization available for magnetic particles, their inducible magnetiza-

tion and the ability to be directed to the specific sites in the body in the presence of an external magnetic field have made them powerful tools as carriers, labels, and probes in nanobiotechnology studies. Magnetic particle-mediated technologies offer targeted, safe, and efficient biomolecule or drug delivery systems in different *in vivo* and *in vitro* systems [64–67]. Remote actuation of magnetic particles, induced by various magnetic fields has been used in different biophysical and biomedical applications such as microfluidics, lab-on-a-chip biosensing, homogeneous bioassays, and magnetophoresis [67]. One of the very recent remote magnetic actuation approaches is based on the use of rotating magnetic fields, where the direction and/or amplitude of the magnetic field varies over time [67]. Depending on the designed rotating magnetic field and used magnetic particles, a broad range of mechanical forces could be transduced to magnetic particles for various biophysical and biomedical applications. The generated rotational force or torque could be at very low ranges (pN·nm range) in magnetic tweezers to study mechanical properties of single biomolecules [68, 69] or at very high ranges to mechanically destruct cancer cells [70]. Rotational actuation of magnetic particles has been used for fluid mixing at very small volumes in lab-on-a-chip devices [71, 72]. Magneto-mechanical destructive effects have been mostly achieved through magnetic particles having specific shapes and/or nanosharp edges [73, 74]. Although the magneto-mechanical actuation of magnetic particles is a relatively new field of study, recent studies have shown a promising application of these systems in nanomedicine and drug delivery [75].

1.6 Thesis statement

1.6.1 Significance of the study

Vision impairment is a significant global health problem that has a serious economic and social impact on many populations world-wide. Even though a majority of global vision problems (∼80%) are treatable or avoidable, lack of proper health care services in many countries leaves millions at high risk of vision loss. That is, to the extent that in 2013 WHO member states adopted a global action plan (Universal Eye Health: a Global Action Plan 2014–2019) towards the reduction of preventable vision impairments, especially in low-income and middle-income countries where ∼90% of affected people live [3, 76]. However, although reports show that there has been a decrease from 4.6% in 1990 to 3.4% in 2015 in the age-standardized prevalence of blindness and visual impairment, because of growth and aging of the populations, the number of the affected individuals has been increasing substantially. Thus, it is believed that, fundamental gaps remain between goals and accomplishments [3, 77, 78]. Cataract and XFS are progressive age-related diseases. XFS is systematically related to several diseases and is known as the most common identifiable cause of glaucoma and a cause for cataract formation, where its co-presentation with cataract has been reported to be between 0.4 and 30.2%, depending on the country of study [6, 79]. Both cataract and glaucoma are among the priority eye diseases reported by WHO that if left untreated will cause serious vision problems and blindness. The only treatment for cataract is surgery which is not accessible for millions in the world causing for growing number of avoidable vision loss world-wide. In the case of XFS, patients with XFS are at a cumulative risk of developing glaucoma and it is thought that 20-60% of open-angle glaucoma cases could be associated with XFS [49, 80]. There is no pharmacotherapy available for XFS or XFG to eliminate

protein aggregates or prevent their formation. Various approaches such as IOP-lowering medications, argon laser trabeculoplasty, selective laser trabeculoplasty, and different forms of surgeries could be used for the management of IOP in XFG. Even though those medical therapy options are not available to many people world-wide, because of poorer prognosis of XFG compared to POAG and its progressive nature, long-term post-operative management of IOP in XFG patients still remains a clinical challenge [81, 82]. Thus, the development of non-surgical approaches seems necessary to provide accessible and affordable therapy for all patients.

1.6.2 Objective of the study

Many studies have been exploring the use of phage display library techniques for the identification of peptides that bind amyloid plaques associated with Alzheimer's disease (AD) and other protein aggregation-based neurological disorders [83, 84]. In addition to this, several studies are now trying to apply these targeting motifs to various types of therapeutics or drug delivery vehicles for the treatment and/or detection of AD [85]. That said, there are no known existing publications that explore a strategy for the identification of peptides for binding fibril structures associated with XFS; this is even more surprising when considering the systemic association of XFS as exfoliation-like fibrils have been observed in multiple organs. Thus, it is the primary goal of this study to develop protocols for the application of phage display techniques to the aggregates associated with cataract and XFS. The secondary goals associated with this research are the identification of peptide structures that may inhibit the fibril formation and/or break up existing fibrils. It is thought that subsequent pharmacotherapies will be dependent on the ability to preferentially target these fibrillar structures, and it is thought that this study will be the precursor to further systematic studies on developing peptides for this express

purpose. In terms of XFS, It is thought that combination of targeting ability of magnetic particles (due to the conjugated targeting peptides identified *via* phage display) and magneto-mechanical destructive forces (due to the remote actuation of magnetic particles) could provide a proper approach to study the effect of derived mechanical forces on fibrillar aggregates associated with XFS materials.

1.7 Scope of the thesis

This thesis consists of six chapters. Chapter 1 is the introduction, and major conclusions have been summarized in chapter 6. The Scope of the four central chapters has been summarized below.

Chapter 2 is a literature review on exfoliation syndrome. This review addresses current knowledge on risk factors contributing to XFS as well as cellular and molecular mechanisms involved in both development and progression of this disease.

Chapter 3 presents an *in vitro* model for cataracts where fibrillation of recombinantly expressed human βB2-crystallin was carried out in denaturing conditions. Upon confirmation of fibril formation with electron microscopy studies, biopanning of phage-displayed peptide libraries was conducted against fibrillar aggregates of βB2-crystallin. Later, the targeting ability of identified peptides was investigated.

Chapter 4 is an electron microscopy study conducted to investigate the morphological variations of XFS fibrils. In this work, the ultrastructure of XFS aggregates isolated from the lens capsules of different patients being in different stages of the disease was studied *via* electron microscopy.

Chapter 5 covers a comprehensive study on XFS which was conducted using human eye lens capsules. An *ex vivo* biopanning strategy has been developed to identify XFS materials-targeting peptides. Subsequent studies included

investigation on the targeting ability of identified peptide ligands, potential applications of engineered peptides in removal of XFS materials from the lens capsule surface, and studies on the biocompatibility of designed therapeutic system.

1.8 References

[1] G. A. Stevens et al., "Global prevalence of vision impairment and blindness: magnitude and temporal trends, 1990-2010.," *Ophthalmology*, vol. 120, no. 12, pp. 2377–2384, Dec. 2013.

[2] World Health Organization. "VISION2020: The Right to Sight. Global Initiative for the Elimination of Avoidable Blindness: *Action Plan* 2006–2011". 2007;1–97. World Health Organization Geneva, Switzerland.

[3] R. R. A. Bourne et al., "Magnitude, temporal trends, and projections of the global prevalence of blindness and distance and near vision impairment: a systematic review and meta-analysis," *Lancet. Glob. Heal.*, vol. 5, no. 9, pp. e888–e897, 2017.

[4] D. Pascolini and S. P. Mariotti, "Global estimates of visual impairment: 2010.," *Br. J. Ophthalmol.*, vol. 96, no. 5, pp. 614–618, 2012.

[5] World Health Organization. "Blindness and vision impairment," [Online]. Available: https://www.who.int/news-room/fact-sheets/detail/blindness-and-visual-impairment.

[6] G. W. Belovay, D. K. Varma, and I. I. K. Ahmed, "Cataract surgery in pseudoexfoliation syndrome.," *Curr. Opin. Ophthalmol.*, vol. 21, no. 1, pp. 25–34, Jan. 2010.

[7] R. Ritch, U. Schlötzer-Schrehardt, and A. G. P. Konstas, "Why is glaucoma associated with exfoliation syndrome?," *Prog. Retin. Eye Res.*, vol. 22, no. 3, pp. 253–275, 2003.

[8] R. W. Nickells, G. R. Howell, I. Soto, and S. W. M. John, "Under pressure: cellular and molecular responses during glaucoma, a common neurodegeneration with axonopathy.," *Annu. Rev. Neurosci.*, vol. 35, pp. 153–179, 2012.

[9] H. A. Quigley and A. T. Broman, "The number of people with glaucoma worldwide in 2010 and 2020.," *Br. J. Ophthalmol.*, vol. 90, no. 3, pp. 262–267, Mar. 2006.

[10] Y. C. Tham, X. Li, T. Y. Wong, H. A. Quigley, T. Aung, and C.-Y. Cheng, "Global prevalence of glaucoma and projections of glaucoma burden through 2040: a systematic review and meta-analysis.," *Ophthalmology*, vol. 121, no. 11, pp. 2081–2090, Nov. 2014.

[11] World Health Organization. "Global data on visual impairments 2010.," 2010.

[12] E. Chan, O. A. R. Mahroo, and D. J. Spalton, "Complications of cataract surgery.," *Clin. Exp. Optom.*, vol. 93, no. 6, pp. 379–389, Nov. 2010.

[13] N. M. N. Haddad, J. K. Sun, S. Abujaber, D. K. Schlossman, and P. S. Silva, "Cataract surgery and its complications in diabetic patients.," *Semin. Ophthalmol.*, vol. 29, no. 5–6, pp. 329–337, 2014.

[14] T. W. Blackstad, O. A. Sunde, and J. Trœtteberg, "On the ultrastructure of the deposits of busacca in eyes with glaucoma simplex and so-called senile exfoliation of the anterior lens capsule1).," *Acta Ophthalmol.*, vol. 38, no. 5, pp. 587–598, Oct. 1960.

[15] N. Ashton, M. Shakib, R. Collyer, and R. Blach, "Electron Microscopic Study of Pseudo-Exfoliation of the Lens Capsule. I. Lens Capsule and Zonular Fibers.," *Invest. Ophthalmol.*, vol. 4, no. 2, pp. 141–153, 1965.

[16] A. J. Dark, B. W. Streeten, and C. C. Cornwall, "Pseudoexfoliative disease of the lens: a study in electron microscopy and histochemistry.," *Br. J. Ophthalmol.*, vol. 61, no. 7, pp. 462–472, Jul. 1977.

[17] S. Meehan, Y. Berry, B. Luisi, C. M. Dobson, J. A. Carver, and C. E. MacPhee, "Amyloid fibril formation by lens crystallin proteins and its implica-

tions for cataract formation," *J. Biol. Chem.*, vol. 279, no. 5, pp. 3413–3419, 2004.

[18] K. Papanikolopoulou et al., "Formation of amyloid fibrils in vitro by human γD-crystallin and its isolated domains," *Mol. Vis.*, vol. 14, p. 81, 2008.

[19] Y. Wang et al., "Formation of amyloid fibrils in vitro from partially unfolded intermediates of human γC-crystallin," *Invest. Ophthalmol. Vis. Sci.*, vol. 51, no. 2, pp. 672–678, 2010.

[20] A. M. Alperstein, J. S. Ostrander, T. O. Zhang, and M. T. Zanni, "Amyloid found in human cataracts with two-dimensional infrared spectroscopy," *Proc. Natl. Acad. Sci. U. S. A.*, vol. 116, no. 14, pp. 6602–6607, 2019.

[21] P. M. Bettelheim FA, "Light scattering of normal human lens I. Application of random density and orientation fluctuation theory.," *Biophys. J.*, vol. 26, no. 1, pp. 85–99, 1979.

[22] H. J. K. Wilfried W. de Jong, Nicolette H. Lubsen, "Molecular evolution of the eye lens.," *Prog. Retin. Eye Res.*, vol. 13, no. 2, pp. 391–442, 1994.

[23] H. Bloemendal, W. De Jong, R. Jaenicke, N. H. Lubsen, C. Slingsby, and A. Tardieu, "Ageing and vision: Structure, stability and function of lens crystallins.," *Prog. Biophys. Mol. Biol.*, vol. 86, no. 3, pp. 407–485, 2004.

[24] M. Delaye and A. Tardieu, "Short-range order of crystallin proteins accounts for eye lens transparency.," *Nature*, vol. 302, no. 5907, pp. 415–417, 1983.

[25] G. Dvorak-Theobald, "Pseudo-exfoliation of the lens capsule: relation to true exfoliation of the lens capsule as reported in the literature and role in the production of glaucoma capsulocuticulare.," *Am. J. Ophthalmol.*, vol. 37, no. 1, pp. 1–12, 1954.

[26] C. L. Karp, J. R. Fazio, W. W. Culbertson, and W. R. Green, "True

Exfoliation of the Lens Capsule," *Arch. Ophthalmol.*, vol. 117, no. 8, pp. 1078–1080, Aug. 1999.

[27] S. Ashok Vardhan et al., "Association of pseudoexfoliation with systemic vascular diseases in a South Indian population," *JAMA Ophthalmol.*, vol. 135, no. 4, pp. 348–354, 2017.

[28] G. E. Erkayhan and S. Dogan, "Cataract Surgery and Possible Complications in Patients with Pseudoexfoliation Syndrome.," *Eurasian J. Med.*, vol. 49, no. 1, pp. 22–25, Feb. 2017.

[29] A. Kurt and T. Yaşar, "Complications of Phacoemulsification and Extracapsular Cataract Extraction Surgery in Eyes with Pseudoexfoliation Syndrome," *Ophthalmol. Res. An Int. J.*, vol. 8, no. 2, pp. 1–8, 2018.

[30] L. Ilveskoski, C. Taipale, E. J. Holmström, and R. Tuuminen, "Macular edema after cataract surgery in eyes with and without pseudoexfoliation syndrome," *Eur. J. Ophthalmol.*, pp. 1–6, 2018.

[31] M. P. Fautsch et al., "Aqueous humor outflow: What do we know? Where will it lead us?," *Investig. Ophthalmol. Vis. Sci.*, vol. 47, no. 10, pp. 4181–4187, 2006.

[32] W. D. Stamer and A. F. Clark, "The many faces of the trabecular meshwork cell.," *Exp. Eye Res.*, vol. 158, pp. 112–123, May 2017.

[33] M. M. Civan and A. D. C. Macknight, "The ins and outs of aqueous humour secretion.," *Exp. Eye Res.*, vol. 78, no. 3, pp. 625–631, Mar. 2004.

[34] "Glaucoma now second leading cause of blindness," *Bull. World Health Organ.*, vol. 82, pp. 844–951, 2004.

[35] R. Ritch, "Exfoliation syndrome-the most common identifiable cause of open-angle glaucoma.," *J. Glaucoma*, vol. 3, no. 2, pp. 176–177, 1994.

[36] E. Vesti and T. Kivela, "Exfoliation syndrome and exfoliation glaucoma.,"

Prog. Retin. Eye Res., vol. 19, no. 3, pp. 345–368, May 2000.

[37] U. Schlotzer-Schrehardt and G. O. H. Naumann, "Ocular and systemic pseudoexfoliation syndrome.," *Am. J. Ophthalmol.*, vol. 141, no. 5, pp. 921–937, 2006

[38] M. A. Desai and R. K. Lee, "The medical and surgical management of pseudoexfoliation glaucoma.," *Int. Ophthalmol. Clin.*, vol. 48, no. 4, pp. 95–113, 2008.

[39] R. M. Conway, U. Schlotzer-Schrehardt, M. Kuchle, and G. O. H. Naumann, "Pseudoexfoliation syndrome: pathological manifestations of relevance to intraocular surgery.," *Clin. Experiment. Ophthalmol.*, vol. 32, no. 2, pp. 199–210, Apr. 2004.

[40] B. K. Derham and J. J. Harding, "Alpha-crystallin as a molecular chaperone.," *Prog. Retin. Eye Res.*, vol. 18, no. 4, pp. 463–509, 1999.

[41] W. W. de Jong, W. Hendriks, J. W. M. Mulders, and H. Bloemendal, "Evolution of eye lens crystallins: the stress connection," *Trends Biochem. Sci.*, vol. 14, no. 9, pp. 365–368, 1989.

[42] P. V. Rao, Q. ling Huang, J. Horwitz, and J. S. Zigler, "Evidence that α-crystallin prevents non-specific protein aggregation in the intact eye lens," *BBA - Gen. Subj.*, vol. 1245, no. 3, pp. 439–447, 1995.

[43] C. Slingsby and N. J. Clout, "Structure of the crystallins.," *Eye*, vol. 13, pp. 395–402, 1999.

[44] K. L. Moreau and J. A. King, "Protein misfolding and aggregation in cataract disease and prospects for prevention.," *Trends Mol. Med.*, vol. 18, no. 5, pp. 273–282, 2012.

[45] H. Ecroyd and J. A. Carver, "Crystallin proteins and amyloid fibrils.," *Cell. Mol. Life Sci.*, vol. 66, no. 1, pp. 62–81, Jan. 2009.

[46] S. D. Moran, T. O. Zhang, S. M. Decatur, and M. T. Zanni, "Amyloid fiber formation in human γd-crystallin induced by UV-B photodamage.," *Biochemistry*, vol. 52, no. 36, pp. 6169–6181, 2013.

[47] B. Ovodenko et al., "Proteomic analysis of exfoliation deposits," *Investig. Ophthalmol. Vis. Sci.*, vol. 48, no. 4, pp. 1447–1457, 2007.

[48] M. Zenkel, P. Lewczuk, A. Jünemann, F. E. Kruse, G. O. H. Naumann, and U. Schlötzer-Schrehardt, "Proinflammatory cytokines are involved in the initiation of the abnormal matrix process in pseudoexfoliation syndrome/glaucoma," *Am. J. Pathol.*, vol. 176, no. 6, pp. 2868–2879, 2010.

[49] U. S.-S. Robert Ritch, "Exfoliation syndrome," *Surv. Ophthalmol.*, vol. 45, no. 4, pp. 265–315, 2001.

[50] M. Zenkel and U. Schlötzer-Schrehardt, "The composition of exfoliation material and the cells involved in its production," *J. Glaucoma*, vol. 23, no. 8, pp. S12–S14, 2014.

[51] A. Henninot, J. C. Collins, and J. M. Nuss, "The Current State of Peptide Drug Discovery: Back to the Future?," *J. Med. Chem.*, vol. 61, no. 4, pp. 1382–1414, Feb. 2018.

[52] Z. Jiang, J. Guan, J. Qian, and C. Zhan, "Peptide ligand-mediated targeted drug delivery of nanomedicines.," *Biomater. Sci.*, vol. 7, no. 2, pp. 461–471, Jan. 2019.

[53] R. C. Ladner, A. K. Sato, J. Gorzelany, and M. de Souza, "Phage display-derived peptides as therapeutic alternatives to antibodies.," *Drug Discov. Today*, vol. 9, no. 12, pp. 525–529, Jun. 2004.

[54] J. L. Lau and M. K. Dunn, "Therapeutic peptides: Historical perspectives, current development trends, and future directions," *Bioorganic Med. Chem.*, vol. 26, no. 10, pp. 2700–2707, 2018.

[55] J. Pande, M. M. Szewczyk, and A. K. Grover, "Phage display: Concept, innovations, applications and future.," *Biotechnol. Adv.*, vol. 28, no. 6, pp. 849–858, 2010.

[56] G. P. Smith and V. A. Petrenko, "Phage display," *Chem. Rev.*, vol. 97, no. 2, pp. 391–410, 1997.

[57] S. S. Sidhu, H. B. Lowman, B. C. Cunningham, and J. A. Wells, "Phage display for selection of novel binding peptides.," *Methods Enzymol.*, vol. 328, pp. 333–363, 2000.

[58] C. K. Kang, V. Jayasinha, and P. T. Martin, "Identification of peptides that specifically bind Abeta1-40 amyloid in vitro and amyloid plaques in Alzheimer's disease brain using phage display.," *Neurobiol. Dis.*, vol. 14, no. 1, pp. 146–156, Oct. 2003.

[59] B. Bohrmann et al., "Gantenerumab: a novel human anti-Abeta antibody demonstrates sustained cerebral amyloid-beta binding and elicits cell-mediated removal of human amyloid-beta.," *J. Alzheimers. Dis.*, vol. 28, no. 1, pp. 49–69, 2012.

[60] I. Ercan, K. U. Tufekci, E. Karaca, S. Genc, and K. Genc, "Peptide Derivatives of Erythropoietin in the Treatment of Neuroinflammation and Neurodegeneration.," *Adv. Protein Chem. Struct.* Biol., vol. 112, pp. 309–357, 2018.

[61] J. Lubkowski, F. Hennecke, A. Pluckthun, and A. Wlodawer, "Filamentous phage infection: crystal structure of g3p in complex with its coreceptor, the C-terminal domain of TolA.," *Structure*, vol. 7, no. 6, pp. 711–722, Jun. 1999.

[62] K. McNamara and S. A. M. Tofail, "Nanoparticles in biomedical applications," *Adv. Phys. X*, vol. 2, no. 1, pp. 54–88, 2017.

[63] S. Parveen, R. Misra, and S. K. Sahoo, "Nanoparticles: a boon to drug

delivery, therapeutics, diagnostics and imaging.," *Nanomedicine nanotechnology, Biol. Med.*, vol. 8, no. 2, pp. 147–166, Feb. 2012.

[64] J. Dobson, "Magnetic micro- and nano-particle-based targeting for drug and gene delivery.," *Nanomedicine (Lond).*, vol. 1, no. 1, pp. 31–37, Jun. 2006.

[65] J. Gao, H. Gu, and B. Xu, "Multifunctional magnetic nanoparticles: design, synthesis, and biomedical applications.," *Acc. Chem. Res.*, vol. 42, no. 8, pp. 1097–1107, Aug. 2009.

[66] M. K. Yu, J. Park, and S. Jon, "Targeting strategies for multifunctional nanoparticles in cancer imaging and therapy," *Theranostics*, vol. 2, no. 1, pp. 3–44, 2012.

[67] C. P. Moerland, L. J. van IJzendoorn, and M. W. J. Prins, "Rotating magnetic particles for lab-on-chip applications - a comprehensive review," *Lab Chip*, vol. 19, no. 6, pp. 919–933, Mar. 2019.

[68] F. Mosconi, J. F. Allemand, and V. Croquette, "Soft magnetic tweezers: a proof of principle.," *Rev. Sci. Instrum.*, vol. 82, no. 3, p. 34302, Mar. 2011.

[69] S. Forth, M. Y. Sheinin, J. Inman, and M. D. Wang, "Torque measurement at the single-molecule level.," *Annu. Rev. Biophys.*, vol. 42, pp. 583–604, 2013.

[70] Y. Cheng et al., "Rotating magnetic field induced oscillation of magnetic particles for in vivo mechanical destruction of malignant glioma.," *J. Control. Release*, vol. 223, pp. 75–84, Feb. 2016.

[71] Y. Gao, A. van Reenen, M. A. Hulsen, A. M. De Jong, M. W. J. Prins, and J. M. J. Den Toonder, "Chaotic fluid mixing by alternating microparticle topologies to enhance biochemical reactions," *Microfluid. Nanofluidics*, vol. 16, no. 1–2, pp. 265–274, 2014.

[72] T. Franke, L. Schmid, D. A. Weitz, and A. Wixforth, "Magneto-mechanical mixing and manipulation of picoliter volumes in vesicles," *Lab Chip*, vol. 9, no. 19, pp. 2831–2835, 2009.

[73] M. Chen et al., "Remote Control of Mechanical Forces via Mitochondrial-Targeted Magnetic Nanospinners for Efficient Cancer Treatment," *Small*, vol. 16, no. 3, pp. e1905424–e1905424, Jan. 2020.

[74] A. Elbourne et al., "Antibacterial Liquid Metals: Biofilm Treatment via Magnetic Activation," *ACS Nano*, vol. 14, no. 1, pp. 802–817, Jan. 2020.

[75] Y. I. Golovin et al., "Towards nanomedicines of the future: Remote magneto-mechanical actuation of nanomedicines by alternating magnetic fields," *J. Control. Release*, vol. 219, pp. 43–60, Dec. 2015.

[76] "WHO. Draft action plan for the prevention of avoidable blindness and visual impairment 2014–2019. Universal eye health: a global action plan 2014–2019. Geneva: *World Health Organization*, 2013."

[77] C. Sabanayagam and C.-Y. Cheng, "Global causes of vision loss in 2015: are we on track to achieve the Vision 2020 target?," *Lancet. Glob. Heal.*, vol. 5, no. 12, pp. e1164–e1165, Dec. 2017.

[78] J. Ramke and C. E. Gilbert, "Universal eye health: are we getting closer?," *Lancet. Glob. Heal.*, vol. 5, no. 9, pp. e843–e844, Sep. 2017.

[79] P. Puska and A. Tarkkanen, "Exfoliation syndrome as a risk factor for cataract development: five-year follow-up of lens opacities in exfoliation syndrome.," *J. Cataract Refract. Surg.*, vol. 27, no. 12, pp. 1992–1998, Dec. 2001.

[80] P. Challa, "Genetics of pseudoexfoliation syndrome.," *Curr. Opin. Ophthalmol.*, vol. 20, no. 2, pp. 88–91, Mar. 2009.

[81] G. Hollo, A. Katsanos, and A. G. Konstas, "Management of exfoliative

glaucoma: challenges and solutions.," *Clin. Ophthalmol.*, vol. 9, pp. 907–919, 2015.

[82] S. Nazarali, F. Damji, and K. F. Damji, "What have we learned about exfoliation syndrome since its discovery by John Lindberg 100 years ago?," *Br. J. Ophthalmol.*, vol. 102, no. 10, pp. 1342–1350, Oct. 2018.

[83] S. A. Funke and D. Willbold, "Peptides for therapy and diagnosis of Alzheimer's disease.," *Curr. Pharm. Des.*, vol. 18, no. 6, pp. 755–767, 2012.

[84] Y. Nagai et al., "Inhibition of polyglutamine protein aggregation and cell death by novel peptides identified by phage display screening.," *J. Biol. Chem.*, vol. 275, no. 14, pp. 10437–10442, Apr. 2000.

[85] C. Zhang et al., "Dual-functional nanoparticles targeting amyloid plaques in the brains of Alzheimer's disease mice.," *Biomaterials*, vol. 35, no. 1, pp. 456–465, Jan. 2014.

Chapter 2

Recent advances in risk factors associated with ocular exfoliation syndrome

Abstract

Exfoliation syndrome is generally considered a progressive age-related systemic disorder of the extracellular matrix, which is clinically characterized through the observation of flaky white aggregates on ocular tissues. Exfoliation syndrome is directly linked to exfoliative glaucoma in elderly patients, where it is known as the most common identifiable cause of open-angle glaucoma. Despite the identification of various risk factors associated with exfoliation syndrome, the exact pathogenesis of this syndrome has not been fully elucidated. There is a growing number of genome-wide association studies in different populations around the world to identify genetic factors underlying exfoliation syndrome. Besides variants in *LOXL1* and *CACNA1A* genes, new loci have been recently identified which are believed to be associated with exfoliation syndrome. Among different genetic factors, functional variants might help to better understand mechanisms underlying this systemic disorder. Besides genetic factors, epigenetic regulation of different gene expression patterns has been thought to play a role in its pathogenesis. Other factors have been also considered to be involved in the development of exfoliation syndrome at cellular organelles level where mitochondrial impairment and autophagy dysfunction have been suggested in relation to exfoliation syndrome. This review addresses the most recent findings on genetic factors as well as cellular and

molecular mechanisms involved in both the development and progression of exfoliation syndrome.

Keywords: Exfoliation syndrome, exfoliation glaucoma, fibrillar aggregates, age-related disease, LOXL1.

2.1 Introduction

In 1917 the presence of 'greyish' flakes located in central bands on the anterior lens capsule, as well as 'greyish' fringes at the pupillary border, were reportedly first observed in elderly patients by an ophthalmology resident using the recently invented slit-lamp microscopy and iris transillumination techniques [1]. Within only a few short years these anomalous deposits (exfoliation materials) were being identified in patients with and without cataract, and by 1923 it was already being conjectured that a link between exfoliation and glaucoma existed [1]. Despite more than a century elapsing since their original observation, the general pathobiology of these exfoliation materials remains ill-defined and an area of intense research.

Exfoliation syndrome (XFS), or pseudoexfoliation [2], is typically considered an age-related fibrillopathy. XFS is characterized clinically through the observation of an accumulation of white precipitates within the anterior segment of the eye, particularly on the anterior lens capsule and pupillary border of the iris. Over the 1960s and 70s, utilizing newly available electron microscopy techniques, it was found that XFS materials were present in a variety of ocular tissues: trabecular meshwork, ciliary body, anterior lens capsule, iris vessels, and bulbar and palpebral conjunctiva [3-8]. Other than the eye, similar fibrillar deposits were found in other organs including skin, blood vessels, gallbladder, lungs, kidneys, heart and meninges suggesting exfoliation as a systemic disorder of the extracellular matrix [9, 10].

It was also observed that ocular XFS materials consisted of fibrils of various thicknesses [11], with a highly cross-linked glycoprotein-proteoglycan aggregate composed of a variety of proteins including fibrillin-1, vitronectin, laminin, fibronectin, latent transforming growth factor-β (TGF-β) binding protein (LTBP), extracellular chaperone clusterin, cross-linking enzymes, such

as lysyl oxidase-like 1 (LOXL1), as well as non-protein components including glycosaminoglycans [12–14]. Most of these proteins exist in extracellular matrix structures in the normal eye, however, mechanisms responsible for their misfolding and abnormal accumulation are largely unknown. Some of these proteins, such as TGF-β1 and LOXL1, are known as major factors in underlying XFS pathways. For instance TGF-β1, along with oxidative stress, has been shown to be cooperatively involved in the accumulation of some proteins found in XFS materials, where chronic oxidative stress and elevated levels of TGF-β1 may disturb the balance between matrix metalloproteinases and their tissue inhibitors resulting in accumulation of extracellular matrix fibrils [15–17]. In addition to this, a common degenerative layer deep in the lens capsule, at the anterior equatorial region, was reported for XFS specimens; possibly thought to be the origin of XFS material [18]. Since then the origin of XFS material has not been clearly identified, however, it is believed that several cell types (i.e. corneal and trabecular endothelial cells) could be involved. Ocular cells being in an active state of fibrillogenesis have been extensively reviewed elsewhere [9, 19].

All anterior segment structures may be affected by the presence of XFS materials, thus, potentially resulting in several clinical and surgical complications [20–23]. Although not believed to increase mortality, XFS is thought to impair normal eye functions [24–28]. Aqueous humor continuously flows into the anterior chamber of the eye at a rate of 2.4 ± 0.6 μl/min, or 1.0% to 1.5% of the anterior chamber volume per minute [29, 30]. This flow must proceed unimpeded through the trabecular meshwork-Schlemm's canal route so as to maintain a consistent intraocular pressure (IOP), curvature of the cornea, and shape and refractive properties of the eye [31–33]. Obstruction or dysfunction of trabecular meshwork cells may lead to elevated IOP and ultimately result in glaucoma; the leading cause of irreversible blindness, affecting $\sim$76 million

people world-wide [34]. Elevated IOP, due to trabecular blockage from XFS materials, iris pigment particles, and apparent local production of fibrillar aggregates by trabecular cells [35], is likely the impetus for the development of exfoliation glaucoma (XFG); the most common identifiable cause of open-angle glaucoma world-wide [36]. Uveosclearal outflow may account for 4-60% of the total outflow from the eye and occurs due to the lack of an epithelial barrier between the ciliary body and anterior chamber [31, 37]. XFS materials have been found in the very first portion of uveoscleral pathway impeding outflow and leading to an increase of 2–3 mmHg in IOP compared to non-XFS eyes. The possible decrease of uveoscleral outflow in eyes with primary open-angle glaucoma (POAG) is still unknown [38, 39]. Compared to POAG, XFG associates with a higher mean IOP levels, a higher rate of optic nerve damage, and a greater diurnal IOP fluctuations. Thus, XFG patients are likely to have earlier and more frequent filtering surgery [40, 41]. In addition to the risk of developing glaucoma, XFS has been suggested as a risk factor for many intraocular complications, including complicated cataract surgery, dispersion of melanin granules, inadequate mydriasis, circular posterior synechiae, blood-aqueous barrier dysfunction, anterior segment hypoxia, corneal decompensation, accelerated cataracts, retinal vascular diseases, cerebrovascular and cardiovascular complications, zonular instability and lens subluxation [40, 42–46]. It has been suggested that higher rates of cataract development in XFS patients could be a result of more frequent apoptosis in lens epithelial cells [47].

Since its discovery, XFS was mistakenly believed to be a 'type' or 'form' of glaucoma. Thus, the search for possible molecular or cellular risk factors for XFS have only started recently [48]. Investigations regarding the causative risk factors for XFS has led to the identification of some genetic factors, initially, but as of late several other risk factors have been identified. The purpose of this review is to summarize recent findings on genetic risk factors and epigenetic

regulators associated with XFS, highlighting functional variants that mechanistically link to its development. Moreover, intracellular events related to dysfunction of normal clearance pathways (i.e. autophagy) have been observed in *in vitro* models of XFS have been considered. Additionally, a comment has been made about the applicability of some of these risk factors as potential biomarkers for early diagnosis.

2.2 Genetic factors: *LOXL1*

Several genetic factors are associated with XFS. Perhaps the most studied gene of interest being a member of lysyl oxidase family, *viz.*, Lysyl oxidase-like 1 (*LOXL1*) [49]. The protein expressed from *LOXLI* (i.e. LOXL1) is necessary for elastic fiber homeostasis [50], where elastic fibers are a complex network of biopolymers in the extracellular matrix that provide inherent elasticity to tissues. Lysyl oxidase is an extracellular copper-dependent enzyme that covalently assembles the soluble precursor tropoelastin, which is secreted from cells into the extracellular space. Reactive aldehyde groups are formed by lysyl oxidase inducing oxidative deamination of lysine residues. Covalent crosslinking occurs *via* either the condensation of formed aldehydes with adjacent enzyme-derived aldehyde residues or the ϵ-amino group of peptidyl lysine [50]. This conjugation leads to the formation of a highly cross-linked, insoluble elastin meshwork [51].

Abnormalities in lysyl oxidase expression at the translation and transcription levels are associated with many diseases and disorders [52]. A genome-wide association study (GWAS) for a Scandinavian population was used to identify DNA sequence variants associated with glaucoma induced by the presence of XFS materials (i.e. exfoliation glaucoma, XFG). Two protein-coding single-nucleotide polymorphisms (SNPs) of *LOXL1* were identified: rs1048661 (Arginine 141 Leucine) and rs3825942 (Glycine 153 Aspartate) in the exon

1, and rs2165241 SNP located in intron 1 of the *LOXL1* gene on 15q24.1 chromosome [49]. Since then several studies have verified the association of genetic variants of *LOXL1* with XFS in different populations, however, risk allele for *LOXL1* SNP rs3825942 which was consistently reported to be G allele, has been found to be the opposite allele (A allele) in the South African black population [53]. Additionally, recombinantly expressed LOXL1, with those specific variants, has been shown to still have amine oxidase activity [54], implying that a more complex mechanism involving non-native *LOXL1* could be crucial to XFS and XFG pathogenesis [55, 56]. It is also thought that dysregulations in the expression of this gene could be a contributing factor for XFS development [57].

In order to find the correlation between LOXL1 expression and the two previously reported SNPs (rs1048661 and rs3825942), expression levels and localization of *LOXL1* was investigated in XFS, XFG, and control human eyes obtained at autopsy. Ocular expression of LOXL1 was approximately 20% less for rs1048661 SNP (R141L), however, rs3825942 SNP (G153D) was not identified to affect the expression level of LOXL1 [58]. Co-localized with different elastic fiber components, LOXL1 was shown to be over-expressed at the early stages of XFS, potentially supporting the idea it is an initial step in the formation of XFS materials [58]. In terms of functional variants, a SNP (rs11638944:C>G) has been identified within intron 1 of *LOXL1*, affecting expression levels of this gene. An overall decrease in LOXL1 mRNA levels for cells that carry the risk sequence of this locus was observed. It has been suggested that the risk sequence had an increased activity at the transcriptional level that was associated with decreased binding affinity of transcription factor (RXRα) and enhanced differential splicing of LOXL1 pre-mRNA along with nonsense-mediated mRNA decay [59]. Differential splicing coupled to nonsense-mediated mRNA decay was later shown to regulate expression of

LOXL1 at the posttranscriptional level in response to XFS-associated environmental and nutritional factors [60]. Given the potential contribution of variants residing in non-protein-coding regions to complex disease, a deep sequencing approach has been conducted to search for those non-coding variants having potential function in intergenic regions flanking the *LOXL1* locus. A common non-coding variant rs7173049A>G was found downstream of *LOXL1*, suggested to be associated with decreased risk of XFS in different ethnic groups, where the minor allele G was shown to be constantly enriched in controls. Protective function of rs7173049-G allele is believed to be through the upregulation of *STRA6*, which is involved in cellular uptake of vitamin A and was shown to be significantly downregulated in XFS eyes [61]. Another deep sequencing analysis has been conducted across *LOXL1* locus in a collection of 5570 XFS cases and 6279 controls drawn from nine countries. Among different studied ethnic groups, a rare allele (rs201011613) was identified exclusively in the Japanese population at *LOXL1* which potentially could provide a protective function against XFS *via* p.Tyr407Phe substitution in the catalytic domain of LOXL1. It is believed that altered elastin metabolism in extracellular matrix due to protective effect of identified variant could improve cell-matrix adhesion and possibly slow down the exfoliative process [62, 63].

A recent multi-ethnic GWAS was used to further confirm that the XFS risk was associated with the expected *LOXL1* locus, as well as, identifying a variant across the *CACNA1A* locus. This GWAS utilized a cohort of 1484 XFS patient samples with 1188 controls for the discovery stage, followed by a validation stage study, in which blood samples of 2628 XFS and 8947 control cases were collected from nine countries. One SNP (rs4926244) residing within an intronic region of *CACNA1A* gene near the $3'$ end was found to be associated in the GWAS discovery stage with p-value of 5.5×10^{-5}, as well as being strongly associated in the GWAS validation stage ($P = 4.17 \times 10^{-5}$).

Association of *CACNA1A* rs4926244 with XFS was further evaluated and confirmed in a third stage of study including 4273 XFS patients and 11780 control individuals from eight additional countries [55]. *CACNA1A* encodes the transmembrane pore-forming alpha-1 subunit of human voltage-gated calcium (P/Q-type) channels [64]. The presence of increased calcium concentration has been associated with XFS fibrils [65], it has been hypothesized that there might be a connection between the decreased mRNA and protein expression of CACNA1A and altered calcium metabolism resulting in the formation of XFS aggregates [55, 66].

Another comprehensive GWAS consisting of samples drawn from six continents has identified new loci associated with XFS. The discovery stage for this GWAS included 9035 XFS cases and 17008 controls from 24 countries followed by the replication stage including 4803 XFS cases and 93267 controls enrolled from 18 different countries. Five new loci having genome-wide significant association including *POMP*, *TMEM136*, *AGPAT1*, *RBMS3*, and *SEMA6A* were identified with increased risk of XFS [62]. Besides *CACNA1A* and *LOXL1*, other newly identified genes also have functional roles that might be involved in the pathobiology of XFS [62, 66].

2.3 Genetic factors: *CLU*

Clusterin, or Apolipoprotein-J (encoded by *CLU* gene), is a ubiquitous multifunctional glycoprotein found in almost all mammalian tissues including most ocular cells and various biological fluids [67, 68]. Clusterin plays a role in lipid transport, apoptosis, complement inhibition, cell-cell and cell-substratum interaction, membrane recycling and clearance of cellular debris [69, 70]. Furthermore, it is an extracellular chaperon that can bind to the exposed hydrophobic regions of denatured and misfolded proteins for inhibiting stress-induced precipitation of slowly aggregating proteins [71, 72]. This

stress-response protein is an amyloid associated molecule that can co-localize with fibrillar aggregates where co-deposition of clusterin has been identified in many systemic and cerebral forms of amyloid fibril-associated disorders [73]. Its co-localization with fibrillar deposits has been also confirmed in XFS [74]. Simultaneous topography and recognition (TREC) imaging has been used to detect clusterin in exfoliation material. Anti-clusterin antibody-modified AFM tips have been use to characterize unprocessed human lens capsules to study the structure of clusterin associated with exfoliation material. Compared to normal tissue, the distribution pattern of clusterin was found to be small localized spots in normal cases and significantly larger patches for XFS tissues [75].

Although clusterin is overexpressed in various stress and pathological conditions, it is downregulated in the anterior chamber of the exfoliative eyes. This suggests the possible contribution of common CLU variants in exfoliation development [67, 73, 76–79]. A CLU SNP (rs3087554) was observed in an Australian population that was identified to be nominally associated with XFS. The study included 86 XFS cases and 2422 controls in which rs3087554 was found to be associated at the genotypic level ($P = 0.044$), but not at the allelic level or when controls with minimum 73 years old were only considered ($P > 0.07$) [80]. Later, an intronic variant (rs2279590) was identified in CLU gene associated with XFS in a study involving 333 German XFS patients and 342 controls [81]. Association of rs3087554 and rs2279590 variants were later investigated in an Indian population including 136 XFS patients and 89 controls, where only CLU SNP rs2279590 was identified to be associated with XFS in that studied population [78]. Association of these variants was not observed in a later study conducted in a South Indian population study (299 XFS/XFG individuals and 244 controls) [82]. The possible association of rs3087554 and rs2279590 polymorphisms with XFS outcomes was recently

screened in a Polish population study including 81 XFS patients and 91 control subjects. No significant differences in allele or genotype frequencies was observed between XFS cases and controls, and only haplotype distribution was found statistically different between studied groups [83]. Common variants in *CLU* in association with XFS/XFG have been only identified at the nominal level, and further investigation need to be done before considering them as strong genetic factor for XFS [66, 84].

Research on the genetic risk factors for XFS is an area of intense research, and other susceptibility loci and SNPs have been identified in association with this syndrome in certain populations [85–89]. GWASs and next-generation sequencing technologies have been used to elucidate potential genetic causal variants underlying XFS, which could help better understanding the disease mechanism and provide specific treatment approaches [66].

2.4 Epigenetic factors

Although many risk alleles and potential biological pathways have been identified for different eye disorders, their complex aetiologies have not yet been explained by genetic factors alone [90]. Besides environmental factors, it is believed that possible epigenetic variations associated with different ocular diseases and blinding conditions may play an important role in XFS, as has been observed in other complex disorders [91, 92]. Epigenetic variations are believed to be involved in cataract, glaucoma, and ocular surface disorders [93]. For example, it has been shown that the CpG islands are hypermethylated in the promoter region of the *LOXL1* gene found in anterior lens capsule epithelial cells collected from XFS patients (Uyghur population). In this case reduced *LOXL1* mRNA and protein levels suggests the possible role of DNA methylation in silencing the *LOXL1* gene [94].

2.4.1 Epigenetic factors: lncRNA

Long non-coding RNAs (lncRNAs) are an important epigenetic regulator of the human genome. Transcripts longer than 200 nucleotides that have limited or no protein-coding capacity, lncRNAs can regulate gene expression at transcription and post-transcription levels or epigenetically at chromatin modification level [95, 96]. A growing body of research indicates that dysregulation of lncRNAs is associated with Alzheimer's, Parkinson's, cancer, and glaucoma. Thus, lncRNA identification might facilitate the prognosis and understanding of the pathological mechanism of XFS [97]. With the aim of identifying a functional role for the variants of the *LOXL1* gene, a deep sequencing approach has been applied to screen the entire *LOXL1* genomic locus in XFS patients from different populations: black South African, US Caucasian, German, and Japanese. The genomic region of peak XFS-association lies immediately upstream of *LOXL1* antisense RNA 1 (LOXL1-AS1). The promoter of this region has been shown to be regulated by risk alleles associated with exfoliation. Expression of this lncRNA has been shown to decrease in response to oxidative stress in lens epithelial cells and to increase in response to cyclic mechanical stress in Schlemm's canal cells *in vitro* [98], supporting a possible role for LOXL1-AS1 lncRNA in cellular stress response and XFS pathogenesis [98]. Because of the potential cell-type- or tissue-type-specific expression of lncRNAs, they may be therapeutic targets but no specific therapy for XFS or XFG has yet been proposed using lncRNAs [99, 100].

2.4.2 Epigenetic factors: miRNA

MicroRNAs (miRNA) are another group of epigenetic regulators. These are small ($\sim$22 nucleotides) non-coding RNAs that post-translationally regulate gene expression [101]. In the trabecular meshwork, miRNAs are known to be involved in cell contraction and extracellular matrix turnover, suggesting

they may be a potential therapeutic candidate for POAG [102]. Some have indicated that XFS is a type of elastosis associated syndrome, with excessive production of elastic microfibrillar components, which may indicate the possible involvement of extracellular matrix formation modulators [65]. Increased levels of a major modulator, transforming growth factor TGF-β1 and its latent form binding proteins (LTBPs 1 and 2), in aqueous humor of XFS patients suggested their role in the accumulation of the abnormal extracellular elastic material [65]. It appears that interactions between TGF-β cytokines family and miR-29 miRNA family modulates synthesis of extracellular matrix in trabecular meshwork cells [103]. miR-29b, a member of miR-29 miRNA family, has been shown to negatively regulate genes coding for extracellular matrix proteins in trabecular meshwork cells, where under chronic oxidative stress conditions its down-regulation might contribute to overexpression of those genes [104]. *In vitro* studies using human trabecular meshwork cell lines have shown that while TGF-β1 did not have significant effect on the expression of miR-29 miRNAs, TGF-β2 was found to downregulate all three members of miR-26 family including (miR-29a, miR-29b, and miR-29c). This downregulation of miR-29 miRNAs subsequently could lead to induction of several extracellular matrix proteins. miR-29b was found to also downregulate TGF-β1 significantly. These two observations highlight the potential role of the miR-29 family in controlling outflow process of aqueous humor affected by altered levels of TGF-βs [103].

miRNAs have been identified in aqueous humor and it has been assumed that any changes in their expression level could be associated with anterior chamber-related disease [105]. By conducting a microarray analysis of the differential expression of miRNA in the aqueous humor of glaucoma patients, several glaucoma-related extracellular miRNAs have been identified [106]. Further investigation, through analyzing both POAG and XFG patients, showed

that three miRNAs between POAG and control, five miRNAs between XFG and controls, and one miRNA (miR-302d-3p) between POAG and XFG exhibited significant differences in expression [107]. These miRNAs are likely to be involved in some glaucoma pathways including focal adhesion, tight junctions, and TGF-β signaling pathways [107]. Disease-specific miRNAs being differentially expressed in different types of glaucoma might play a role in targeted therapy or diagnosis.

It is believed that studying the polymorphisms in the miRNA biogenesis pathway could reveal information for disease prognosis and pharmacogenomics [104, 105]. The association of polymorphisms in genes involved in the biogenesis of miRNAs in XFS, XFG, and POAG populations showed that: (1) rs1057035 SNP in the 3′-untranslated region of the *DICER* gene (Dicer enzyme, a member of RNase III family) was associated with a decreased risk of XFS; and (2) rs55671916 SNP in the 3′-untranslated region of *XPO5* gene (XPO5 is involved in the nuclear export of pre-miRNAs) was associated with increased risk of XFG. It is thought that further studies on target genes of these small RNAs might elucidate more information on the genetic aspects of XFS and XFG [108].

2.4.3 Epigenetic factors: Novel Biomarkers

miRNAs are also strong candidates for predictive and diagnostic biomarkers because of their abundance in body fluids. In a recent study, miRNA levels in plasma and aqueous humor of glaucoma and XFS patients has been screened using Japanese and Caucasian patient cohorts. Twenty cell-free circulating miRNAs have been identified to be highly expressed in the plasma and aqueous humor of XFS/OAG cases, compared to controls. Among these twenty, a combination of three miRNAs (miR-637, miR-1306-5p, miR-3159) showed the highest specificity and sensitivity to glaucoma cases [109]. miRNA-based

biomarkers could provide an easy blood-based screening test for early diagnosis XFS and XFG [109].

Besides previously discussed approaches to find biomarkers, metabolomics analysis is also a promising means for biomarker discovery. Metabolomics involves analyses of substrates and products of metabolism in the cells and biofluids [110]. Since the metabolome is the final product of gene expression, any alterations at genomic or proteomic levels will be highly amplified at the metabolic pathways level, making metabolomic biomarkers a highly sensitive candidate for early-stage disease identification [110, 111]. It is believed that this group of biomarkers could be used in early diagnosis of XFS and glaucoma [112]. Plasma samples of XFS and XFG patients have been analyzed to identify specific metabolomic biomarker for XFS. Lower levels of neuroprotective spermine and spermidine polyamines in the plasma of XFS patients compared to the controls have been suggested as possible metabolomic signature for XFS [112, 113].

2.5 Dysfunction of clearance of protein-aggregates: Autophagy

Autophagy is an intracellular membrane trafficking system that delivers cytosolic constituents to the lysosome for subsequent degradation. Autophagy has been shown to be regulated and induced in response to nutrient starvation or other stress conditions. Autophagy is responsible for clearance of protein aggregates, which is crucial to cellular homeostasis as ubiquitin-proteasomal degradation pathways cannot digest these large assemblies [114]. Given the importance of autophagic clearance of protein aggregates, autophagy-related gene variants (*ATG* genes) may be implicated in XFS pathology. A study of 108 XFS/XFG patients and 118 healthy individuals in a Spanish population, however, showed that SNPs in three *ATG* genes (*ATG16L*, *ATG2B*, and

ATG5) were not significantly different in the allelic and genotype frequency of SNPs [115]. This finding does not leave out the possible connection between autophagy dysfunction and XFS pathogenesis. An *in vitro* study using fibroblast cells excised from Tenon's capsule of XFS and POAG patients during filtration surgery and strabismus surgery showed that, compared to POAG counterparts, Tenon's cells from XFS patients had different phenotypic signs of reduced clearance of autophagosmes due to autophagy dysfunction [116]. In a following *in vitro* study it was shown that those functional and structural differences were statistically significant between POAG and XFS-derived Tenon capsule fibroblasts [117]. Once autophagy was induced by starvation, autophagosomes in POAG cells were clustered around nuclear microtubule organizing center (MTOC), a normal microtubule-based migration observed in normal cells. On the contrary, no obvious MTOC was identified in XFS cells upon starvation induction, resulting in the dispersion of the majority of organelles in the cytoplasm [117]. It has been recently shown that autophagic degradation of misfolded LOXL1 resulting from gene variants was impeded in Tenon capsule fibroblasts, representing an *in vitro* model of XFG [118]. Those model cell lines failed in the establishment of MTOC, resulting in impaired localization of lysosomes, endosomes, and autophagosomes in the cytoplasm.

It is now well established that mutual interplay between mitochondria and lysosomes is crucial in maintaining cell homeostasis, and impaired autophagy has been linked with many different diseases [119]. Non-functioning mitochondria have been observed in XFS *in vitro* models, which could reduce the efficiency of respiration, leading to reduced ATP with increased reactive oxygen species production [116]. During aging, some *ATG*s are downregulated and autophagy function declines in humans, which is believed to be linked with age-related disease [120]. Given the association between its dysfunction and different diseases, autophagy has been considered as potential therapeutic

target [116, 120–122]. Understanding the effect of dysfunctional autophagy and impaired mitochondria in XFS progression is a new field of research, and more studies need to be done to uncover their role in XFS pathology and to identify potential therapeutic targets.

2.6 Conclusions

Exfoliation syndrome (XFS) has been studied at different levels of macromolecules, genetic factors, intracellular organelles and environmental factors. Almost all the studied factors are potentially linked to the pathogenesis of XFS. In term of genetic factors, several GWASs conducted in different populations have identified several genetic factors potentially associated with XFS. Among identified genetic factors, more attention has been drawn to the common variants of *LOXL1* gene in recent years, where two common variants of this gene have been purposed to be strongly associated with XFS. However, even though almost all studied XFS cases have these SNPs, healthy individuals have been found carrying the same SNPs in their genome. Investigations related to the connection between XFS and genetic factors have been accelerated in recent years; however, it is believed that identified SNPs alone cannot explain the pathomechanism of XFS. A possible role of cellular mechanisms at the cytoplasmic organelle level has been suggested as potential factors associated with this syndrome. Identification of any possible connection between genetic factors and impaired cellular functions might be helpful in understanding mechanisms related to formation of XFS material. Although the vast majority of studies focus on the age-matched groups of XFS or XFG cases; however, they might be in different stages of the disease. Thus, investigation on initial stages of the disease might reveal more information of the main macromolecules involved in the pathogenesis. For instance, mRNA and protein expression of IL-6 and IL-8 has been shown to be significantly in-

creased in the early stages of the XFS. However, in comparison to the control cases, advanced stages of the XFS or XFG do not show significant increase in production of IL-6 and IL-8 [13]. Given the accumulation of a myriad of molecules buried in XFS material, genetic or biochemical studies performed in a disease stage-dependent manner could reveal more information about factors underlying XFS and XFG progression.

2.7 References

[1] A. Tarkkanen and T. Kivelä, "John G. Lindberg and the discovery of exfoliation syndrome.," *Acta Ophthalmol. Scand.*, vol. 80, no. 2, pp. 151–154, 2002.

[2] G. Dvorak-Theobald, "Pseudo-exfoliation of the lens capsule: relation to true exfoliation of the lens capsule as reported in the literature and role in the production of glaucoma capsulocuticulare.," *Am. J. Ophthalmol.*, vol. 37, no. 1, pp. 1–12, 1954.

[3] Davanger M, "The pseudo-exfoliation syndrome. A scanning electron microscopic study. I. The anterior lens surface. *Acta Ophthalmol* 53: 809–820, 1975.

[4] M. Ghosh and J. S. Speakman, "The ciliary body in senile exfoliation of the lens.," *Can. J. Ophthalmol.*, vol. 8, no. 3, pp. 394–403, Jul. 1973.

[5] J. P. Harnisch, "Exfoliation material in different sections of the eye.," *Albrecht Von Graefes Arch. Klin. Exp. Ophthalmol.*, vol. 203, no. 3–4, pp. 181–190, Sep. 1977.

[6] Ringvold A, Electron microscopy of the wall of iris vessels in eyes with and without exfoliation syndrome (pseudoexfoliation of the lens capsule). *Virchows Arch A, Pathol Pathol Anat* 348: 328–341, 1969.

[7] A. Ringvold and T. Vegge, "Electron microscopy of the trabecular meshwork in eyes with exfoliation syndrome. (Pseudoexfoliation of the lens capsule).," *Virchows Arch. A, Pathol. Pathol. Anat.*, vol. 353, no. 2, pp. 110–127, 1971.

[8] M. Shakib, N. Ashton, and R. Blach, "Electron Microscopic Study of Pseudo-exfoliation of the Lens Capsule II. Iris and Ciliary Body," *Invest. Ophthalmol.*, vol. 4, pp. 154–161, Apr. 1965.

[9] R. Ritch and U. Schlotzer-Schrehardt, "Exfoliation syndrome.," *Surv. Ophthalmol.*, vol. 45, no. 4, pp. 265–315, 2001.

[10] U. M. Schl and M. R. Koca, "Pseudoexfoliation Syndrome Ocular Manifestation of a Systemic Disorder?," *Arch, vol.* 110, pp. 1752–2756, 1992.

[11] T. W. Blackstad, O. A. Sunde, and J. Trœtteberg, "On the ultrastructure of the deposits of busacca in eyes with glaucoma simplex and so-called senile exfoliation of the anterior lens capsule1).," *Acta Ophthalmol.*, vol. 38, no. 5, pp. 587–598, Oct. 1960.

[12] B. Ovodenko et al., "Proteomic analysis of exfoliation deposits," *Investig. Ophthalmol. Vis. Sci.*, vol. 48, no. 4, pp. 1447–1457, 2007.

[13] M. Zenkel, P. Lewczuk, A. Jünemann, F. E. Kruse, G. O. H. Naumann, and U. Schlötzer-Schrehardt, "Proinflammatory cytokines are involved in the initiation of the abnormal matrix process in pseudoexfoliation syndrome/glaucoma," *Am. J. Pathol.*, vol. 176, no. 6, pp. 2868–2879, 2010.

[14] P. Challa and W. M. Johnson, "Composition of Exfoliation Material.," *Glaucoma*, vol. 27, no. 7, pp. 29–31, 2018.

[15] M. Zenkel, A. Krysta, F. Pasutto, A. Juenemann, F. E. Kruse, and U. Schlötzer-Schrehardt, "Regulation of Lysyl Oxidase-like 1 (LOXL1) and elastin-related genes by pathogenic factors associated with pseudoexfoliation syndrome.," *Investig. Ophthalmol. Vis. Sci.*, vol. 52, no. 11, pp. 8488–8495, 2011.

[16] D. Chiras, G. Kitsos, M. B. Petersen, I. Skalidakis, and C. Kroupis, "Oxidative stress in dry age-related macular degeneration and exfoliation syndrome.," *Critical Reviews in Clinical Laboratory Sciences*, vol. 52, no. 1. Informa Healthcare USA, Inc., pp. 12–27, 2015.

[17] U. Schlotzer-Schrehardt, "New pathogenetic insights into pseudoexfoli-

ation syndrome/glaucoma. Therapeutically relevant?," *Ophthalmologe*, vol. 109, no. 10, pp. 944–951, Oct. 2012.

[18] N. Ashton, M. Shakib, R. Collyer, and R. Blach, "Electron Microscopic Study of Pseudo-Exfoliation of the Lens Capsule. I. Lens Capsule and Zonular Fibers.," *Invest. Ophthalmol.*, vol. 4, pp. 141–153, 1965.

[19] M. Zenkel and U. Schlötzer-Schrehardt, "The composition of exfoliation material and the cells involved in its production.," *J. Glaucoma*, vol. 23, no. 8 Suppl 1, pp. S12-4, 2014.

[20] S. Ashok Vardhan et al., "Association of pseudoexfoliation with systemic vascular diseases in a South Indian population," *JAMA Ophthalmol.*, vol. 135, no. 4, pp. 348–354, 2017.

[21] G. Egemen Erkayhan and S. Dogan, "Cataract Surgery and Possible Complications in Patients with Pseudoexfoliation Syndrome," *Eurasian J. Med.*, vol. 49, no. 1, pp. 22–25, 2016.

[22] L. Ilveskoski, C. Taipale, E. J. Holmström, and R. Tuuminen, "Macular edema after cataract surgery in eyes with and without pseudoexfoliation syndrome," *Eur. J. Ophthalmol.*, pp. 1–6, 2018.

[23] A. Kurt and T. Yaşar, "Complications of Phacoemulsification and Extracapsular Cataract Extraction Surgery in Eyes with Pseudoexfoliation Syndrome," Ophthalmol. *Res. An Int. J.*, vol. 8, no. 2, pp. 1–8, 2018.

[24] K. Grødum, A. Heijl, and B. Bengtsson, "Glaucoma and mortality," *Graefe's Arch. Clin. Exp. Ophthalmol.*, vol. 242, no. 5, pp. 397–401, 2004.

[25] A. Ringvold, S. Blika, and L. Sandvik, "Pseudo-exfoliation and mortality," *Acta Ophthalmol. Scand.*, vol. 75, no. 3, pp. 255–256, 2009.

[26] K. R. Shrum, M. G. Hattenhauer, and D. Hodge, "Cardiovascular and cerebrovascular mortality associated with ocular pseudoexfoliation," *Am. J.*

Ophthalmol., vol. 129, no. 1, pp. 83–86, 2000.

[27] J. K. Slettedal, L. Sandvik, and A. Ringvold, "Ocular pseudoexfoliation syndrome and life span.," *EBioMedicine*, vol. 2, no. 7, pp. 765–769, Jul. 2015.

[28] R. Svensson and C. Ekstrom, "Pseudoexfoliation and mortality: a population-based 30-year follow-up study.," *Acta Ophthalmol.*, vol. 93, no. 2, pp. 162–164, Mar. 2015.

[29] R. F. Brubaker, "Flow of aqueous humor in humans [The Friedenwald Lecture].," *Invest. Ophthalmol. Vis. Sci.*, vol. 32, no. 13, pp. 3145–3166, Dec. 1991.

[30] M. Goel, R. G. Picciani, R. K. Lee, and S. K. Bhattacharya, "Aqueous Humor Dynamics: A Review," *Open Ophthalmol. J.*, vol. 4, pp. 52–59, 2010.

[31] M. P. Fautsch et al., "Aqueous humor outflow: What do we know? Where will it lead us?," *Investig. Ophthalmol. Vis. Sci.*, vol. 47, no. 10, pp. 4181–4187, 2006.

[32] W. D. Stamer and A. F. Clark, "The many faces of the trabecular meshwork cell," *Exp. Eye Res.*, vol. 158, pp. 112–123, 2017.

[33] M. M. Civan and A. D. C. Macknight, "The ins and outs of aqueous humour secretion.," *Exp. Eye Res.*, vol. 78, no. 3, pp. 625–631, Mar. 2004.

[34] Y.-C. Tham, X. Li, T. Y. Wong, H. A. Quigley, T. Aung, and C.-Y. Cheng, "Global prevalence of glaucoma and projections of glaucoma burden through 2040: a systematic review and meta-analysis.," *Ophthalmology*, vol. 121, no. 11, pp. 2081–2090, Nov. 2014.

[35] U. Schlotzer-Schrehardt and G. O. Naumann, "Trabecular meshwork in pseudoexfoliation syndrome with and without open-angle glaucoma. A morphometric, ultrastructural study.," *Invest. Ophthalmol. Vis. Sci.*, vol. 36, no. 9, pp. 1750–1764, Aug. 1995.

[36] R. Ritch, "Exfoliation syndrome-the most common identifiable cause of open-angle glaucoma.," *J. Glaucoma*, vol. 3, no. 2, pp. 176–177, 1994.

[37] S. F. Nilsson, "The uveoscleral outflow routes.," *Eye (Lond).*, vol. 11 (Pt 2), pp. 149–154, 1997.

[38] A. Alm and S. F. E. Nilsson, "Uveoscleral outflow-a review.," *Exp. Eye Res.*, vol. 88, no. 4, pp. 760–768, Apr. 2009.

[39] T. V Johnson, S. Fan, C. B. Camras, and C. B. Toris, "Aqueous humor dynamics in exfoliation syndrome.," *Arch. Ophthalmol.* (Chicago, Ill. 1960), vol. 126, no. 7, pp. 914–920, Jul. 2008.

[40] U. Schlötzer-schrehardt and G. O. H. Naumann, "Trabecular Mechanisms of Intraocular Pressure Elevation Pseudoexfoliation Syndrome," in Mechanisms of the Glaucomas: Disease Processes and Therapeutic Modalities, *Humana press*, 2008, pp. 117–138.

[41] E. Vesti and T. Kivela, "Exfoliation syndrome and exfoliation glaucoma.," *Prog. Retin. Eye Res.*, vol. 19, no. 3, pp. 345–368, May 2000.

[42] I. F. Aboobakar, W. M. Johnson, W. D. Stamer, M. A. Hauser, and R. R. Allingham, "Major review: Exfoliation syndrome; advances in disease genetics, molecular biology, and epidemiology," *Exp. Eye Res.*, vol. 154, pp. 88–103, 2017.

[43] R. M. Conway, U. Schlötzer-Schrehardt, M. Küchle, and G. O. H. Naumann, "Pseudoexfoliation syndrome: Pathological manifestations of relevance to intraocular surgery," *Clin. Exp. Ophthalmol.*, vol. 32, no. 2, pp. 199–210, 2004.

[44] M. A. Desai and R. K. Lee, "The medical and surgical management of pseudoexfoliation glaucoma.," *Int. Ophthalmol. Clin.*, vol. 48, no. 4, pp. 95–113, 2008.

[45] R. Ritch, "Ocular and systemic manifestations of exfoliation syndrome," *J. Glaucoma*, vol. 23, no. 8, pp. S1–S8, 2014.

[46] H. Chung, S. Arora, K. F. Damji, and E. Weis, "Association of pseudoexfoliation syndrome with cardiovascular and cerebrovascular disease: a systematic review and meta-analysis," *Can. J. Ophthalmol.*, vol. 53, no. 4, pp. 365–372, 2018.

[47] P. Oltulu and R. Oltulu, "The Association of Cataract and Lens Epithelial Cell Apoptosis in Patients with Pseudoexfoliation Syndrome," *Curr. Eye Res.*, vol. 43, no. 3, pp. 300–303, 2018.

[48] R. Ritch, "Systemic Associations of Exfoliation Syndrome.," *Asia-Pacific J. Ophthalmol.* (Philadelphia, Pa.), vol. 5, no. 1, pp. 45–50, 2016.

[49] G. Thorleifsson et al., "Common sequence variants in the LOXL1 gene confer susceptibility to exfoliation glaucoma.," *Science*, vol. 317, no. 5843, pp. 1397–1400, Sep. 2007.

[50] X. Liu et al., "Elastic fiber homeostasis requires lysyl oxidase-like 1 protein," *Nat. Genet.*, vol. 36, no. 2, pp. 178–182, 2004.

[51] K. S. Midwood and J. E. Schwarzbauer, "Elastic Fibers: Building Bridges Between Cells and Their Matrix.," *Curr Biol.*, vol. 12, no. 02, pp. 279–281, 2002.

[52] L. I. Smith-Mungo and H. M. Kagan, "Lysyl oxidase: Properties, regulation and multiple functions in biology," *Matrix Biol.*, vol. 16, no. 7, pp. 387–398, 1998.

[53] S. E. I. Williams et al., "Major LOXL1 risk allele is reversed in exfoliation glaucoma in a black South African population," *Mol. Vis.*, vol. 16, pp. 705–712, Apr. 2010.

[54] S. Kim and Y. Kim, "Variations in LOXL1 associated with exfoliation

glaucoma do not affect amine oxidase activity," *Mol. Vis.*, vol. 18, pp. 265–270, 2012.

[55] T. Aung et al., "A common variant mapping to CACNA1A is associated with susceptibility to exfoliation syndrome," *Nat. Genet.*, vol. 47, no. 4, pp. 387–392, 2015.

[56] I. F. Aboobakar and R. R. Allingham, "Genetics of exfoliation syndrome and glaucoma.," *Int. Ophthalmol. Clin.*, vol. 54, no. 4, pp. 43–56, 2014.

[57] M. Zenkel and U. Schlötzer-Schrehardt, "Expression and regulation of LOXL1 and elastin-related genes in eyes with exfoliation syndrome," *J. Glaucoma*, vol. 23, no. 8, pp. S62–S63, 2014.

[58] U. Schlötzer-Schrehardt et al., "Genotype-correlated expression of lysyl oxidase-like 1 in ocular tissues of patients with pseudoexfoliation syndrome/glaucoma and normal patients," *Am. J. Pathol.*, vol. 173, no. 6, pp. 1724–1735, 2008.

[59] F. Pasutto et al., "Pseudoexfoliation syndrome-associated genetic variants affect transcription factor binding and alternative splicing of LOXL1," *Nat. Commun.*, vol. 8, no. May, 2017.

[60] D. Berner et al., "Posttranscriptional regulation of LOXL1 expression *via* alternative splicing and nonsense-mediated mRNA decay as an adaptive stress response," *Investig. Ophthalmol. Vis. Sci.*, vol. 58, no. 13, pp. 5930–5940, 2017.

[61] D. Berner et al., "The protective variant rs7173049 at LOXL1 locus impacts on retinoic acid signaling pathway in pseudoexfoliation syndrome.," *Hum. Mol. Genet.*, vol. 28, pp. 2531–2548, Apr. 2019.

[62] T. Aung et al., "Genetic association study of exfoliation syndrome identifies a protective rare variant at LOXL1 and five new susceptibility loci," *Nat.*

Genet., vol. 49, no. 7, pp. 993–1004, 2017.

[63] T. Aung, A. S. Chan, and C.-C. Khor, "Genetics of Exfoliation Syndrome.," *J. Glaucoma*, vol. 27 Suppl 1, pp. S12–S14, Jul. 2018.

[64] D. Pietrobon, "CAv2.1 channelopathies," *Pflugers Arch. Eur. J. Physiol.*, vol. 460, no. 2, pp. 374–393, 2010.

[65] U. Schlötzer-Schrehardt, M. Zenkel, M. Küchle, L. Y. Sakai, and G. O. H. Naumann, "Role of Transforming Growth Factor-β1 and its Latent Form Binding Protein in Pseudoexfoliation Syndrome," *Exp. Eye Res.*, vol. 73, no. 6, pp. 765–780, 2001.

[66] U. Schlötzer-Schrehardt, "Molecular Biology of Exfoliation Syndrome," *J. Glaucoma*, vol. 27, no. 7, pp. S32–S37, 2018.

[67] M. Zenkel, F. E. Kruse, A. G. Jünemann, G. O. H. Naumann, and U. Schlötzer-Schrehardt, "Clusterin deficiency in eyes with pseudoexfoliation syndrome may be implicated in the aggregation and deposition of pseudoexfoliative material," *Investig. Ophthalmol. Vis. Sci.*, vol. 47, no. 5, pp. 1982–1990, 2006.

[68] S. E. Jones and C. Jomary, "Clusterin.," *Int. J. Biochem. Cell Biol.*, vol. 34, no. 5, pp. 427–431, May 2002.

[69] A. M. Rodríguez-Piñeiro, M. P. de la Cadena, Á. López-Saco, and F. J. Rodríguez-Berrocal, "Differential Expression of Serum Clusterin Isoforms in Colorectal Cancer," *Mol. Cell. Proteomics*, vol. 5, no. 9, pp. 1647–1657, 2006.

[70] M. E. Rosenberg and J. Silkensen, "Clusterin: Physiologic and pathophysiologic considerations," *Int. J. Biochem. Cell Biol.*, vol. 27, no. 7, pp. 633–645, 1995.

[71] M. E. Fini, A. Bauskar, S. Jeong, and M. R. Wilson, "Clusterin in the

eye: An old dog with new tricks at the ocular surface," *Exp. Eye Res.*, vol. 147, pp. 57–71, 2016.

[72] S. Poon, T. M. Treweek, M. R. Wilson, S. B. Easterbrook-Smith, and J. A. Carver, "Clusterin is an extracellular chaperone that specifically interacts with slowly aggregating proteins on their off-folding pathway," *FEBS Lett.*, vol. 513, no. 2–3, pp. 259–266, 2002.

[73] M. Calero, A. Rostagno, E. Matsubara, B. Zlokovic, B. Frangione, and J. Ghiso, "Apolipoprotein J (clusterin) and Alzheimer's disease," *Microsc. Res. Tech.*, vol. 50, no. 4, pp. 305–315, 2000.

[74] I. Doudevski, A. Rostagno, M. Cowman, J. Liebmann, R. Ritch, and J. Ghiso, "Clusterin and complement activation in exfoliation glaucoma," *Investig. Ophthalmol. Vis. Sci.*, vol. 55, no. 4, pp. 2491–2499, 2014.

[75] R. Creasey et al., "Detecting protein aggregates on untreated human tissue samples by atomic force microscopy recognition imaging," *Biophys. J.*, vol. 99, no. 5, pp. 1660–1667, 2010.

[76] J. Stafiej et al., "Immunohistochemical analysis of microsomal glutathione S-transferase 1 and clusterin expression in lens epithelial cells of patients with pseudoexfoliation syndrome," *Exp. Ther. Med.*, vol. 13, no. 3, pp. 1057–1063, 2017.

[77] B. J. Fan, L. R. Pasquale, J. H. Kang, H. Levkovitch-Verbin, J. L. Haines, and J. L. Wiggs, "Association of clusterin (CLU) variants and exfoliation syndrome: An analysis in two Caucasian studies and a meta-analysis," *Exp. Eye Res.*, vol. 139, pp. 115–122, 2015.

[78] B. Padhy, G. G. Nanda, M. Chowdhury, D. Padhi, A. Rao, and D. P. Alone, "Role of an extracellular chaperone, Clusterin in the pathogenesis of Pseudoexfoliation Syndrome and Pseudoexfoliation Glaucoma," *Exp. Eye*

Res., vol. 127, pp. 69–76, 2014.

[79] J. Magalhães and M. J. Saraiva, "Clusterin overexpression and its possible protective role in transthyretin deposition in familial amyloidotic polyneuropathy," *J. Neuropathol. Exp. Neurol.*, vol. 70, no. 12, pp. 1097–1106, 2011.

[80] K. P. Burdon et al., "Genetic analysis of the clusterin gene in pseudoexfoliation syndrome.," *Mol. Vis.*, vol. 14, pp. 1727–1736, Sep. 2008.

[81] M. Krumbiegel et al., "Exploring functional candidate genes for genetic association in german patients with pseudoexfoliation syndrome and pseudoexfoliation glaucoma.," *Invest. Ophthalmol. Vis. Sci.*, vol. 50, no. 6, pp. 2796–2801, Jun. 2009.

[82] S. K. Dubey, J. F. Hejtmancik, S. R. Krishnadas, R. Sharmila, A. Haripriya, and P. Sundaresan, "Evaluation of genetic polymorphisms in clusterin and tumor necrosis factor-alpha genes in South Indian individuals with pseudoexfoliation syndrome.," *Curr. Eye Res.*, vol. 40, no. 12, pp. 1218–1224, 2015.

[83] H. Lesiewska, K. Linkowska, J. Stafiej, T. Grzybowski, J. Swobodziński, and G. Malukiewicz, "CLU polymorphisms in patients with pseudoexfoliation syndrome in polish population," *J. Ophthalmol.*, vol. 2019, 2019.

[84] J. L. Wiggs, J. H. Kang, B. Fan, H. Levkovitch-Verbin, and L. R. Pasquale, "A Role for Clusterin in Exfoliation Syndrome and Exfoliation Glaucoma?," *J. Glaucoma*, vol. 27 Suppl 1, pp. S61–S66, Jul. 2018.

[85] K. Zagajewska et al., "GWAS links variants in neuronal development and actin remodeling related loci with pseudoexfoliation syndrome without glaucoma," *Exp. Eye Res.*, vol. 168, no. June 2017, pp. 138–148, 2018.

[86] Y. N. Ma, T. Y. Xie, and X. Y. Chen, "Multiple Gene Polymorphisms Associated with Exfoliation Syndrome in the Uygur Population," *J. Ophthalmol.*, vol. 2019, 2019.

[87] M. Nakano et al., "Novel common variants and susceptible haplotype for exfoliation glaucoma specific to Asian population," *Sci. Rep.*, vol. 4, pp. 1–6, 2014.

[88] M. Krumbiegel et al., "Genome-wide association study with DNA pooling identifies variants at CNTNAP2 associated with pseudoexfoliation syndrome," *Eur. J. Hum. Genet.*, vol. 19, no. 2, pp. 186–193, 2011.

[89] J. L. Wiggs et al., "Common variants at 9p21 and 8q22 are associated with increased susceptibility to optic nerve degeneration in glaucoma," *PLoS Genet.*, vol. 8, no. 4, pp. 1–12, 2012.

[90] V. F. Oliver, K. A. van Bysterveldt, and S. L. Merbs, "Chapter 22-Epigenetics in Ocular Medicine," TOBT-ME Tollefsbol, (ed.). Medical Epigenetics. Boston: *Academic Press*, 2016, pp. 391–412.

[91] W. M. Johnson, L. K. Finnegan, M. A. Hauser, and W. D. Stamer, "LncRNAs, DNA Methylation, and the Pathobiology of Exfoliation Glaucoma," *J. Glaucoma*, vol. 27, no. 3, pp. 202–209, 2018.

[92] A. W. Hewitt, J. J. Wang, H. Liang, and J. E. Craig, "Epigenetic effects on eye diseases," *Expert Rev. Ophthalmol.*, vol. 7, no. 2, pp. 127–134, 2014.

[93] H. A. Alkozi, R. Franco, and J. J. Pintor, "Epigenetics in the eye: An overview of the most relevant ocular diseases," *Front. Genet.*, vol. 8, no. 144, pp. 1–7, 2017.

[94] H. Ye et al., "LOXL1 hypermethylation in pseudoexfoliation syndrome in the uighur population," *Investig. Ophthalmol. Vis. Sci.*, vol. 56, no. 10, pp. 5838–5843, 2015.

[95] J. Cao, "The functional role of long non-coding RNAs and epigenetics," *Biol. Proced. Online*, vol. 16, no. 11, pp. 1–13, 2014.

[96] T. R. Mercer, M. E. Dinger, and J. S. Mattick, "Long non-coding RNAs:

insights Into Functions," *Nat. Rev. Genet.*, vol. 10, pp. 155–159, 2009.

[97] P. Wan, W. Su, and Y. Zhuo, "The Role of Long Noncoding RNAs in Neurodegenerative Diseases," *Mol. Neurobiol.*, vol. 54, pp. 2012–2021, 2017.

[98] M. A. Hauser et al., "Genetic variants and cellular stressors associated with exfoliation syndrome modulate promoter activity of a lncRNA within the LOXL1 locus," *Hum. Mol. Genet.*, vol. 24, no. 22, pp. 6552–6563, 2015.

[99] G. Arun, S. D. Diermeier, and D. L. Spector, "Therapeutic Targeting of Long Non-Coding RNAs in Cancer," *Trends Mol. Med.*, vol. 24, no. 3, pp. 257–277, 2018.

[100] T. Wu and Y. Du, "LncRNAs: From Basic Research to Medical Application," *Int. J. Biol. Sci.*, vol. 13, pp. 295–307, 2017.

[101] V. Ambros, "The functions of animal microRNAs," *Nature*, vol. 431, no. 7006, pp. 350–355, 2004.

[102] P. Gonzalez, G. Li, J. Qiu, J. Wu, and C. Luna, "Role of microRNAs in the trabecular meshwork.," *J. Ocul. Pharmacol. Ther.*, vol. 30, no. 2–3, pp. 128–137, 2014.

[103] C. Luna, G. Li, J. Qiu, D. L. Epstein, and P. Gonzalez, "Cross-talk between miR-29 and transforming growth factor-betas in trabecular meshwork cells," Investig. *Ophthalmol. Vis. Sci.*, vol. 52, no. 6, pp. 3567–3572, 2011.

[104] C. Luna, G. Li, J. Qiu, D. L. Epstein, and P. Gonzalez, "Role of miR-29b on the regulation of the extracellular matrix in human trabecular meshwork cells under chronic oxidative stress.," *Mol. Vis.*, vol. 15, pp. 2488–2497, Nov. 2009.

[105] J. J. Dunmire, E. Lagorous, R. A. Bouhenni, M. Jones, and D. P. Edward, "MicroRNA in aqueous humor from patients with cataract," *Exp. Eye Res.*, vol. 108, pp. 68–71, 2013.

[106] Y. Tanaka et al., "Profiles of extracellular miRNAs in the aqueous humor of glaucoma patients assessed with a microarray system," *Sci. Rep.*, vol. 4, pp. 1–7, 2014.

[107] M. D. Drewry et al., "Differentially expressed microRNAs in the aqueous humor of patients with exfoliation glaucoma or primary open-angle glaucoma," *Hum. Mol. Genet.*, vol. 27, no. 7, pp. 1263–1275, 2018.

[108] A. Chatzikyriakidou et al., "MicroRNA-related polymorphisms in pseudoexfoliation syndrome, pseudoexfoliative glaucoma, and primary open-angle glaucoma," *Ophthalmic Genet.*, vol. 39, no. 5, pp. 603–609, 2018.

[109] A. G. Hindle et al., "Identification of candidate miRNA biomarkers for glaucoma," *Investig. Ophthalmol. Vis. Sci.*, vol. 60, no. 1, pp. 134–146, 2019.

[110] C. H. Johnson, J. Ivanisevic, and G. Siuzdak, "Metabolomics: Beyond biomarkers and towards mechanisms," *Nat. Rev. Mol. Cell Biol.*, vol. 17, no. 7, pp. 451–459, 2016.

[111] M. S. Monteiro, M. Carvalho, M. L. Bastos, and P. Guedes de Pinho, "Metabolomics Analysis for Biomarker Discovery: Advances and Challenges," *Curr. Med. Chem.*, vol. 20, no. 2, pp. 257–271, 2013.

[112] S. McNally and C. J. O'Brien, "Metabolomics/proteomics strategies used to identify biomarkers for exfoliation glaucoma," *J. Glaucoma*, vol. 23, no. 8, pp. S51–S54, 2014.

[113] S. Leruez et al., "A Plasma Metabolomic Signature of the Exfoliation Syndrome Involves Amino Acids, Acylcarnitines, and Polyamines.," *Invest. Ophthalmol. Vis. Sci.*, vol. 59, no. 2, pp. 1025–1032, Feb. 2018.

[114] I. Dikic, "Proteasomal and Autophagic Degradation Systems," *Annu. Rev. Biochem.*, vol. 86, no. 1, pp. 193–224, 2017.

[115] L. de Juan-Marcos, F. A. Escudero-Dominguez, E. Hernandez-Galilea, F. Cruz-Gonzalez, I. Follana-Neira, and R. Gonzalez-Sarmiento, "Investigation of Association between Autophagy-Related Gene Polymorphisms and Pseudoexfoliation Syndrome and Pseudoexfoliation Glaucoma in a Spanish Population.," *Semin. Ophthalmol.*, vol. 33, no. 3, pp. 361–366, 2018.

[116] A. Want et al., "Autophagy and mitochondrial dysfunction in tenon fibroblasts from exfoliation glaucoma patients," *PLoS One*, vol. 11, no. 7, pp. 1–21, 2016.

[117] J. M. Wolosin, R. Ritch, and A. M. Bernstein, "Is Autophagy Dysfunction a Key to Exfoliation Glaucoma?," *J. Glaucoma*, vol. 27, no. 3, pp. 197–201, 2018.

[118] A. M. Bernstein, R. Ritch, and J. M. Wolosin, "Exfoliation syndrome: A disease of autophagy and LOXL1 proteopathy.," *J. Glaucoma*, vol. 27, no. 7, pp. S44–S53, 2018.

[119] M. Audano, A. Schneider, and N. Mitro, "Mitochondria, lysosomes, and dysfunction: their meaning in neurodegeneration," *J. Neurochem.*, vol. 147, no. 3, pp. 291–309, 2018.

[120] A. M. Leidal, B. Levine, and J. Debnath, "Autophagy and the cell biology of age-related disease," *Nat. Cell Biol.*, vol. 20, no. 12, pp. 1338–1348, 2018.

[121] L. Galluzzi, J. M. Bravo-San Pedro, B. Levine, D. R. Green, and G. Kroemer, "Pharmacological modulation of autophagy: therapeutic potential and persisting obstacles," *Nat. Rev. Drug Discov.*, vol. 16, pp. 487–511, 2017.

[122] B. Levine and G. Kroemer, "Biological Functions of Autophagy Genes: A Disease Perspective," *Cell*, vol. 176, no. 1–2, pp. 11–42, 2019.

Chapter 3

Peptides for targeting βB2-crystallin fibrils

Abstract

Crystallins are a major family of proteins located within the lens of the eye. Cataracts are thought to be due to the formation of insoluble fibrillar aggregates, which are largely composed of proteins from the crystallin family. Today the only cataract treatment that exists is surgery and this can be difficult to access for individuals in the developing world. Development of novel pharmacotherapeutic approaches for the treatment of cataract rests on the specific targeting of these structures. βB2-crystallin, a member of β-crystallin family, is a large component of the crystallin proteins within the lens, and as such was used to form model fibrils *in vitro*. Peptides were identified, using phage display techniques, that bound to these fibrils with high affinity. Fibrillation of recombinantly expressed human βB2-crystallin was performed in 10% (v/v) trifluoroethanol (TFE) solution (pH 2.0) at various temperatures, and its amyloid-like structure was confirmed using Thioflavin-T (ThT) assay, transmission electron microscopy (TEM), and X-ray fiber diffraction (XRFD) analysis. Affinity of identified phage-displayed peptides was analyzed using enzyme-linked immunosorbent assay (ELISA). Specific binding of a cyclic peptide (CKQFKDTTC) showed the highest affinity, which was confirmed using a competitive inhibition assay.

Keywords: Phage display; βB2-crystallin; amyloid-like fibril; fibrillar ag-

gregate; cataract; targeting peptide.

3.1 Introduction

Cataracts are the leading cause of blindness and affect the quality of life of approximately 50% of the aged population worldwide [1, 2]. Cataract development is thought to stem from the aggregation of crystallins into amorphous and amyloid-like fibrillar structures [3, 4] that ultimately grow to sufficient size to scatter light as it traverses the lens. There is no pharmacological treatment for this disease [5]; available treatment is surgical replacement of the lens with an artificial polymer-mimic. This treatment is difficult to access for a large portion of patients worldwide (especially in developing countries) [6]. Surgery is expensive, invasive, performed only when quality of life is drastically affected [2], and involves possible surgical risks and complications such as posterior capsular opacification [5]. Screening the interaction of small molecules with misfolded or aggregated proteins is considered a promising strategy for discovering and designing drugs to prevent protein aggregation and/or eliminate formed fibrils [7]. Identification of peptide-based fibrillogenesis inhibitors is a growing field offering drugs with specific targeting capabilities [8, 9]. Phage display is a powerful tool for identifying peptides with specific affinity for different targets, without a priori information regarding the target or binding mechanism [10]. Thus, this technique has been widely used to identify high affinity binders for fibrillar aggregates including peptides [11] and single-chain variable fragments (scFv) [12]. For example, phage display techniques have been used to identify peptides with specific binding affinity to fibrillar amyloid-like aggregates, but not monomeric Aβ peptides [13]. The identification of these specific binders allows for the specific, local delivery of fibril blocker and/or fibril destroying reagents and may provide a platform for diagnostic functionality [11, 13].

Normal lens tissue is an avascular, transparent structure that functions to focus incoming light onto the retina [14]. Crystallins are the major protein fam-

ily found within the lens, accounting for approximately 90% of the lens' total protein content [3, 5]. Three classes of crystallin proteins have been identified: α-, β- and γ-crystallin. α-crystallin proteins are well known to have a chaperone function and belong to a small heat-shock protein (sHsp) family, whereas β- and γ-crystallins primarily play a role in maintaining lens structure [4]. Crystallin proteins are found in high concentration within the lens (200–450 mg/ml) and are thought to have very low turnover rates. Their high concentration, while being necessary for providing a proper refractive index, may be a factor in influencing protein aggregation should even very minor perturbations in protein structure occur *in vivo* [3, 15, 16]. Whether the aggregates of cataractous material are amorphous or fibrillar, or a combination of both is a matter of debate [17]. In fact, it has been shown that crystallin proteins denature under even mild conditions to form fibrillar amyloid-like structures *in vitro* [18-20]. In addition, recent *ex vivo* studies have shown fibrillation of crystallins during cataract development, suggesting that fibril formation plays an important role in cataract formation [21]. Other modifications to the crystallin proteins thought to induce aggregation include age-associated conformational changes [14], deamidation [22], oxidation, glycation, truncation [5], methylation, and ultraviolet radiation [23]. These changes to the lens proteins, coupled with their low turnover and high concentration, are thought to be the impetus for the formation of aggregates large enough to affect the optical function of the lens [16, 24]. Furthermore, the formation of insoluble fibrillar aggregates within the lens is also thought to disturb the short-range order between crystallins required for lens transparency and furthers opacification and cataract formation [18].

It has been suggested that because β-crystallins compromise approximately 40% of young human lens crystallins, and undergo high modification with aging; they may have a significant influence on development of age-related

cataract [23]. βB2-crystallin is the major protein component within the β-crystallins family, assembles into dimeric and oligomeric structures, plays a critical role in maintaining solubility of other β-crystallins, and functions to provide lens transparency [25-27]. βB2-crystallin is a basic member of β-crystallins [27], and its subunits have two tightly folded domains that are connected by a linker peptide. Each domain is folded in two Greek key motifs composed of four β-sheet structures (Fig. 3.1) [25]. Aggregation of recombinantly expressed human βB2-crystallin has been studied previously as a model for cataracts [28]. One of the most common method for forming fibrils involves using the 2,2,2-trifluoroethanol (TFE) solution that yields final fibril properties similar to that of amyloid fibrils [29, 30]. It has been demonstrated that bovine crystallin proteins form amyloid-like structures in the presence of TFE [18]. In this study, we follow previous work by using TFE to form fibrils of recombinantly expressed human βB2-crystallin in acidic solution [18]. Resulting fibril formation was characterized using the Thioflavin-T (ThT) assay, electron microscopy and X-ray fiber diffraction (XRFD) analysis.

It is thought that through the identification of peptides having strong and specific interaction with fibrillar βB2-crystallin, as a representative protein of β-crystallin family, might lead to a wide variety of treatment options. Identified peptides with specific affinity to βB2-crystallin fibrillar aggregates could have potential therapeutic effects on cataract. Even peptides without inhibitory or fibril destroying capability could be employed as drug mediators [31]. Mechanical, chemical, or thermal agents having fibril disruption potential could be conjugated to targeting peptides providing a new therapeutic approach for cataract [31]. Screening of random phage-displayed peptide libraries against fibrillar aggregates of individual crystallins could yield ligands with specific affinity to each type of crystallin proteins. In this study ELISA and competitive inhibition assay highlight high-affinity peptides to

βB2-crystallin fibrils selected from phage display process. This is the first time in the literature that small peptide binders have been identified against fibrillar aggregates of recombinantly expressed human βB2-crystallin.

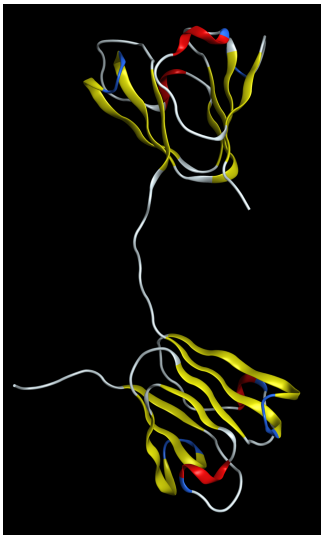

Figure 3.1: Ribbon model structure of Human βB2-crystallin. Monomer structure of human βB2-crystallin shown in ribbon representation. β-sheet reach domains are connected to each other through linker peptide. Figure was generated using Molecular Operating Environment (MOE) software, (PDB ID: 1YTQ) [27].

3.2 Materials and methods

3.2.1 Expression and purification of human βB2-crystallin protein

DNA sequence of human βB2-crystallin gene was cloned into a pET-15b vector. βB2-crystallin protein was expressed with an N-terminal histidine tag in *E. coli* BL21 (DE3) host strains. Bacterial cells containing the recombinant plasmids were inoculated into LB medium supplemented with 100 μg/mL ampicillin. When the OD_{600} of the bacterial culture reached 0.6, the cells were induced by 1.0 mM isopropyl β-D-1-thiogalactopyranoside (IPTG) for 18 hr at 37 °C. The cells were subsequently harvested by centrifugation at 6000 $\times$ g for 20 min at 4 °C and resuspended in buffer A (25 mM Tris, protease inhibitor EDTA-free tablet, pH 8.0, Roche). Cell disruption was performed by

sonication on ice (4 cycles, 15 sec at 45% power) using a microtip probe sonicator (Fisher Scientific ultrasonic dismembrator, Model 500). Cell lysate was ultracentrifuged at 223000 × g for 120 min at 10 °C. The supernatant was removed and loaded on the Ni-NTA column pre-equilibrated with buffer A. The column was then washed with buffer B (25 mM Tris, 0.1% Triton X-100, pH 8.0), buffer C (25 mM Tris, 1 M NaCl, pH 8.0), and buffer D (25 mM Tris, 25 mM Imidazole, pH 8.0) sequentially and βB2-crystallin protein was eluted with a linear gradient of 500 mM imidazole in buffer A. Eluted fractions containing recombinant protein were pooled followed by dialysis against buffer A at 4 °C. Then, $CaCl_2$ was added to the final concentration of 2 mM. Purified protein solution was mixed with enterokinase (0.02 μg of the enzyme per 1 mg of the crystallin protein) and incubated for 22 hr at room temperature (RT). His-tag digest was monitored by SDS-PAGE analysis. To remove the His-tag and enterokinase enzyme, digested samples were passed through Ni-NTA resin and trypsin inhibitor agarose. To inhibit all possible traces of enterokinase activity, phenylmethylsulfonyl fluoride (PMSF) protease inhibitor was added to the recombinant protein solution with 0.1 mM final concentration. The protein sample was finally concentrated using an Amicon® ultra-15 centrifugal filter unit.

Expression of βB2-crystallin protein was verified through SDS-PAGE, and liquid chromatography–mass spectrometry (LC-MS) analysis. (Protein identification by mass spectrometry was carried out in Alberta proteomics and mass spectrometry facility (University of Alberta, Edmonton, Alberta, Canada).

3.2.2 Fibrillation of βB2-crystallin protein

Fibrillation protocol was followed as described elsewhere [18]. Concentrated solutions of βB2-crystallin protein were diluted in 10% (v/v) trifluoroethanol (TFE) solution, pH 2.0 (adjusted with HCl) to a final concentration of 10

mg/ml and incubated for 24 hr at RT. To study the effect of elevated temperature on fibril formation, the same incubation process was carried out at 60 °C as well. After incubation at both RT and 60 °C, cloudiness of solution was observed in both cases. For further evaluation of the fibril formation process, aliquots were collected at 0, 4, 10, and 24 hr time points and stored at -20 °C to stop the fibrillation process.

3.2.3 Thioflavin T (ThT) assay

ThT assay was carried out as described [17]. Fresh solution of 5 μM ThT in 50 mM glycine-NaOH buffer, pH 9.0 was prepared and syringe filtered (0.22 μm). In triplicate, 2 μl of each fibril solution was diluted into 200 μl of ThT assay solution in Corning® 96-well clear bottom black polystyrene fluorescence microplates; similar to those used for phage panning. ThT fluorescence studies of samples were carried out by a FlexStation® 3 multimode plate reader at excitation wavelength of 440 nm and emission scanning wavelengths from 450-550 nm (emission of ThT is at 490 nm and maximum peak intensities reported). Intensity values represent relative fluorescence units (RFU). Statistical difference at $P < 0.05$ level was analyzed by one-way ANOVA test.

3.2.4 Electron microscopy

Transmission electron microscopy (TEM) was used to visualize the fibrils formed from βB2-crystallin proteins. Pretreatment of carbon coated TEM grids was performed by glow discharge method. 5 μl of each sample was immediately deposited onto negatively glow discharged TEM grids. Sample preparation for electron microscopy was continued by blotting the excess water from sample with filter paper and negatively staining with 2% (w/v) uranyl acetate. Then samples were washed several times with water and air dried. Micrographs were taken on JEOL 2200FS TEM with accelerating voltage at

200 KV. TEM images were taken in two bright field and annual dark field modes. Gatan microscopy suite software was used to analyse the micrographs.

3.2.5 X-ray fiber diffraction (XRFD) analysis of fibrillar aggregates

Samples of βB2-crystallin incubated at 60 °C for 24 hr were used for XRFD analysis. Sample preparation for XRFD analysis was performed by deposition of 5 μl of protein sample on glass slide. The samples were dried and collected as a small clump. The dried clump samples were then placed in the air to avoid the unnecessary peaks from substrate. A Bruker model D8/Discover X-ray diffractometer with Cu K alpha radiation (40 kV, 40 mA) was employed to determine the X-ray diffraction patterns of βB2-crystallin fibrils. 2θ ranges of each sample was from 0 to 26.5 degree with a step size of 0.01 degree. To reduce the beam intensity at the low angle (< 2 degree), the beam stopper was used. The collected data was carefully analyzed using EVATM software. Smoothing and baseline correction of XRFD results was performed using OriginPro 8.6 (OriginLab®) software. The data was analyzed using circles at the indicated distances.

3.2.6 Phage panning

A random phage display library representing circular 7-mer peptides on M13 phages (New England Biolabs, Ph.D.™-C7C library) was used for screening against target molecules. Library screening and phage amplification protocols were adapted from Ph.D.™-C7C Phage display Peptide Library (New England Biolabs). To immobilize the fibrillar target molecules on the solid support, 200 μl aliquot of βB2-crystallin fibrils was added at a concentration of 100 μg/ml in 0.1 M $NaHCO_3$, pH 8.6 to the wells of a 96-well polystyrene microplate, and incubated overnight at 4 °C with gentle rocking. The next day the coating

solution was removed from the wells, and solution of 5 mg/ml BSA in 0.1 M $NaHCO_3$ pH 8.6 was subsequently added for 1 hr at 4 °C to block the uncoated surfaces, and wells washed 6 times with TBST buffer (50 mM Tris-HCl, pH 7.5, 150 mM NaCl containing 0.1% v/v Tween-20). Screening of phage display library against fibrillar aggregates was carried out by adding a 100 μl aliquot of phage library containing 1×10^{11} plaque-forming units (pfu) of phage (pfu/ml) in TBST buffer to each well. After 2 hr incubation at RT with gentle shacking the nonbinding phages were removed from the wells and the wells were subsequently washed 10 times with TBST buffer. Then, phages bound to the βB2-crystallin fibrils were eluted with 100 μl 0.2 M glycine-HCl (pH 2.2) containing 1 mg/ml bovine serum albumin (BSA). After 15 min the solution of recovered phages was neutralized with 15 μl 1 M Tris-HCl buffer, pH 9.1. Prior to phage amplification, a portion of eluted solution was used for plaque assay titration to quantify the phage in recovered material. Amplification of eluted phages was performed by infection of *E. coli* ER2738 cells (New England Biolabs). Amplified phages were subsequently precipitated by 20% (w/v) polyethylene glycol–8000, 2.5 M NaCl and resuspended in TBS buffer (50 mM Tris-HCl (pH 7.5), 150 mM NaCl). Washing buffers containing 0.2% and 0.3% Tween-20 were used in second and third round of biopanning respectively (Fig. 3.2).

3.2.7 DNA sequencing of selected phage clones

After each round of panning, bacterial clones infected by phages were grown up to early logarithmic phase in LB medium at 37 °C. Bacterial cells were harvested at 5000 rpm for 15 min at RT. DNA of selected phage clones was purified with QIAprep® Spin M13 kit (Qiagen). The extracted DNA and primers (provided by phage display peptide library kit) were mixed in a tube to a final volume of 10 ul and characterized using Sanger DNA sequencing

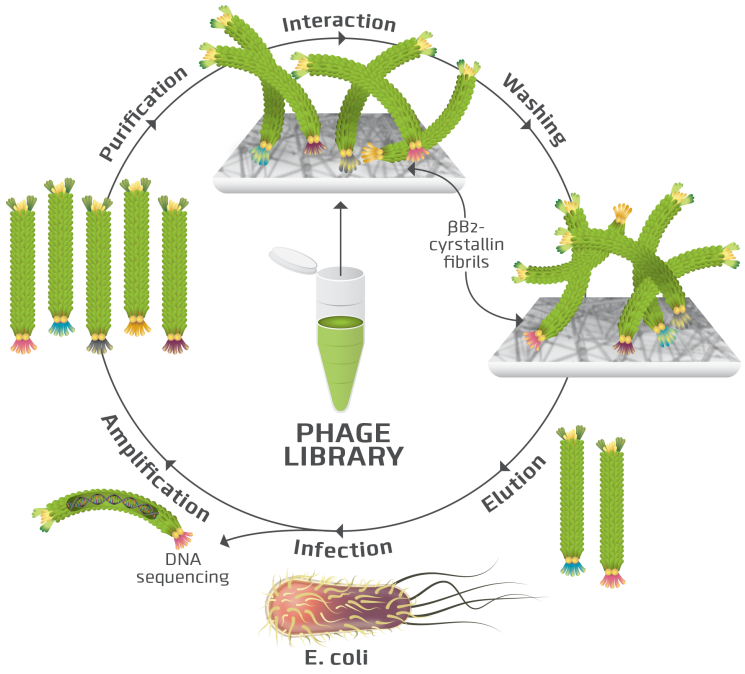

Figure 3.2: Phage display process. Schematic representation of phage library screening against fibrillar aggregates of βB2-crystallin protein. After immobilization of βB2-crystallin fibrils on the plastic support, random library of phaged-isplayed peptides was screened against fibrillar aggregates. Nonbinding phages were subsequently removed through washing and highly attached phages were eluted and amplified for further analysis.

method.

3.2.8 ELISA for phage binding assay

37 phages were selected through three rounds of phage screening against fibrillar aggregates. Enzyme-linked immunosorbent assay (ELISA) was carried out to identify phages having highest affinity for βB2-crystallin fibrils. Direct coating of target molecules on 96-well polystyrene microplate was performed by adding 100 μl of βB2-crystallin fibrils at concentration of 50 μg/ml in 0.1 M $NaHCO_3$, pH 8.6 to each well and incubation overnight at 4 °C. After removing the excess protein solution, each well was filled with a 10 μl aliquot of amplified phages (1×10^{11} pfu/10 μl) in 190 μl phosphate-buffered saline (PBS) containing 2% BSA. The plate was then incubated at RT by gentle shaking for 2 hr. The wells were then washed 6 times with 0.1% PBST buffer

(PBS buffer containing 0.1% Tween-20). Next, 200 μl of diluted (1:5000) solution of HRP/anti-M13 monoclonal conjugate (GE Healthcare) in PBS buffer containing 2% BSA was added to the wells having immobilized fibrillar target molecules as well as control wells without any target molecules. After 30 min incubation at RT with gentle shacking, the excess antibody solution was removed and wells were washed with PBST 0.05% buffer (PBS buffer containing 0.05% Tween-20) for 6 times. A 100 μl aliquot of freshly prepared 3,3',5,5'-tetramethylbenzidine (TMB) chromogen solution (Pierce^{TM} TMB Substrate Kit) was added to each well and incubated at RT for 3 min with gentle shacking, followed by stopping the reaction with 100 μl 2M sulfuric acid. The absorbance of each well was measured at 450 nm using FlexStation® 3 multimode plate reader. In all ELISA assays proper controls were applied to compare the binding of peptides displayed on the surface of the phages onto the polystyrene surface with and without immobilized target molecules. One-way ANOVA test was used to analyse the level of significance ($p < 0.05$) between results.

3.2.9 Competitive inhibition assay

Competitive and inhibitory ELISA assay was carried out to investigate the binding specificity of identified peptide (CKQFKDTTC) with the highest absorbance observed in regular ELISA assay. A 7-mer non-binding cyclic peptide (CTNANHYFC) was used as a control. Direct coating of target molecules (βB2-crystallin fibrils) was followed as described in phage ELISA binding assay. BSA blocking buffer was subsequently used to block nonspecific binding. 100 μl of synthetic cyclic peptides at different concentrations (0, 0.008, 0.04, 0.2, and 1 mg/ml) was added to immobilized fibrillar target molecule wells and incubated at RT for 2 hr. A 100 μl aliquot of counterpart phage (1×10^{10} pfu/ml) was added subsequently to each well and incubated for 30 min

at RT. After washing the wells 6 times with 0.1% PBST buffer, 200 μl of diluted HRP/anti-M13 monoclonal conjugate was added to them and color development procedure was followed as described in ELISA section.

3.3 Results and discussion

3.3.1 Fibril formation: ThT assay

Recombinantly expressed human βB2-crystallin was incubated in 10% (v/v) TFE solution (pH 2.0), at RT or 60 °C, which is thought to partially unfold the protein and allow fibrillation to occur [18]. It is suggested that ThT fluoresces upon interaction with amyloid-like aggregates through incorporation into β-sheet motifs, and is the gold-standard assay for quantifying the presence of fibrils [32]. A control solution of βB2 protein was incubated with ThT to prove that the β-sheet rich native form of βB2-crystallin does not affect the ThT fluorescent intensity. Moreover, the increased fluorescent emission of ThT upon incorporation into the β-sheet structures within fibrils allowed for the formation of βB2-crystallin fibrils to be evaluated (Fig. 3.3). Similar to previous reports using bovine crystallins [18], results summarized in (Fig. 3.3) showed that both temperature and incubation time in TFE solutions affected fibril formation for systems of identical protein concentration. The increase in temperature from RT to 60 °C, for all time points, led to statistically significant ($p < 0.05$) increases in fibril formation. However, there was no significant difference in fibril content for all RT time points. There was also no significant difference in fibril content between 4 and 10 hr time points at 60 °C, but there was between 10 and 24 hr incubation at this temperature.

3.3.2 Fibril formation: Electron microscopy studies

Aliquots, collected from different fibrillation experiments, were further analyzed for fibril formation using transmission electron microscopy (TEM). It

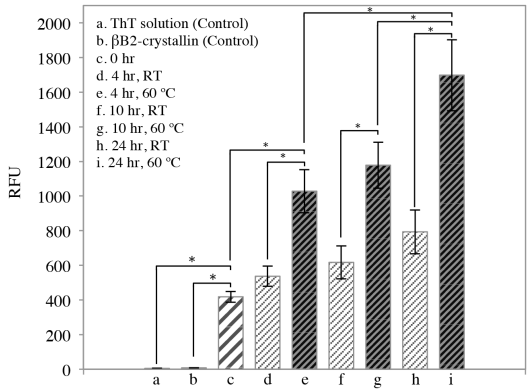

Figure 3.3: ThT assay results. ThT assay of fibrillar aggregates formed from recombinantly expressed human βB2-crystallin protein in 10% (v/v) TFE, pH 2.0 at RT and 60 °C. Fluorescence intensity of ThT assay for native (control) and βB2-crystallin incubated under various fibril forming solution conditions was performed by excitation of ThT molecule at 440 nm. Fluorescence emission was scanned from 450-600 nm and maximum peak intensity reported. (* represents $p < 0.05$, data represent mean 1 $\pm$ SD, $n \geq 3$).

was observed that upon incubation in the TFE solution, βB2-crystallins aggregated into fibrillar structures (Fig. 3.4). The most obvious fibrillar aggregates were observed in samples incubated at 60 °C for 10 hr (Fig. 3.4C). TEM micrographs of 10 hr incubation in two different temperatures revealed that increasing the temperature had a noticeable influence on fibril formation. Fibrils formed at RT were shorter than those formed at 60 °C and mostly were bound to each other and made huge aggregates (Fig. 3.4B). This difference in TEM micrographs of βB2-crystallin fibrils formed at RT or 60 °C may explain the significant difference observed for the ThT assay results for these conditions (Fig. 3.3). It may be that increasing the TFE solution temperature increases the chance for exposed β-sheet secondary structures to interact with each other leading to formation of longer fibrils at 60 °C compared to RT in the same time intervals. Micrographs of samples incubated for 24 hr at 60 °C (Appendix 1, Fig. A1) showed that, after longer incubation times, individual fibrils bound to each other and formed larger aggregates. Thus, βB2-crystallin fibrils formed at 60 °C, 10 hr were selected for affinity screening studies.

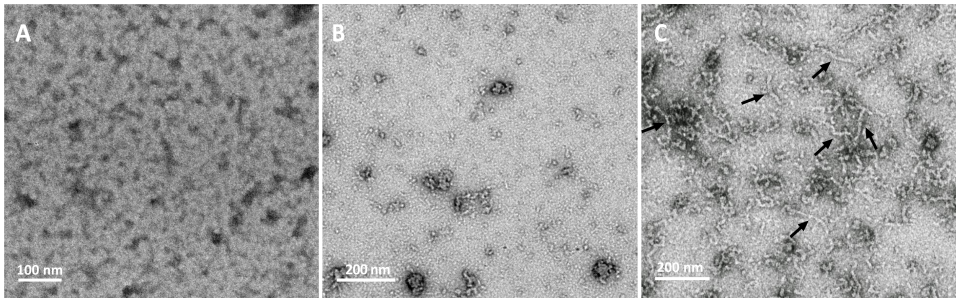

Figure 3.4: Electron microscopy images. Representative TEM images of recombinantly expressed βB2-crystallin protein before TFE incubation (A), 10 hr incubation in 10% (v/v) TFE, pH 2.0 at RT (B), and 10 hr incubation in 10% (v/v) TFE, pH 2.0 at 60 °C (C).

3.3.3 X-ray fiber diffraction (XRFD) analysis of βB2-crystallin fibrils

It has been demonstrated that the overwhelming majority of fibrillar structures formed from different proteins share a common cross-β structure [33]. This structural unit has been also reported for bovine crystallin-based fibrils [18]. Previously reported XRFD patterns for amyloid fibrils have shown meridional reflections at 4.7 to 4.8 $\mathring{A}$ and equatorial reflections at $\sim$10 $\mathring{A}$ [34, 35]. Our XRFD analysis indicated that human recombinant βB2-crystallin fibrillar aggregates had a structural pattern similar to common XRFD patterns of amyloid fibrils (Fig. A2). In cross-β sheet pattern of βB2-crystallin fibrils formed at 60 °C, β-sheet secondary structures with stacking distance of $\sim$4.664 $\mathring{A}$ and an intersheet distance of $\sim$9.967 $\mathring{A}$ have organized into amyloid-like fibrillar aggregates (Fig. 3.5A). XRFD analysis also indicated an interstrand distance of $\sim$4.654 $\mathring{A}$ and intersheet distance of $\sim$11.75-9.531 $\mathring{A}$ for βB2-crystallin fibrils formed at RT (Fig. 3.5B). Meridional and equatorial reflection patterns are similar between βB2-crystallin fibrils and other amyloid-like structures such as lysozyme fibrils [36]. This may indicate that intermolecular interactions between exposed β-sheets of partially unfolded βB2-crystallin proteins have led to the vertical alignment of the proteins to the fibril's axis. This also confirms the results of electron microscopy and ThT assay studies, as XRFD

analysis of βB2-crystallin fibrils formed at RT and 60 °C showed that samples collected from 60 °C incubation had more, well-defined amyloid-like structures (Fig. 3.5).

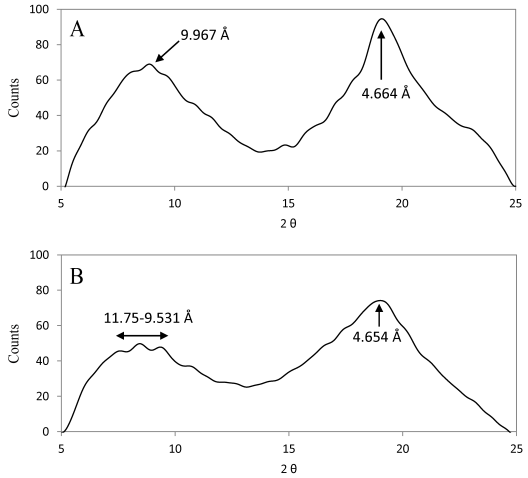

Figure 3.5: X-ray diffraction pattern analysis of βB2-crystallin fibrils. Representative X-ray diffraction pattern of βB2-crystallin fibrils. βB2-crystallin protein (10 mg/ml) was incubated for 24 hr in 10% (v/v) TFE, pH 2.0 at (A) 60 °C and (B) RT. Formed fibrillar aggregates were subsequently analyzed to determine X-ray diffraction patterns. The collected data was analyzed using EVATM software. Peaks represent stacking distance ($\sim$4.664 $\mathring{A}$ for fibrils formed at 60 °C and $\sim$4.654 $\mathring{A}$ for fibrils formed at RT) and intersheet distance ($\sim$9.967 $\mathring{A}$ for fibrils formed at 60 °C and $\sim$11.75-9.531 $\mathring{A}$ for fibrils formed at RT) of β-sheet secondary structures in cross-β sheet pattern of βB2-crystallin fibrils.

3.3.4 Identification of high binding peptides

Phage display screening was performed to identify cyclic peptides having high affinity to fibrillar aggregates of βB2-crystallin. Three rounds of phage display yielded 48 colonies (16 colonies from each round) and 37 sequences were identified. It was expected that by using a BSA blocking buffer, as well as increasing the surfactant concentration in the washing buffer, the nonspecific interaction of phage with the container surface or target fibrils would be minimized. This was verified as no peptides identified were similar to those previously obtained that bind BSA [37] or polystyrene [38]. Besides, all peptides were scanned within SAROTUP in order to eliminate any target un-related sequences. None of the selected sequences for βB2-crystallin were found in MimoDB, represent-

ing the previously identified peptide binders. SAROTUP is an online tool to scan and exclude peptides that might be identified because of interaction of phage library with possible contaminations or target-unrelated components of biopanning system [39]. MimoDB is a database of identified peptides through phage display approach that can also be used to exclude possible non-specific and target-unrelated peptides [40].

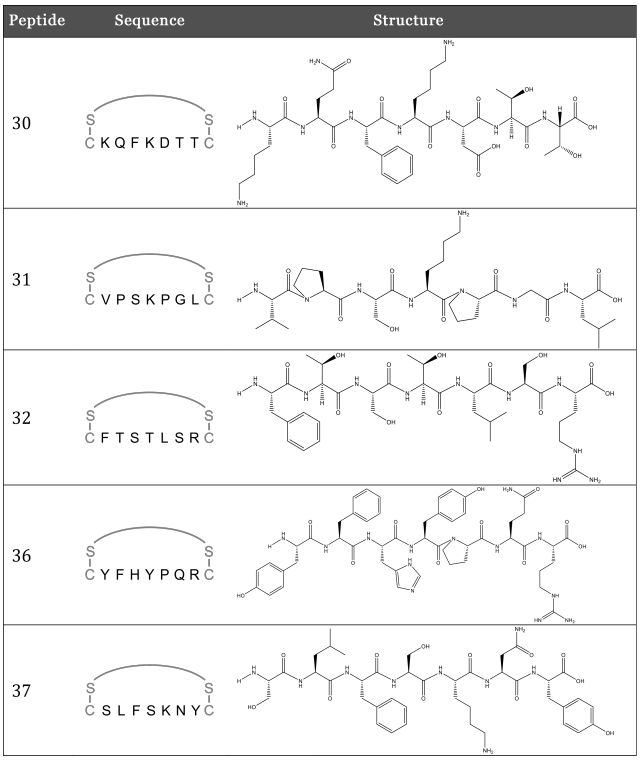

Table 3.1: Identified peptides having highest affinity to βB2-crystallin fibrils.

3.3.5 Identification of high binding peptides: ELISA assay

Although amyloid like fibrillar aggregates of different proteins share a common core structural pattern, their surface properties should depend on both the amino acid sequence of each protein within the aggregate as well as the overall fibril morphology. And, as reported, due to complex distribution of hydrophobic and charge regions on their surface, amyloid-like structures can

interact with different species having different physicochemical properties [41]. Thus, predicting high-affinity peptide binders to βB2-crystallin fibrils is too complicated to develop without a priori knowledge of the fibril morphology. Phage display techniques, however, allow for the identification of high-affinity binding peptides to complex targets where binding affinity is expected to increase from one round to the next, without a prior knowledge of the target itself. An ELISA affinity assay was carried out and binding affinity of phage-displayed peptides to βB2-crystallin fibrils increased with subsequent rounds (Fig. 3.6). The final peptides showed a significantly higher affinity than those from previous rounds of phage display. To show this we included them in (Fig. 3.6) with all the phage display results, however comparing them to each other may be difficult as the absorbances likely were within the non-linear response of the technique. So to clarify this, a second analysis of these peptides only was conducted, where the interaction time of TMB substrate and HRP enzyme was decreased from 3 to 1 min (Fig. 3.7). Peptides having the highest affinity to βB2-crystallin fibrils are listed in Table 3.1, and their sequences were analyzed using online peptide property calculator software (www.genscript.com). All five peptides were basic peptides having positive net charge in physiological pH. Although, normally, one expects successive rounds of phage display to lead to a consensus sequence of a unique peptide binder (or binders of similar structure), this was not observed to be the case for these fibril targets. This is likely due to the fact that these fibrils form highly variable surface structures with varied charge, hydrophilic and hydrophobic exposed domains. Thus, these fibrils likely form a surface rich in multiple binding domains, unlike targeting single proteins that may provide limited binding sites for the phage peptides to interact with. This is likely why a relatively diverse set of amino acid sequences can have such a high affinity with the fibril surface and likely why, despite having different specific sequences, these peptides have a

similar chemical make-up (i.e. basic, positive net charge, with some aromatic structures).

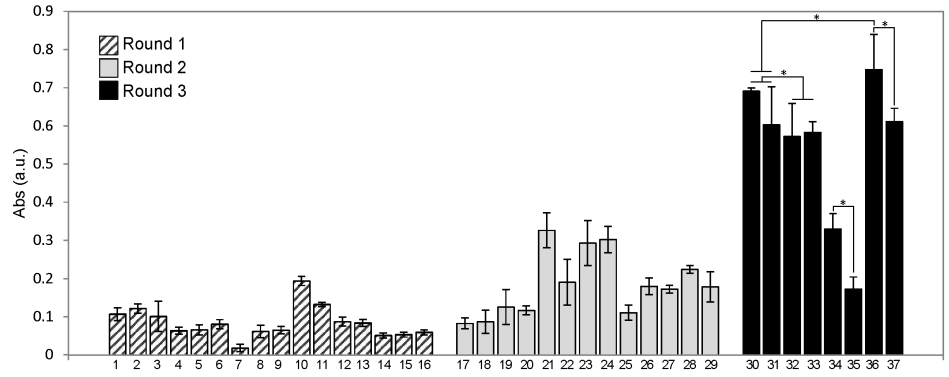

Figure 3.6: ELISA assay results. ELISA result of phage binding to βB2-crystallin fibrils after three rounds of phage display (* represents $p < 0.05$, data represent mean $\pm$ 1 SD, $n \geq 3$). Note: Most round 3 results yielded raw absorbance (a.u.) ≥ 1; these results are post background subtraction, best 5 were taken and repeated.

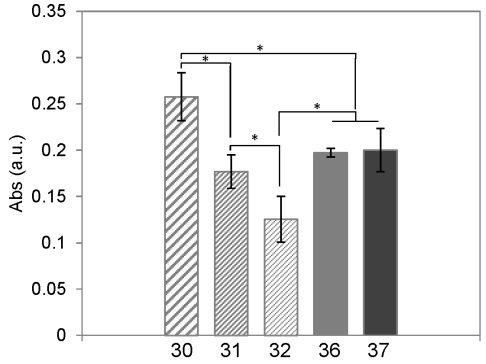

Figure 3.7: ELISA assay results. ELISA result of identified phage-displayed peptides from round 3 having highest affinity to βB2-crystallin fibrils (* represents $p < 0.05$, data represent mean $\pm$ 1 SD, $n \geq 3$).

3.3.6 Competitive Inhibition Assay

Phage-ELISA binding assay was previously performed to investigate binding affinity of phage-displayed peptide to the fibrillar aggregates of βB2-crystallin. However, the question remains whether the identified peptide itself could maintain its specific binding ability. To this purpose, a phage vs. peptide competitive inhibition assay was carried out to determine whether the cyclic free

peptide (CKQFKDTTC) and corresponding phage-displayed peptide could compete for the same binding site on the βB2-crystallin fibrils. The results showed that preincubation of fibrillar target molecules with identified peptide, inhibited binding of phage in a concentration-dependent manner (Fig. 3.8). The control cyclic peptide (CTNANHYFC) did not show any inhibitory effect on phage-displayed peptide binding.

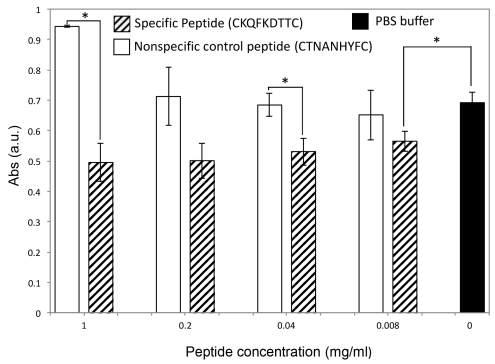

Figure 3.8: Competitive Inhibition Assay. Competitive inhibition ELISA assay result of free cyclic peptide (CKQFKDTTC) with highest affinity to βB2-crystallin fibrils (* represents $p < 0.05$, data represent mean $\pm$ 1 SD, $n \geq 3$).

3.4 Conclusions

Small peptide molecules having specific interaction with fibrillar aggregates of proteins can serve as anti-aggregation drugs or diagnostic agents in amyloidogenic diseases. Given the evidence implicating fibrillation of lens crystallin proteins in cataract development, we sought to identify peptides specifically targeting the fibrillar state of βB2-crystallin, the major β-crystallin in the lens. This work primarily focused on fibrillation of recombinantly expressed human lens βB2-crystallin in 10% (v/v) (TFE) solution, pH 2.0, at RT and 60 °C. Fibril formation of βB2-crystallin was verified by ThT assay and electron microscopy studies. Statistical analysis of ThT assay results showed that elevated temperature and incubation time increased chance of fibrillation of

recombinantly expressed human βB2-crystallin as observed in case of bovine crystallins [18].

XRFD analysis showed that βB2-crystallin fibrils formed amyloid-like structure having a core pattern of cross-β sheet, a common structural feature of amyloid fibrils [33]. We observed that interstrand and intersheet distances of β-sheets in amyloid-like structure of βB2-crystallin fibrils follow the common structural pattern observed in other fibrillar aggregates.

Specific binding of identified phage-displayed peptides was documented using ELISA assay. Basic peptides identified after third round of phage panning showed significantly high absorbance in ELISA assay; representing a high affinity of displayed peptide on the surface of phage to βB2-crystallin fibrils. Specific binding of identified peptide (with highest absorbance in ELISA) to fibrillar aggregates of βB2-crystallin was demonstrated using competitive binding inhibition ELISA assay, through which competitive binding between phage clone and corresponding encoded peptide was analysed. It is thought that the identification of these peptides will advance the treatment of cataract in patients through non-invasive techniques.

3.5 Acknowledgements

The authors acknowledge Jae-Young Cho for his assistance with the XRFD analysis, and Julie Qian for her assistance with the transmission electron microscopy. This work was supported by Ingenuity lab, province of Alberta, University of Alberta (department of chemical and materials engineering), Alberta innovates technology futures, Natural Sciences and Engineering Research Council of Canada (NSERC).

3.6 References

[1] O. Okoye, B. I. Eze, and C. M. Chuka-Okosa, "Eliminating the barriers to uptake of cataract surgery in a resource-poor setting: A focus on direct surgical cost," *Niger. J. Clin. Pract.*, vol. 18, no. 3, pp. 333–336, 2015.

[2] M. S. Kosinski-Collins and J. King, "*In vitro* unfolding, refolding, and polymerization of human gamma D crystallin, a protein involved in cataract formation.," *Protein Sci.*, vol. 12, no. 3, pp. 480–90, 2003.

[3] A. Surguchev and A. Surguchov, "Conformational diseases: looking into the eyes," *Brain Res. Bull.*, vol. 81, no. 1, pp. 12–24, 2010.

[4] H. Ecroyd and J. A. Carver, "Crystallin proteins and amyloid fibrils," *Cell. Mol. Life Sci.*, vol. 66, no. 1, pp. 62–81, 2009.

[5] K. L. Moreau and J. A. King, "Protein misfolding and aggregation in cataract disease and prospects for prevention," *Trends Mol. Med.*, vol. 18, no. 5, pp. 273–282, 2012.

[6] J. Liao et al., "Meta-analysis of genome-wide association studies in multi-ethnic Asians identifies two loci for age-related nuclear cataract," *Hum. Mol. Genet.*, vol. 23, no. 22, pp. 6119–6128, 2014.

[7] T. Härd and C. Lendel, "Inhibition of amyloid formation," *J. Mol. Biol.*, vol. 421, no. 4–5, pp. 441–465, 2012.

[8] Y. S. Eisele et al., "Targeting protein aggregation for the treatment of degenerative diseases," *Nat. Rev. Drug Discov.*, vol. 14, no. 11, p. 759, 2015.

[9] K. L. Sciarretta, D. J. Gordon, and S. C. Meredith, "Peptide-based inhibitors of amyloid assembly," *Methods Enzymol.*, vol. 413, pp. 273–312, 2006.

[10] M. Hamzeh-Mivehroud, A. A. Alizadeh, M. B. Morris, W. B. Church,

and S. Dastmalchi, "Phage display as a technology delivering on the promise of peptide drug discovery," *Drug Discov. Today*, vol. 18, no. 23–24, pp. 1144–1157, 2013.

[11] B. P. Orner, L. Liu, R. M. Murphy, and L. L. Kiessling, "Phage display affords peptides that modulate beta-amyloid aggregation," *J. Am. Chem. Soc.*, vol. 128, no. 36, pp. 11882–11889, 2006.

[12] W. D. Marcus, H. Wang, S. M. Lindsay, and M. R. Sierks, "Characterization of an antibody scFv that recognizes fibrillar insulin and beta-amyloid using atomic force microscopy.," *Nanomedicine*, vol. 4, no. 1, pp. 1–7, Mar. 2008.

[13] C. K. Kang, V. Jayasinha, and P. T. Martin, "Identification of peptides that specifically bind Abeta1-40 amyloid *in vitro* and amyloid plaques in Alzheimer's disease brain using phage display.," *Neurobiol. Dis.*, vol. 14, no. 1, pp. 146–156, Oct. 2003.

[14] K. Srivastava, J. M. Chaves, O. P. Srivastava, and M. Kirk, "Multicrystallin complexes exist in the water-soluble high molecular weight protein fractions of aging normal and cataractous human lenses," *Exp. Eye Res.*, vol. 87, no. 4, pp. 356–366, 2008.

[15] W. W. de Jong, N. H. Lubsen, and H. J. Kraft, "Molecular evolution of the eye lens," *Prog. Retin. Eye Res.*, vol. 13, no. 2, pp. 391–442, 1994.

[16] C. M. Dobson, "Protein-misfolding diseases: Getting out of shape," *Nature*, vol. 418, no. 6899, p. 729, 2002.

[17] H. Ecroyd, M. Garvey, D. C. Thorn, J. A. Gerrard, and J. A. Carver, "Amyloid fibrils from readily available sources: milk casein and lens crystallin proteins," in *Protein Nanotechnology*, Springer, 2013, pp. 103–117.

[18] S. Meehan, Y. Berry, B. Luisi, C. M. Dobson, J. A. Carver, and C. E.

MacPhee, "Amyloid fibril formation by lens crystallin proteins and its implications for cataract formation," *J. Biol. Chem.*, vol. 279, no. 5, pp. 3413–3419, 2004.

[19] Y. Wang et al., "Formation of amyloid fibrils *in vitro* from partially unfolded intermediates of human γC-crystallin," *Invest. Ophthalmol. Vis. Sci.*, vol. 51, no. 2, pp. 672–678, 2010.

[20] K. Papanikolopoulou et al., "Formation of amyloid fibrils *in vitro* by human γD-crystallin and its isolated domains," *Mol. Vis.*, vol. 14, p. 81, 2008.

[21] T. O. Zhang, A. M. Alperstein, and M. T. Zanni, "Amyloid β-Sheet Secondary Structure Identified in UV-Induced Cataracts of Porcine Lenses using 2D IR Spectroscopy," *J. Mol. Biol.*, vol. 429, no. 11, pp. 1705–1721, 2017.

[22] K. J. Lampi, P. A. Wilmarth, M. R. Murray, and L. L. David, "Lens β-crystallins: the role of deamidation and related modifications in aging and cataract," *Prog. Biophys. Mol. Biol.*, vol. 115, no. 1, pp. 21–31, 2014.

[23] B. G. Mohr, C. M. Dobson, S. C. Garman, and M. Muthukumar, "Electrostatic origin of *in vitro* aggregation of human γ-crystallin," *J. Chem. Phys.*, vol. 139, no. 12, p. 09B614¬1, 2013.

[24] J. I. Clark, "Self-assembly of protein aggregates in ageing disorders: the lens and cataract model," *Philos. Trans. R. Soc. B Biol. Sci.*, vol. 368, no. 1617, p. 20120104, 2013.

[25] K. J. Lampi, K. K. Amyx, P. Ahmann, and E. A. Steel, "Deamidation in human lens betaB2-crystallin destabilizes the dimer.," *Biochemistry*, vol. 45, no. 10, pp. 3146–3153, Mar. 2006.

[26] J. F. Hejtmancik, P. T. Wingfield, and Y. V Sergeev, "β¬Crystallin association," *Exp. Eye Res.*, vol. 79, no. 3, pp. 377¬383, 2004.

[27] M. A. Smith, O. A. Bateman, R. Jaenicke, and C. Slingsby, "Mutation

of interfaces in domain-swapped human betaB2-crystallin.," *Protein Sci.*, vol. 16, no. 4, pp. 615–625, Apr. 2007.

[28] M. Michiel et al., "Aggregation of deamidated human betaB2-crystallin and incomplete rescue by alpha-crystallin chaperone.," *Exp. Eye Res.*, vol. 90, no. 6, pp. 688–698, Jun. 2010.

[29] P. Marinelli, V. Castillo, and S. Ventura, "Trifluoroethanol modulates amyloid formation by the all α-helical URN1 FF domain," *Int. J. Mol. Sci.*, vol. 14, no. 9, pp. 17830–17844, 2013.

[30] S. Srisailam et al., "Amyloid-like Fibril Formation in an All β-Barrel Protein partially structured intermediate state (s) is a precursor for fibril formation," *J. Biol. Chem.*, vol. 278, no. 20, pp. 17701–17709, 2003.

[31] S. Cetinel, L. Unsworth, and C. Montemagno, "Peptide-based treatment strategies for cataract," *J. Glaucoma*, vol. 23, pp. S73–S76, 2014.

[32] A. Hawe, M. Sutter, and W. Jiskoot, "Extrinsic fluorescent dyes as tools for protein characterization," *Pharm. Res.*, vol. 25, no. 7, pp. 1487–1499, 2008.

[33] T. P. J. Knowles, M. Vendruscolo, and C. M. Dobson, "The amyloid state and its association with protein misfolding diseases," *Nat. Rev. Mol. cell Biol.*, vol. 15, no. 6, p. 384, 2014.

[34] M. Sunde, L. C. Serpell, M. Bartlam, P. E. Fraser, M. B. Pepys, and C. C. F. Blake, "Common core structure of amyloid fibrils by synchrotron X-ray diffraction," *J. Mol. Biol.*, vol. 273, no. 3, pp. 729–739, 1997.

[35] E. D. Eanes and G. G. Glenner, "X-ray diffraction studies on amyloid filaments," *J. Histochem. Cytochem.*, vol. 16, no. 11, pp. 673–677, 1968.

[36] B. A. Vernaglia, J. I. A. Huang, and E. D. Clark, "Guanidine hydrochloride can induce amyloid fibril formation from hen egg-white lysozyme," *Biomacro-*

molecules, vol. 5, no. 4, pp. 1362–1370, 2004.

[37] M. Vodnik, U. Zager, B. Strukelj, and M. Lunder, "Phage display: selecting straws instead of a needle from a haystack," *Molecules*, vol. 16, no. 1, pp. 790–817, 2011.

[38] M. Vodnik, B. Štrukelj, and M. Lunder, "HWGMWSY, an unanticipated polystyrene binding peptide from random phage display libraries," *Anal. Biochem.*, vol. 424, no. 2, pp. 83–86, 2012.

[39] J. Huang, B. Ru, S. Li, H. Lin, and F.-B. Guo, "SAROTUP: scanner and reporter of target-unrelated peptides," *Biomed Res. Int.*, vol. 2010, 2010.

[40] J. Huang et al., "MimoDB 2.0: a mimotope database and beyond," *Nucleic Acids Res.*, vol. 40, no. D1, pp. D271–D277, 2011.

[41] B. Moores et al., "Effect of surfaces on amyloid fibril formation," *PLoS One*, vol. 6, no. 10, p. e25954, 2011.

Chapter 4

Structural polymorphisms in fibrillar aggregates associated with exfoliation syndrome

Abstract

Exfoliation syndrome is largely considered an age-related disease that presents with fibrillar aggregates in the anterior segment of the eye. A growing body of literature has investigated structural diversity of amyloids and fibrillar aggregates associated with neurodegenerative disease. However, in case of exfoliation syndrome, there is a dearth of information on the biophysical characteristics of these fibrils and structural polymorphisms. Herein, structural diversity of fibrils isolated from the anterior lens capsule of patients was evaluated using transmission electron microscopy techniques. It was apparent that, despite having a low sample number of different patients, there exists a wide range of fibril morphologies. As it is not precisely understood how these fibrils form, or what they are composed of, it is difficult to postulate a mechanism responsible for these differences in fibril structure. However, it is apparent that there is a wider range of fibril structure than initially appreciated. Moreover, these data may suggest the variance in fibril structure arises from patient-specific fibril composition and/or formation mechanisms.

Key words: Exfoliation syndrome, glaucoma, fibrillar aggregates, structural polymorphism.

4.1 Introduction

Exfoliation syndrome (XFS) presents with fibrillar aggregates in many tissues throughout the body and within the eye it is largely, but not solely, located in the anterior segment [1, 2]. Exfoliation materials mostly contain elastic fiber components and are thought to be formed through overproduction of elastic microfibrils and their assembly into fibrillar aggregates [3]. These aggregates can lead to cataract formation and impede aqueous humor drainage, leading to increased intraocular pressure (IOP) that causes exfoliation glaucoma. Briefly, movement of the iris sphincter region over the anterior surface of the lens capsule during physiologic pupillary motion may liberate XFS materials from the capsule which then deposits in the trabecular meshwork. In addition, the exfoliation particles can act as sandpaper during iridozonular friction, leading to rupture of a weak iris pigment epithelium, pigment loss from the iris, and subsequent distribution of pigment particles within the anterior chamber [4, 5]. Early electron microscopy studies yielded the presence of cross-banded fibrillar structures and filamentous subunits in a ground of amorphous aggregates of ocular tissues from XFS patients [6, 7]. Upon further examination, using thioflavin dyes, XFS materials in human eye tissue sections showed an intense yellow fluorescence commonly associated with amyloid plaques [7–9]. Similarly, congo red staining of these tissues provided results also usually associated with amyloid structures. Although congo red dichroism of XFS materials has been observed for this system [8], it has not always generated consistent results [2, 10] and has generally been observed to be variable through many studies of other systems [11, 12]. Despite immunofluorescence studies showing selective binding of an anti-amyloid antiserum to XFS materials [7], and some studies suggesting structural similarities between amyloid fibrils and XFS materials [13, 14], the similarity between amyloid and XFS aggregates is debated [4].

Correlating the precise similarities between the structure of XFS and amyloid fibrils is outside the scope of this study; as high-resolution studies of XFS fibril core structure would be required to properly address this question. That said, structural polymorphisms are a key characteristic of amyloid fibrils, where variations in the structure of fibrillar aggregates might be correlated with variations in disease phenotype or biological mechanisms underlying disease development [15, 16]. So important is this characterization that patient-specific structural variations in amyloid fibrils have been thought to be key to developing structure-specific diagnostic agents [15, 16]. Thus, amyloid polymorphisms and structural variations of fibrillar aggregates associated with neurodegenerative diseases have been extensively characterized [15, 16]. However, early microscopy studies of XFS materials primarily focused on finding fibrils in different ocular structures, as opposed to precisely defining their biophysical characteristics [17].

For other fibril forming diseases it is acknowledged that structural polymorphisms play an important role in their pathomechanism [18, 19]; however, this topic seems largely unstudied for XFS. Mature XFS fibrils are electron-dense structures that may show a periodic cross-banding pattern. The formation mechanism for fibrils are largely undefined, however, it could be that they are formed through lateral binding of microfibrillar subunits [20]. Despite the fact that conformational diversity of fibrillar aggregates might lead to different physiological consequences [21], there are limited studies done to determine the potential diversity of XFS fibrils between patients. Previous transmission electron microscopy (TEM) analysis of XFS fibrils on human lens capsules have suggested that XFS materials are generally composed of two main types of fibrillar structures: (i) fibril diameter of $\sim$20 nm and length of $\sim$1 μm, with common banding patterns every $\sim$25 or 50 nm (25 nm being less frequent); (ii) fibril diameter of $\sim$40 nm and length from 0.3 – 0.5 μm, with a less fre-

quent banding pattern. It has been hypothesized that these fibrils form from protofilaments having a range of diameters from ∼5 to ∼9 nm with banding pattern of ∼11 nm [4]. However, patient to patient variability in the structural polymorphisms of these formed fibrils has not been reported.

In this study, we confirmed the presence of XFS fibrils on human lens capsules using different microscopy techniques. Isolated XFS deposits from the anterior lens capsules of various patients, at different stages of the disease (Table 4.1), were imaged using TEM techniques to evaluate the structural characteristics of these fibrils. A large variety in structural features of these fibrils were observed. Despite the small sample size of patients studied a large number of differences in fibril structure was observed. It seems obvious that further structural studies need to be conducted to fully characterize these fibrillar structures.

Sample name	Patient age	Patient sex	Amount of XFS materials
L	61	Male	Low
M1	72	Male	Moderate
M2	66	Male	Moderate
M3	83	Male	Moderate
H	67	Male	Heavy

Table 4.1: XFS samples used for TEM studies.

4.2 Materials and methods

4.2.1 Sample collection

All human tissue samples were collected according to protocols approved by the Research Ethics Boards of the University of Alberta, and University of Calgary. The exclusion criteria included eyes with previous severe trauma or infrared radiation exposure, history of diabetes mellitus, and patients with previously reported amyloidosis. Tissue samples were transferred and kept at 4 °C in BSS® intraocular irrigation solution (Alcon). Lens capsules used

for microscopy studies of XFS fibrils on the tissue were preserved in fixative buffer (2.5% glutaraldehyde, 4% paraformaldehyde in 0.1 M phosphate buffer, pH 7.4) prior to processing. Lens capsules used for removing XFS materials were washed with ultrapure water (Milli-Q) to remove excess salts prior to processing. Capsules were placed on the coverslip in 25 μl of 1 mM sodium azide and XFS materials were removed through a light abrasion of the surface with the side of a gel loading pipette tip (GELoader, epT.IPS, 20 μL, Eppendorf, Germany). For light microscopy observation, tissue sections were stained with Richardson's stain (0.1% methylene blue in 0.1% sodium borate, 0.1% azure II).

4.2.2 Scanning electron microscopy (SEM) of lens capsule having XFS materials

Upon washing with 0.1 M phosphate buffer, the lens capsule was dehydrated in a graded series of ethanol with 20% increase in concentration every 15 min followed by hexamethyldisilazane (HMDS) treatment, 25% increments every 30 min. Sample was allowed to air dry overnight, and subsequently sputter-coated with gold–palladium film. SEM images were obtained using a Philips FEI-XL30 scanning electron microscope (FEI Company, CA, USA).

4.2.3 Transmission electron microscopy (TEM) of XFS deposits on lens capsule

After washing with 0.1 M phosphate buffer, lens capsule was dehydrated through a graded ethanol series. Sample was then infiltrated with a mixture of ethanol and Spurr's resin overnight, followed by 100% Spurr's resin incubation. Thin sections were prepared using an ultramicrotome (Reichert-Jung Ultracut-E, Vienna, Austria) and stained with 4% uranyl acetate solution. Electron micrographs were captured using a Philips–FEI transmission electron microscope (Morgagni-268, Hillsboro, USA) operating at an acceleration

voltage of 80 kV.

4.2.4 TEM of isolated XFS materials

Negative stain electron microscopy was used to assess the different fibrillar deposits of patient-derived XFS samples. XFS materials were removed from the anterior lens capsule surface as described above in sample collection section. XFS patients were classified as having low, moderate, or heavy deposits. 6 μl of each sample was loaded onto a glow-discharged 400 mesh carbon-coated copper grid (Ted Pella Inc. Redding, CA). Typically, samples were adsorbed onto the grid surface for 2 minutes after which excess solution was removed by blotting with Whatman paper. Grids were then washed briefly and negatively stained using freshly filtered 2% uranyl acetate (UA) or 2% phosphotungstic acid (PTA) solutions. The negatively stained samples were analyzed with a FEI Tecnai G20 electron microscope (FEI Company). An acceleration voltage of 200 kV was used to record micrographs on an Eagle 4k $\times$ 4k CCD camera (FEI Company).

4.2.5 Two-dimensional (2D) class averages of the fibril segments

Electron micrographs showing well-defined, isolated fibrillar structures were used for image processing to enhance the signal-to-noise ratio of the fibril ultrastructure. Isolated fibril images were selected and segmented along the fibril axis into 50% overlapping boxes of 200 $\times$ 200 pixels (64 nm $\times$ 64 nm) using EMAN's boxer program [22]. Class averages were calculated using the EMAN's startnrclasses program [22].

4.3 Results and discussion

Patient specific samples were collected and XFS materials isolated from the anterior side of excised lens capsules were further characterized using stereomicroscopy, SEM and TEM techniques. It should be mentioned that the identification of XFS materials may not fully represent the population of materials present before surgery as the surgery itself may inadvertently remove some XFS materials from the capsule; this is despite the fact that standard surgical practices are employed from patient to patient and from surgeon to surgeon. In addition to this, the patient-to-patient variation in deposition patterns of XFS materials on lens capsules may result in differences in amount of XFS materials or even structural types of XFS materials present after surgery. Thus, despite being clinically diagnosed with XFS, only five out of nine tissue samples clearly had fibrils present.

In contrast to complex purification strategies used to process samples from amyloidotic organs, like the brain or liver, that may induce artifacts in their analysis [23] the method for capturing XFS materials is relatively straightforward. Similar to previously reported methods [24], we used a gel-loading pipette tip to remove XFS materials using a gentle mechanical force that removed aggregates without damaging underlying tissues. Thus, it is expected this approach will minimize contamination through capturing collagen fragments or addition of enzymes for degrading the lens capsule itself. Given the well-defined and significant differences in size and structure between XFS and collagen fibers [25], it was apparent that no collagen fibers were observed in our TEM studies of XFS materials [26, 27].

4.3.1 Identification of XFS materials on the lens capsule

XFS coated human lens capsules were analyzed using light and scanning electron microscopy (SEM, Fig. 4.1). Stereomicroscopy was used to confirm the presence of XFS deposits on the anterior side of all lens capsules prior to subsequent processing for electron microscopy characterization. A representative stereomicroscopy result is shown in (Fig. 4.1a) for XFS deposits from a 68-year-old male patient, with a moderate level of XFS, where the lens was stained with trypan blue ophthalmic solution used during cataract surgery. Because of the deep blue color, XFS deposits were not observed clearly in the central zone of the lens capsule, however, XFS deposits were clearly observed in the peripheral zone (Fig. 4.1a). Junctions between intermediate (i.e. devoid of XFS materials) and peripheral zones were also observed (white arrows, Fig. 4.1a). The observed connecting bridge pattern between the central zone and peripheral zone is common for clinically identified XFS [2]. The intermediate clear zone, where the lens capsule is normal and mainly devoid of XFS deposits [28], was also clearly observed in stereomicrographs, and further high-resolution SEM confirmed this area was completely devoid of XFS fibrils (Fig. 4.1b). This zone is believed to be created due to the rubbing of iris sphincter region over the anterior surface of the lens capsule during physiologic pupillary movement [4].

SEM studies of XFS materials were used to confirm the presence of a loosely packed irregular meshwork of XFS fibrils on the surface of the lens capsule, as previously reported (Figs. 4.1c-e) [28]. The lens capsule collected from a 76-year-old female patient, with moderate XFS, was used to evaluate the XFS materials on the lens using SEM (Figs. 4.1b-e). Different locations of the same lens capsule were characterized (Figs. 4.1b-e), the results of which are similar to previously reported structures on the lens capsule. The diameter of

the majority of XFS fibrils were found to be in the range of ∼15 to ∼40 nm (Fig. 4.1f). Thinner fibrils of ∼10 nm diameter were observed that could be protofilaments, which may aggregate laterally to form thicker mature fibrils that are up to ∼80 nm in diameter (Fig. 4.1e). SEM studies on XFS fibrils associated with human lens capsules have shown fibril diameter ranges of ∼50 - 80 nm and ∼35 - 40 nm with subunit filaments having a diameter of ∼10 nm [10, 28]. Spherical aggregates (white arrows, Fig. 4.1c) were observed as reported previously, where others have conjectured them to be cell fragments [10]. Because of the irregular and tangled arrangement of XFS fibrils, it is difficult to ascertain individual fibril length; we could barely identify fibrils exceeding 1 μ in length, however, different SEM studies have reported lengths ranging from ∼3 - 5 μm [10, 28].

Using some of the same lens capsule analyzed using SEM (Fig. 4.1), an expected bush-like, feathery excrescence of XFS materials was also observed using light microscopy (Fig. 4.2a) [2]. As already seen in the SEM micrographs, an irregular orientation of non-branching XFS fibrils was also observed in TEM micrographs (Figs. 4.2b and c). Diameter distribution analysis on TEM micrographs showed that XFS fibrils had a similar width distribution as observed using SEM, where the majority of fibrillar aggregates had diameters ranging from ∼15 - ∼40 nm (Fig. 4.1f). Protofilaments with a diameter of ∼10 nm were observed within the mature XFS matrix (arrow, Fig. 4.2b). These protofilament subunits are thought to laterally aggregate to form fibrils up to 80 nm in width (Figs. 4.1f, 2b) [20]. Previous electron microscopy studies have shown that XFS fibrils usually exhibit a periodic cross-banding pattern [2, 4, 29]. In this study, a banding pattern was observed in some TEM micrographs of XFS fibrils in lens capsule sections (Figs. 4.2c, d). The core structure of XFS fibrils has not been clearly identified, thus a molecular basis for the observed cross-banding patterns is unknown. However, collagen fibers

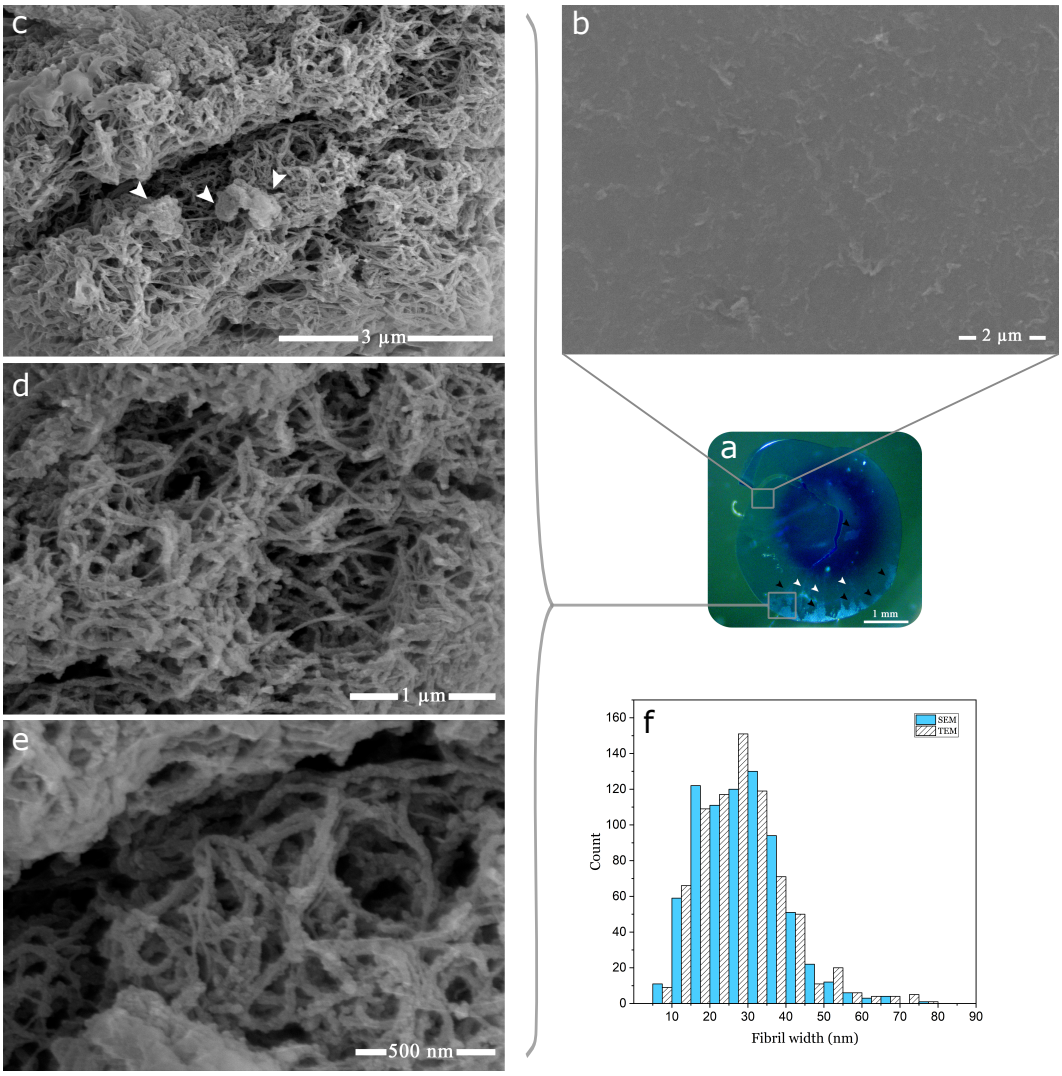

Figure 4.1: Micrographs of the anterior surfaces of lens capsules excised from XFS patients. (a) Lens capsule under stereomicroscope (black arrows indicate XFS deposits, white arrows indicate the junctions between intermediate and peripheral zones). (b) SEM micrograph of a non-XFS rich capsule location. (c-e) SEM micrographs of XFS fibrils found on the capsule surface. (f) Diameter distribution of XFS fibrils on the capsule surface as observed using SEM and TEM.

show a highly ordered banding pattern that is due to the specific packing of tropocollagen monomers, which create regular gap and overlap regions along the fiber [30]. That said, this structure in collagen arises from a controlled fibrillogenesis process, whereas XFS fibrils have only been associated with cells that have an increased metabolism, where previous studies have shown indications of an active fibrillogenesis process [20, 31]. However, it is unclear what

molecular-level interactions are responsible for cross-banding patterns seen in XFS fibrils.

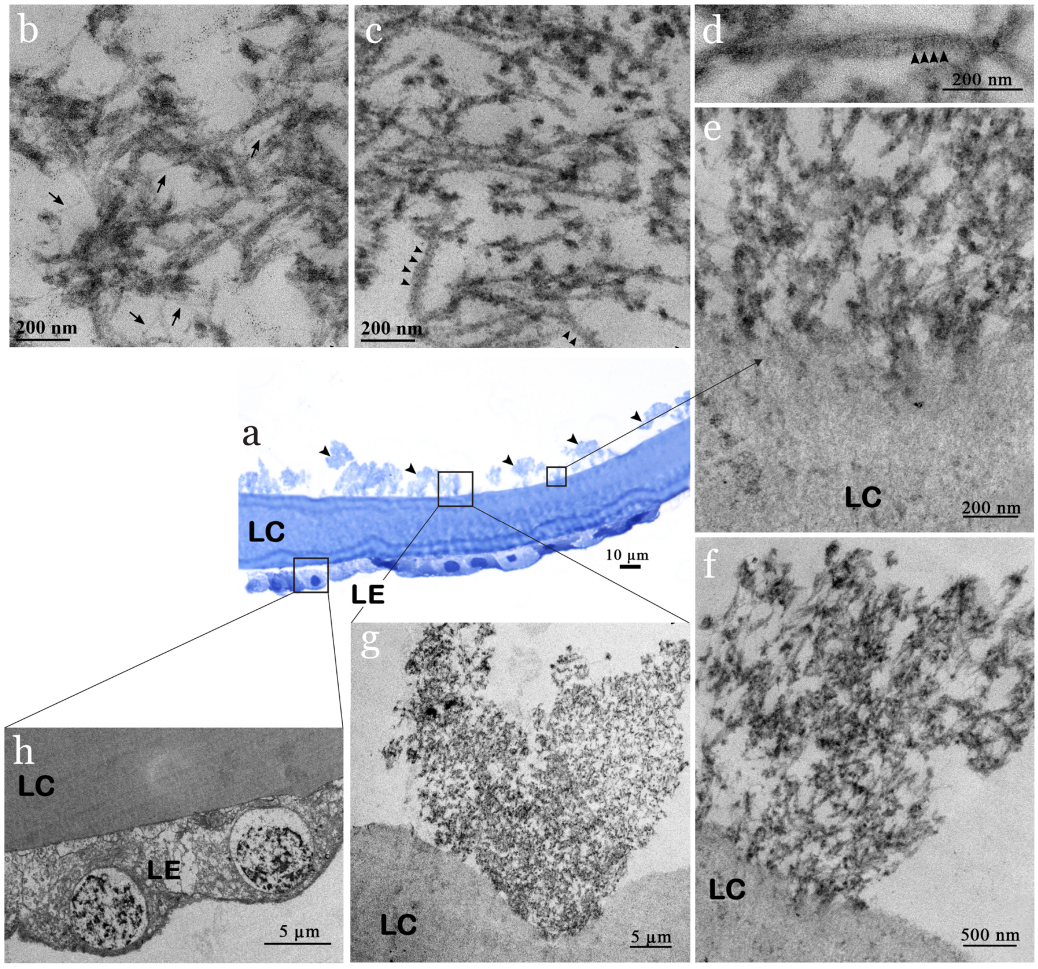

Figure 4.2: Micrographs of the cross-section of anterior lens capsules excised from XFS patients. (a) Light microscope image of sectioned lens capsule showing bush-like excrescence of XFS materials on the surface of lens capsule (arrows). (b) TEM micrograph of XFS fibrils being formed through lateral binding of protofilament subunits. (c, d) XFS fibrils on the anterior lens capsule, with cross-banding pattern (arrows). (e) interface contact between lens capsule and XFS fibril. (f, g) differences in interfacial contacts with XFS materials as well as XFS macrostructure. (h) Lens epithelial cells on the posterior side of lens capsule (LC: lens capsule, LE: lens epithelium).

The epithelial cells located on the posterior side of the lens capsule were evident in both light and TEM micrographs (Figs. 4.2a, h). Previously reported TEM studies have shown that part of the XFS materials found on the anterior lens capsule are in fact intracapsular XFS fibrils, which emerge from the lens epithelium and migrate through the lens capsule to its surface [2, 32].

However, although our data may suggest that a similar structure within the lens capsule exists (arrow, Figs. 4.2e, f), we focused on analyzing the fibrils exposed on the anterior side of the capsule only. Excrescences of XFS fibrils on the anterior lens capsule were also observed as expected (Fig. 4.2g).

4.3.2 XFS materials liberated from the capsule

The ultrastructure of XFS materials obtained from five clinically diagnosed patients were characterized using negative stain TEM (Figs. 4.3-7). Figures 4.3-5 are stained samples from patients with moderate amounts of XFS deposits on their lens capsules. Figures 4.6 and 4.7 are from patients with low and high amount of XFS deposits, respectively. In contrast to previous results, it is apparent that the characterized XFS fibrils have a distinct morphology in each patient sample.

As seen in (Fig. 4.3a), isolated fibrils from a 72-year-old male patient, of moderate XFS, had distinct substructures and contained two or more protofilaments. These fibrils were highly abundant on the EM grid. The width of fibrils with one, two (e.g., Fig. 4.3a first two panels), and three protofilaments were measured to be ∼16, 31, and 48 nm, respectively (Table 4.2). As seen in the last two panels of (Fig. 4.3a), fibrils with higher numbers of protofilament were also observed with an aggregate width of ≥116 nm. Fibril length was between ∼200 to 700 nm. A 2D class average from these fibrils (Fig. 4.3b) allowed for an increase in the signal to noise ratio, thus enhancing the features in the electron micrographs. Upon closer inspection of the 2D class average (Fig. 4.3b), the protofilaments display a clear periodicity with a repeat distance of ∼7-8 nm, suggesting a discrete subunit structure.

Fig. 4.4a shows fibrils that were detected in a sample from a 66-year-old male patient (M2) with moderate XFS. The width of these fibrils was found to be ∼13 nm (Table 4.2), with some fibril lengths exceeding 1 μm. Due to the

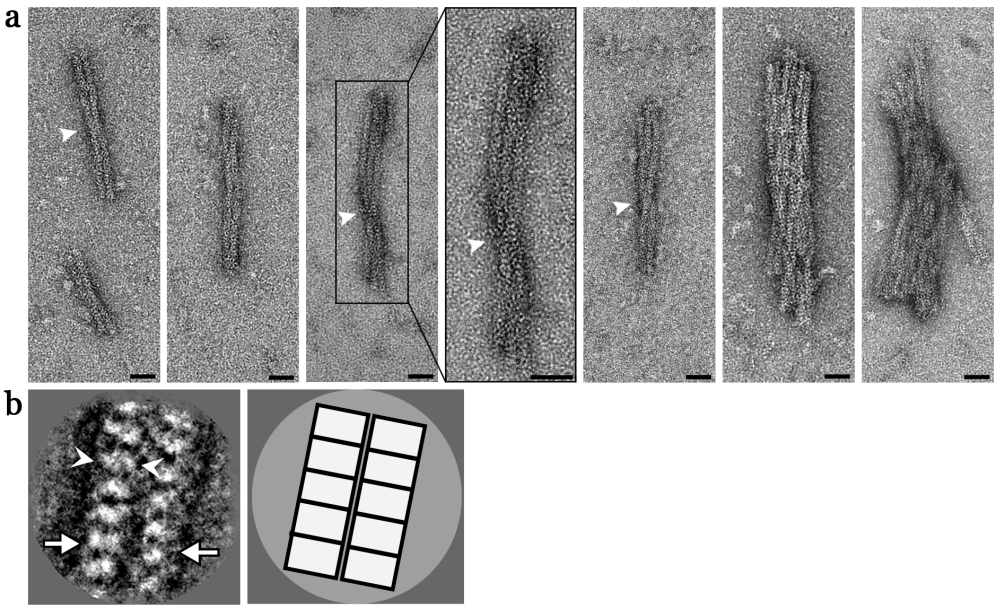

Figure 4.3: Electron micrographs of XFS fibrils from the surface of lens capsule XFS-M1. (a) Electron micrographs of negatively stained (using 2% UA), isolated XFS deposits from the lens capsule of a 72-year-old male patient (M1) being in moderate stages of XFS at the time of surgery. Arrows in (a) indicate helical twist regions (scale bars = 50 nm). (b) First panel: A representative 2D class average of the two protofilament fibril segments after image processing. One and two protofilament is designated by white arrowheads and arrows, respectively (scale bar = 10 nm). Second panel: A schematic illustration of the 2D class average image.

heterogeneity of the fibrils a 2D class average failed to reveal any prominent features. However, the presence of only one density in the 2D class average (Fig. 4.4b) suggests that the ∼13 nm fibrils consist of one protofilament only.

Fibrils obtained from sample M3 are similar to those of sample M2, showing filaments with lengths that can exceed 1 μm (Fig. 4.5a). However, these fibrils had widths between ∼5 and ∼21 nm, with a dominant species at ∼10 nm. The 2D class averages suggested that the 20 nm fibrils are made of two 10 nm protofilaments (Fig. 4.5c), and although not prominent it is likely that the 10 nm fibrils might contain two 5 nm protofilaments (Fig. 4.5c).

Fibrils obtained from a 61-year-old male patient (sample L) had a width of ∼23 nm (Fig. 4.6a) and a length of ∼200 nm to ∼1 μm. In some, but not all, of the 23 nm fibrils two distinct densities were detectable, but this feature was not amplified in the 2D class average (Fig. 4.6b) indicating a less prominent

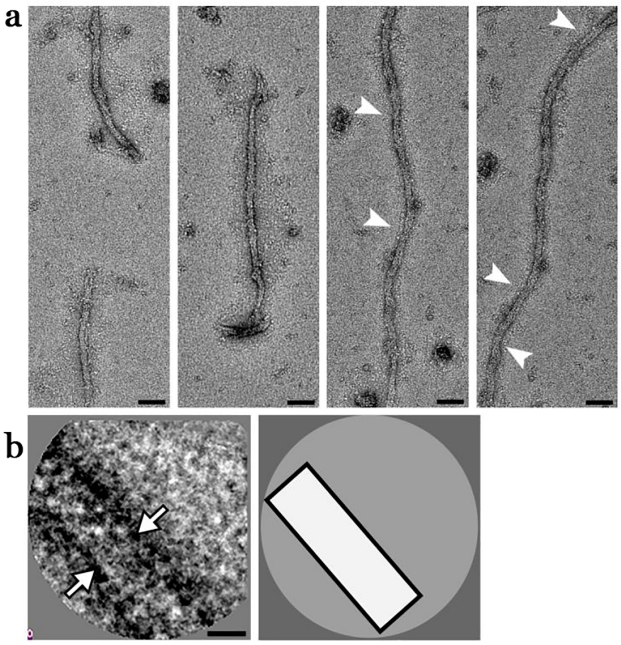

Figure 4.4: Electron micrographs of XFS fibrils from the surface of lens capsule XFS-M2. (a) Electron micrographs of negatively stained (using 2% UA), isolated XFS deposits from a lens capsule of a 66-year-old male patient (M2) being in moderate stages of XFS at the time of surgery. Arrows in (a) indicate helical twist regions (scale bars = 50 nm). (b) Fist panel: A representative 2D class average of the fibril segments after image processing (scale bar = 10 nm). White arrows indicate the density of the fibril in the 2D class average image suggesting it is consist of one protofilament only. Second panel: A schematic illustration of the 2D class average.

substructure.

The only XFS patient sample that showed distinct, observable 5 nm protofilaments that were consistent among all fibrils within this sample came from sample H, who was a patient with high stage XFS (Fig. 4.7a). The fibrils themselves had a diameter of ∼10.5 nm with a length of between 200 to 500 nm. The two 5-nm protofilaments were made visible in the 2D class average (Fig. 4.7b). It was interesting to note that this was the only patient in advanced stages of disease.

Twisting is one of the key markers of structural polymorphism in protein fibrils [33]. XFS fibrils from samples XFS-M1, M2, M3, and H showed a helical twist in their structures (arrow, Figs. 4.3-5, 7). XFS-H fibril showed the most regular helical pitches (arrow, Fig. 4.7), however, other XFS fibrils showed

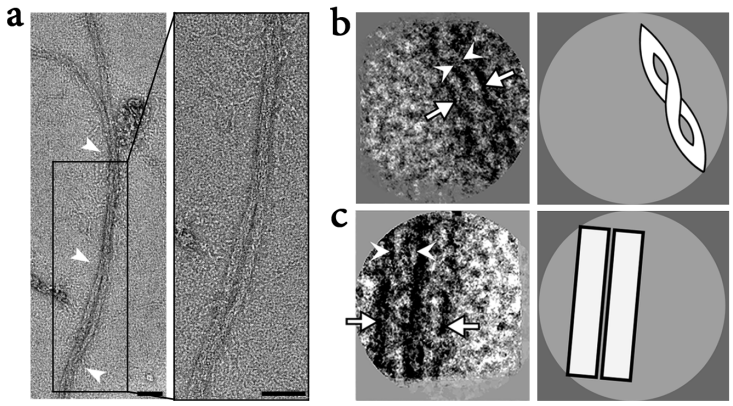

Figure 4.5: Electron micrographs of XFS fibrils from the surface of lens capsule XFS-M3. (a) Electron micrographs of negatively stained (using 2% UA), isolated XFS deposits from a lens capsule of an 83-year-old male patient (sample M3) being in moderate stages of XFS at the time of surgery. Arrows in (a) indicate helical twist regions (scale bars = 50 nm). (b) First panel: A representative 2D class average of the 10 nm filaments displaying two protofilaments. One and two protofilaments are designated by white arrowheads and arrows, respectively. Second panel: A schematic illustration of the 2D class average image (scale bar = 10 nm). (c) First panel: 2D class average of 20 nm fibrils displaying two distinct physical entities. One and two protofilaments are designated by white arrowheads and arrows, respectively. Second panel: A schematic illustration of the 2D class average image (scale bar = 10 nm).

less regular twist regions along the fibril axis. The most irregular twist regions were observed in XFS-M2 fibrils (arrow, Fig. 4.4). To understand the twisted structure of XFS fibrils, their composition and mechanism involving molecular assembly need to be determined. However, twisting is a structural behavior of helical fibrils and amyloids which affect their morphology. It is the result of net interaction arising from two opposing forces; where amino acids tend to twist due to their intrinsic chirality, twisted structures resist further bending stress arising from their elastic distortion [33, 34].

Diameters of XFS protofilaments are as reported in Table 4.2. Only one type of protofilament was observed in the XFS fibrils obtained from the lens capsule of the patient clinically diagnosed with low XFS. Although in some fibrils of this sample two densities were detected, this structural distinction was not readily recognizable in 2D class average images. In the XFS-M2 sample, protofilaments having a diameter of $\sim$13 nm was observed. Samples XFS-M3

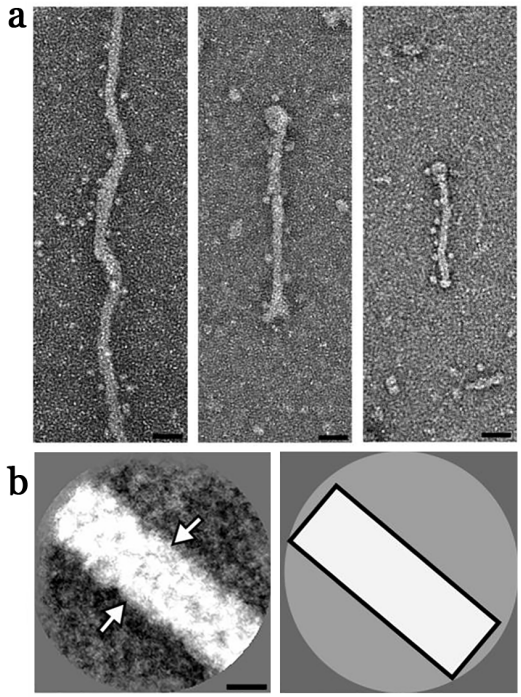

Figure 4.6: Electron micrographs of XFS fibrils from the surface of lens capsule XFS-L. (a) Electron micrographs of negatively stained (using 2% PTA), isolated XFS deposits from a lens capsule of a 61-year-old male patient (sample L) being in low stages of XFS at the time of surgery (scale bars = 50 nm). (b) First panel: A representative 2D class average of the fibril segments. White arrows indicate the density of the fibril in the 2D class average image (scale bar = 10 nm). Second panel: A schematic illustration of the 2D class average image.

and XFS-H both showed two types of protofilaments having similar diameters, whereas, in sample XFS-M3, another type of protofilament with diameter ∼21 nm was observed. It has been previously shown that the diameter of XFS protofilaments found on the lens capsule was ∼10 nm [10]. Moreover, a review suggests that the protofilaments could be in the range of ∼5 to ∼9 nm in width [4]. In this study, the protofilaments were identified based on the most basic visible component of the fibril, meaning that, for instance, in the XFS-M1 sample (Fig. 4.3), three types of fibrils having diameters of 16, 31, and 48 nm, would correspond to one, two, or three protofilaments, respectively (Table 4.2). This is an important aspect of observed structural variation, where it seems that besides the well-known mechanism of lateral aggregation of protofilaments

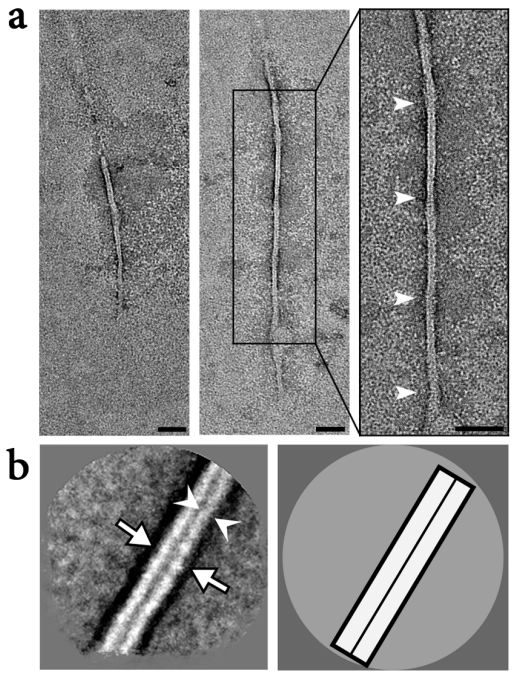

Figure 4.7: Electron micrographs of XFS fibrils from the surface of lens capsule XFS-H. (a) Electron micrographs of negatively stained (2% PTA), isolated XFS deposits from a lens capsule of a 67-year-old male patient (sample H) being in high stages of XFS at the time of surgery. Arrows in (a) indicate helical twist regions (scale bars = 50 nm). (b) First panel: A representative 2D class average of the fibril segments. One and two protofilaments are designated by white arrowheads and arrows, respectively (scale bar = 10 nm). Second panel: A schematic illustration of the 2D class average image.

into mature XFS fibrils, there might be some initial molecular-level assembly processes that could lead to formation of thicker fibrils, presumably without going through lateral aggregation process.

4.4 Conclusions

In this study we evaluated fibrils located on the anterior lens capsules of human eyes for the express purpose of elucidating the extent of their structural

	number of protofilaments	**L**	**M1**	**M2**	**M3**	**H**
Fibril width (nm)	One	∼23	∼16	∼13	∼5	∼5
	Two	-	∼31	-	∼11.5	∼10.5
	Three	-	∼48	-	∼21	-

Table 4.2: Width measurement of fibrils from patients diagnosed with exfoliation syndrome.

diversity. Electron micrographs of fibrils from only five patients revealed significant diversity in fibril morphologies. It is striking that given a small sample size such diversity in fibril structure was noted. These results may suggest different phenotypes or clinical subtypes of XFS, however, additional analyses would be required to resolve this question and reveal more detailed information about unknown aspects of XFS fibrils. Further classification including statistical distribution of structural sub-populations will require significantly more samples. Nevertheless, even with a small sample size it was apparent that fibrils are comprised of protofilaments of various diameters and banding patterns.

Fibril polymorphisms are considered an important facet of other fibril-related diseases, but is largely overlooked when considering XFS. For instance, two distinct fibrillar structures were found in samples extracted post-mortem from the brains of two Alzheimer's disease patients with different clinical histories. Autopsy revealed that both patients had developed characteristic Aβ plaques and neurofibrillary tangles of Alzheimer's disease, however, different fibril structures suggests that this structural diversity might be correlated with variations in disease development [35]. That said, it is also obvious that fibrils associated with Alzheimer's, for example, interact with a vastly different environment, viz., cell dense tissue compared to XFS materials located on the anterior lens capsule. However, XFS fibrils are located throughout the anterior segment and within the Schlemm's canal wall i.e. environments that range from cell free to cell dense. It has been shown that XFS materials are composed of fibrils of varying diameters and lengths [4, 36]. However, certain types of fibrils with dominant structural features in different patients have not been observed before.

Taking amyloid fibrils as a basis, polymorphisms are thought to reflect fibril structures, including: variations in the number of protofilaments, differences

in the relative orientation of protofilaments, and differences in the internal conformation of the protofilament [37, 38]. Furthermore, structural variations of *ex vivo* amyloid fibrils may be influenced by constituent proteins and fibrillogenesis conditions [39]. Considering these factors, further studies on XFS fibrils obtained from different patients may reveal possible links between precursor proteins and dominating fibrillar ultrastructures, which may shed light on disease progression.

4.5 Acknowledgements

The authors would like to acknowledge all tissue donors and clinical staff in the operating rooms of the Royal Alexandra Hospital (Edmonton, AB, Canada) and Rockyview Hospital (Calgary, AB, Canada) who have helped in the process of human tissue sample collection. We also acknowledge Arlene Oatway for her assistance with electron microscopy of tissue samples.

4.6 References

[1] M. Küchle, U. Schlötzer-Schrehardt, and G. O. Naumann, "Occurrence of pseudoexfoliative material in parabulbar structures in pseudoexfoliation syndrome.," *Acta Ophthalmol.*, vol. 69, no. 1, pp. 124–130, Feb. 1991.

[2] J. C. Morrison and W. R. Green, "Light microscopy of the exfoliation syndrome.," *Acta Ophthalmol. Suppl. (Oxf.).*, vol. 184, pp. 5–27, 1988.

[3] U. Schlotzer-Schrehardt and G. O. H. Naumann, "Ocular and systemic pseudoexfoliation syndrome.," *Am. J. Ophthalmol.*, vol. 141, no. 5, pp. 921–937, May 2006.

[4] R. Ritch and U. Schlötzer-Schrehardt, "Exfoliation syndrome," *Surv. Ophthalmol.*, vol. 45, no. 4, pp. 265–315, 2001.

[5] R. Ritch, "Exfoliation syndrome-the most common identifiable cause of open-angle glaucoma.," *J. Glaucoma*, vol. 3, no. 2, pp. 176–178, 1994.

[6] T. W. Blackstad, O. A. Sunde, and J. Trœtteberg, "On the ultrastructure of the deposits of busacca in eyes with glaucoma simplex and so-called senile exfoliation of the anterior lens capsule," *Acta Ophthalmol.*, vol. 38, no. 5, pp. 587–598, 1960.

[7] A. Ringvold and G. Husby, "Pseudo-exfoliation material-an amyloid-like substance.," *Exp. Eye Res.*, vol. 17, no. 3, pp. 289–299, Nov. 1973.

[8] J. Meretoja and A. Tarkkanen, "Occurrence of Amyloid in Eyes with Pseudo-exfoliation," *Ophthalmic Res.*, vol. 9, no. 2, pp. 80–91, 1977.

[9] L. P. Repo, A. Naukkarinen, L. Paljärvi, and M. E. Teräsvirta, "Pseudoexfoliation syndrome with poorly dilating pupil: A light and electron microscopic study of the sphincter area," *Graefe's Arch. Clin. Exp. Ophthalmol.*, vol. 234, no. 3, pp. 171–176, 1996.

[10] A. J. Dark, B. W. Streeten, and C. C. Cornwall, "Pseudoexfoliative disease of the lens: a study in electron microscopy and histochemistry.," *Br. J. Ophthalmol.*, vol. 61, no. 7, pp. 462–472, Jul. 1977.

[11] C. G. Clement and L. D. Truong, "An evaluation of Congo red fluorescence for the diagnosis of amyloidosis," *Hum. Pathol.*, vol. 45, no. 8, pp. 1766–1772, 2014.

[12] R. P. Linke, H. V. Gartner, and H. Michels, "High-sensitivity diagnosis of AA amyloidosis using Congo red and immunohistochemistry detects missed amyloid deposits," *J. Histochem. Cytochem.*, vol. 43, no. 9, pp. 863–869, 1995.

[13] M. Davanger and O. O. Pedersen, "Pseudo-exfoliation material on the anterior lens surface. Demonstration and examination of an interfibrillar ground substance," *Acta Ophthalmol*, vol. 53, no. 1, pp. 3–18, 1975.

[14] J. Berlau et al., "Analysis of aqueous humour proteins of eyes with and without pseudoexfoliation syndrome.," *Graefes Arch. Clin. Exp. Ophthalmol.*, vol. 239, no. 10, pp. 743–746, 2001.

[15] R. Tycko, "Amyloid polymorphism: structural basis and neurobiological relevance.," *Neuron*, vol. 86, no. 3, pp. 632–645, May 2015.

[16] W. Qiang, W. M. Yau, J.-X. Lu, J. Collinge, and R. Tycko, "Structural variation in amyloid-beta fibrils from Alzheimer's disease clinical subtypes.," *Nature*, vol. 541, no. 7636, pp. 217–221, Jan. 2017.

[17] R. Ritch, "Systemic associations of exfoliation syndrome," *Asia-Pacific J. Ophthalmol.*, vol. 5, no. 1, pp. 45–50, 2016.

[18] C. M. Dobson, "Protein aggregation and its consequences for human disease.," *Protein Pept. Lett.*, vol. 13, no. 3, pp. 219–227, 2006.

[19] M. Stefani and C. M. Dobson, "Protein aggregation and aggregate toxic-

ity: new insights into protein folding, misfolding diseases and biological evolution.," *J. Mol. Med. (Berl).*, vol. 81, no. 11, pp. 678–699, Nov. 2003.

[20] M. Zenkel and U. Schlötzer-Schrehardt, "The composition of exfoliation material and the cells involved in its production.," *J. Glaucoma*, vol. 23, no. 8 Suppl 1, pp. S12-4, 2014.

[21] B. H. Toyama and J. S. Weissman, "Amyloid structure: conformational diversity and consequences.," *Annu. Rev. Biochem.*, vol. 80, pp. 557–585, 2011.

[22] S. J. Ludtke, P. R. Baldwin, and W. Chiu, "EMAN: semiautomated software for high-resolution single-particle reconstructions.," *J. Struct. Biol.*, vol. 128, no. 1, pp. 82–97, Dec. 1999.

[23] J. L. Jiménez, G. Tennent, M. Pepys, and H. R. Saibil, "Structural diversity of *ex vivo* amyloid fibrils studied by cryo-electron microscopy," *J. Mol. Biol.*, vol. 311, no. 2, pp. 241–247, 2001.

[24] M. Davanger, "A method of isolating and collecting pseudo-exfoliation material from extracted cataractous lenses.," *Acta Ophthalmol.*, vol. 55, no. 4, pp. 634–640, Aug. 1977.

[25] U. Schlötzer-Schrehardt, M. Küchle, and G. O. Naumann, "Electron-microscopic identification of pseudoexfoliation material in extrabulbar tissue.," *Arch. Ophthalmol.*, vol. 109, no. 4, pp. 565–570, 1991.

[26] W. J. Tromans, R. W. Horne, G. A. Gresham, and A. J. Bailey, "Electron microscope studies on the structure of collagen fibrils by negative staining.," *Z. Zellforsch. Mikrosk. Anat.*, vol. 58, pp. 798–802, 1963.

[27] D. Schwartz and A. Veis, "Structure of bovine anterior lens capsule basement membrane collagen molecules from electron microscopy.," *Biopolymers*, vol. 18, no. 9, pp. 2363–2367, Sep. 1979.

[28] M. Davanger, "The pseudo-exfoliation syndrome. A scanning electron microscopic study. I. The anterior lens surface.," *Acta Ophthalmol.*, vol. 53, no. 6, pp. 809–820, Dec. 1975.

[29] M. Davanger, "On the ultrastructure and the formation of pseudo-exfoliation material.," *Acta Ophthalmol.*, vol. 58, no. 4, pp. 520–527, Aug. 1980.

[30] M. D. Shoulders and R. T. Raines, "Collagen structure and stability.," *Annu. Rev. Biochem.*, vol. 78, pp. 929–958, 2009.

[31] G. O. Naumann, U. Schlotzer-Schrehardt, and M. Kuchle, "Pseudoexfoliation syndrome for the comprehensive ophthalmologist. Intraocular and systemic manifestations.," *Ophthalmology*, vol. 105, no. 6, pp. 951–968, Jun. 1998.

[32] T. I. Bertelsen, P. A. Drabloes, and P. R. Flood, "The socalled senile exfoliation (pseudoexfoliation) of the anterior lens capsule, a product of the lens epithelium. Fibrillopathia epitheliocapsularis. A microscopic, histochemic and electron microscopic investigation.," *Acta Ophthalmol.*, vol. 42, pp. 1096–1113, 1964.

[33] L. R. Volpatti, M. Vendruscolo, C. M. Dobson, and T. P. J. Knowles, "A clear view of polymorphism, twist, and chirality in amyloid fibril formation.," *ACS Nano, vol.* 7, no. 12, pp. 10443–10448, Dec. 2013.

[34] A. Aggeli et al., "Hierarchical self-assembly of chiral rod-like molecules as a model for peptide beta-sheet tapes, ribbons, fibrils, and fibers.," *Proc. Natl. Acad. Sci. U. S. A.*, vol. 98, no. 21, pp. 11857–11862, Oct. 2001.

[35] J. X. Lu, W. Qiang, W. M. Yau, C. D. Schwieters, S. C. Meredith, and R. Tycko, "Molecular structure of beta-amyloid fibrils in Alzheimer's disease brain tissue.," *Cell*, vol. 154, no. 6, pp. 1257–1268, Sep. 2013.

[36] B. W. Street and A. J. D. En, "Pseudoexfoliation syndrome," in A.

Gamer, G.K. Klintworth (Eds.), *Pathobiology of Ocular Disease, Part A*, Marcel Dekker, New York, 1994, pp. 591–629.

[37] M. Fandrich, J. Meinhardt, and N. Grigorieff, "Structural polymorphism of Alzheimer Abeta and other amyloid fibrils.," *Prion*, vol. 3, no. 2, pp. 89–93, 2009.

[38] K. Annamalai et al., "Polymorphism of Amyloid Fibrils *In Vivo*," *Angew. Chem. Int. Ed. Engl.*, vol. 55, no. 15, pp. 4822–4825, Apr. 2016.

[39] E. Vazquez-Fernandez et al., "The Structural Architecture of an Infectious Mammalian Prion Using Electron Cryomicroscopy.," *PLoS Pathog.*, vol. 12, no. 9, p. e1005835, Sep. 2016.

Chapter 5

Towards preventing exfoliation glaucoma by targeting and removing fibrillar aggregates associated with exfoliation syndrome

Abstract

Exfoliation syndrome presents as an accumulation of insoluble fibrillar aggregates that commonly correlates with age and causes ocular complications, most notably open-angle glaucoma. Despite advances in understanding the pathogenesis and risk factors associated with exfoliation syndrome, there has been no significant progress in curative pharmacotherapy of this disease. It is thought that the ability to target the fibrillar aggregates associated with exfoliation may offer a new therapeutic approach, facilitating their direct removal from affected tissues. Phage display techniques yielded two peptides (LPSYNLHPHVPP, IPLLNPGSMQLS) that could differentiate between exfoliative and non-affected regions of the human lens capsule. These peptides were conjugated to magnetic particles using click chemistry to investigate their ability in targeting and removing exfoliation materials from the anterior human lens capsule. The behavior of the fibrillar materials upon binding to these magnetic particles was assessed using magnetic pins and rotating magnetic fields of various strengths. *Ex vivo* studies showed that the magnetic particle-peptide conjugates could generate enough mechanical force to remove large aggregates of exfoliation materials from the lens capsule when exposed to a low-frequency rotating magnetic field (5000 G, 20 Hz). Biocompatibility of targeting peptides with and without conjugated magnetic particles was con-

firmed using MTT cell toxicity assay, live/dead cell viability assay, and DNA fragmentation studies on primary cultured human trabecular meshwork cells. This is a novel, minimally invasive, therapeutic approach for the treatment of exfoliation glaucoma via the targeting and removal of exfoliation materials that could be applied to all tissues within the anterior segment of the eye.

Keywords: exfoliation syndrome, phage display, peptide, targeting, magnetic particle.

5.1 Introduction

Exfoliation syndrome (XFS, a.k.a. pseudoexfoliation) is known as the most common identifiable cause of glaucoma, affecting ∼70 million individuals in the world [1]. XFS is commonly considered an age-related disease that significantly affects the homeostasis of the human eye through the formation of small deposits of white materials throughout the anterior segment of the eye. Although their precise composition is unknown, these white deposits are considered to be amyloid-like fibrils, with varied thicknesses, embedded in a fibrillogranular matrix of glycoprotein-proteoglycan crosslinks [2–6]. When found in the trabecular meshwork, these fibrillar deposits can impede the outflow of aqueous humor and cause large fluctuations in intraocular pressure (IOP) that increases eye pressure to the point that irreversible blindness glaucoma may occur [7–9]. Despite best clinical efforts, IOP levels for patients with exfoliation glaucoma may gradually or suddenly elevate uncontrollably [8]. XFS has been causally related to lens subluxation, zonular instability, blood-aqueous barrier impairment, and several intraoperative and postoperative complications that occur during ocular treatments [10, 11]. Moreover, there is a body of evidence suggesting that XFS is a systemic disease, which presents in blood vessels, lungs, skin, gallbladder, heart, meninges, and it is a potential risk factor for other clinical complications such as coronary artery disease and renal artery stenosis [12–14].

XFS materials are not removed through normal regulatory processes necessary for ocular homeostasis and, despite some success in elucidating pathomechanisms, curative pharmacotherapy to prevent, break down, or remove these materials has not yet been achieved. The ability to treat this disease necessitates the ability to preferentially target the fibrillar structures related to XFS within the *in vivo* context. Compared to the other targeting ap-

proaches, peptide-based therapeutic strategies have benefited from a lower immunogenicity profile, higher binding affinity, and increased specificity related to the small peptide molecules relative to other drug compounds. Phage display is a powerful technique for screening a library of random amino acid sequences to identify peptides that specifically, and robustly, bind to substrates with an antibody-like affinity; a strategy used to identify peptides that bind Alzheimer's disease plaques [17, 18]. Moreover, phage display provides high-throughput screening of random peptide libraries without a priori knowledge of the target properties, which is pertinent as the physicochemical properties of these fibrillar structures is ill-defined.

Herein, we have used *ex vivo* phage display to identify high-affinity binding peptides specific for XFS materials. All phage binding experiments were conducted using extracted human aqueous humor (hAH) so as to mimic the physiological pH and solution properties that are crucial to molecular interactions (ion, protein, osmolarity) [19]. Non-XFS lens capsules were used as a negative panning target to remove peptides that bind to only to the lens capsule itself. The phage library, after negative panning, was introduced to XFS materials found on human lens capsules, and amplified three times to determine high binding affinity sequences. Labeled phage-displayed peptides and wild-type phages were carried out to confirm the selective binding to XFS materials.

Identified XFS-targeting peptides were conjugated to spherical magnetic particles (1μm dia.) to evaluate their ability to target, liberate from the lens surface, and collect XFS materials. Magnetic particles (MPs) have been employed for diagnosis and treatment applications as they have shown relatively good biocompatibility and can be directed to specific sites in the body using external magnetic fields [20]. Furthermore, when exposed to an external low-frequency rotating magnetic field similar MPs have generated mechani-

cal forces that have been utilized for a variety of biomedical applications [21]. Conjugation of alkyne-modified peptides to azide-functionalized MPs was confirmed using surface zeta potential measurements, Fourier-transform infrared spectroscopy (FTIR), and competitive labeling of MPs. The targeting capability of peptide modified MPs was evaluated against their scrambled sequences for binding to human lens capsules with and without XFS materials. Cellular uptake of MP-peptide conjugates was studied using electron microscopy. Cell toxicity of MP-peptide complexes was investigated using different techniques including live/dead cell viability assay, MTT assay, and DNA fragmentation. The effect of magnetic pin and rotating magnetic field on their ability to liberate XFS materials bound to peptide modified MPs was evaluated using XFS lens capsules, *ex vivo*. It was found that the designed peptide-based targeting system along with magnetic field treatment was able to remove XFS materials from a wide range of patient samples. It is thought that these engineered materials will provide a minimally invasive therapeutic strategy for treating XFS that is hitherto unavailable.

5.2 Methods

5.2.1 Patient sample collection

Human tissue samples were collected and analyzed following written informed consent according to the University of Alberta and University of Calgary research ethics board-approved protocols. Human lens capsules were collected from patients aged between 63-84 years, mean 74.8 $\pm$ 5 years, undergoing phacoemulsification cataract surgery, and were stored in balanced salt solution (BSS® intraocular irrigating solution, Alcon) at 4 °C prior to use. Aqueous humor fluid was collected from anterior chamber of the eye using a 30-gauge cannula inserted through the paracentesis site. Patients with history of dia-

betes mellitus, with previous severe trauma to the eye, with previous expositor to infrared radiation and patents with previous diagnosis of amyloid disease were excluded from the study.

5.2.2 Cell line

Primary human trabecular meshwork (hTM) cells were obtained from ScienCell Research Laboratories (Carlsbad, CA), and maintained in TMCM medium (ScienCell, no. 6591). Primary cell culture was passaged according to the manufacturer's instructions. Passage three cells were seeded on tissue culture plates coated with gelatin and media were refreshed every 2-3 days. These monolayer cultures were used in subsequent experiments upon reaching 95-100% confluency.

5.2.3 Isolation of XFS materials-specific peptides

Ph.D.^{TM}-12 phage display peptide library was used for *ex vivo* screening. All human tissues were washed three times with BSS buffer before use. Human lens capsules collected from patients without XFS were used for subtractive screening. The lens capsules were incubated with the phage library (1×10^{11} pfu) in an equal volume of aqueous humor fluid and BSS® irrigating solution for 1 hr at 37 °C in 0.2 ml tube. The solution was removed and 300 μl of ice-cold BSS solution was added to the tube and tissue was washed several times with BSST buffer (BSS solution containing 0.1% v/v Tween-20) to elute off unbound or weakly bound phages. The lens capsule was subsequently stained with 0.06% Trypan blue (same concentration used in anterior segment surgeries to facilitate visualization of target tissues in specific situations) to get better visualization of XFS material under the microscope. Tissue was washed further to remove the excess dye and was placed on a sterile microscope slide and covered with 20 μl BSS buffer and XFS material was carefully removed

from the surface of lens capsule using round tip sterile needles. Care was taken to not remove undesired parts of the lens capsule during the process. The solution containing the scraped XFS material was transferred to a fresh tube containing 100 μl 0.2 M glycine-HCl (pH 2.2) to elute phages bound to the XFS material. After 15 min the solution containing recovered phages was neutralized with 15 μl 1 M Tris-HCl buffer (pH 9.1). The eluted phages were amplified by infection of *E. coli* host strain ER2738 (New England Biolabs). Three rounds of *ex vivo* panning was performed with subtractive panning in the beginning of subsequent round and stepwise increasing of Tween concentration in BSST buffer (0.1, 0.2, 0.3%) to increase the likelihood of identification of XFS material-targeting peptides. Individual clones were then picked for characterization of peptide-encoding inserts using DNA sequencing (Fig. 5.1).

5.2.4 Evaluation of the targeting ability of phage-displayed peptides

Phage labeling

The ability of two highly enriched phage-displayed peptides to bind specifically to XFS materials was evaluated *ex vivo* by fluorescently labeling these phages with Cy5 (Lumiprobe) as described elsewhere [22]. Amplified phages (1×10^{11} pfu) were resuspended in 0.3 M $NaHCO_3$ (pH 8.6) containing 10 μg cy5 dye and incubated for 2 hr at room temperature in the dark. Subsequent to phage/fluorophore incubation, 40 μl of 10 mM lysine was added to interact with remaining free cy5 dye molecules in the solution. The volume of reaction mixture was subsequently brought up to 1 ml with PBS buffer, and the phages were purified with two rounds of 20% (w/v) polyethylene glycol-8000, 2.5 M NaCl precipitation. The labelled phages resuspended in BSS solution.

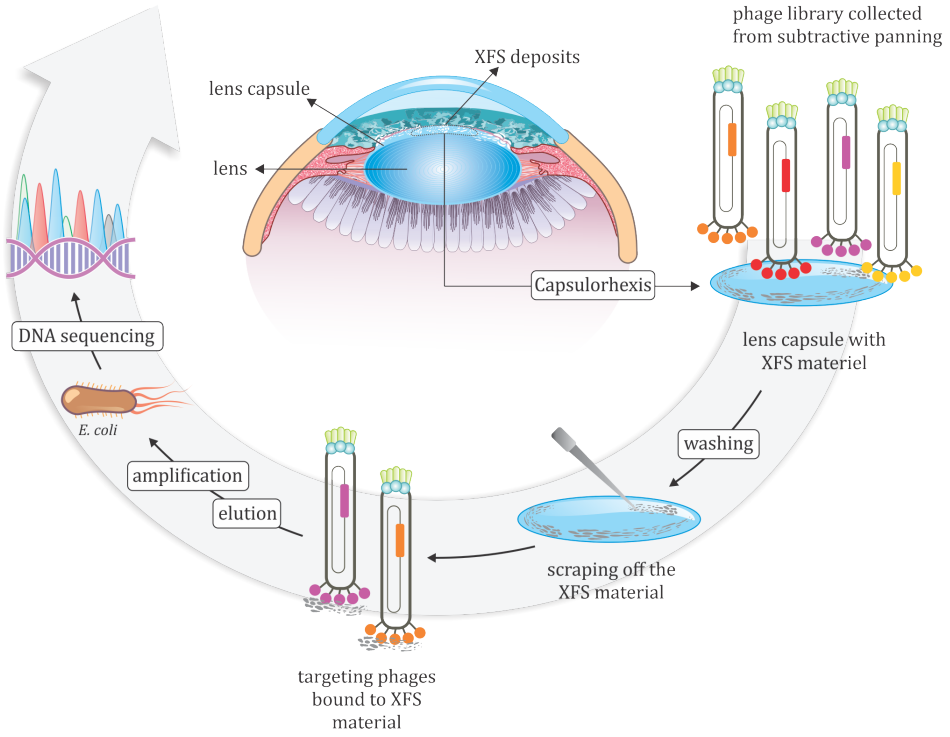

Figure 5.1: *Ex vivo* panning of phage-displayed peptide library on exfoliative human lens capsule. Control human lens capsules without XFS material were subjected to subtractive panning to enrich XFS material-specific binders. Positive screening was carried out on lens capsules collected from patients with XFS and undergoing phacoemulsification cataract surgery. Three rounds of screening were applied and selected phage plaques were analyzed using DNA sequencing.

Ex vivo evaluation of targeting ability of labeled phages

Fluorescently labeled phages carrying identified targeting peptides as well as wild-type phages without peptide-encoding inserts were incubated with exfoliative human lens capsules in a 100 μl solution containing equal volumes of human aqueous humor and BSS solution. The incubation was allowed to continue for 1 hr at 37 °C. After serially washing with BSST buffer (0.1, 0.3%), three times each, the lens capsules were mounted on microscope slides and were examined an Olympus IX81 inverted fluorescence microscope (Olympus Corporation, Tokyo, Japan). The location of XFS materials on the surface of the lens capsule was confirmed in bright-field mode prior to fluorescence imaging.

5.2.5 Magnetic bead-peptide conjugates

Synthetic alkyne-modified peptides (≥95% purity) corresponding to the phage-displayed XFS materials-binding peptides and scrambled sequences were purchased from RS synthesis (Louisville, KY, USA). The peptides were alkyne-modified and their conjugation to azide-functionalized MPs with biocompatible coatings (1 μm MPs, Nanocs Inc, New York) were carried out through copper-catalyzed azide-alkyne click chemistry as described [23]. Azide-functionalized MPs were added to the peptide solution having a final concentration of 600 μM in 100 mM potassium phosphate buffer (pH 7). A premix solution containing 2.5 μl of 20 mM $CuSO_4$ and 5 μl of 50 mM tris(3-hydroxypropyltriazolyl-methyl)amine (THPTA) ligand (Lumiprobe) was prepared immediately prior to use and added to the click reaction solution. 25 μl of 100 mM sodium ascorbate was subsequently added and the reaction was allowed to proceed for 1 hr. Subsequent to click reaction, the peptide-conjugated MPs were first washed with 10 mM EDTA to remove copper ions and then with BSS buffer.

5.2.6 Characterization of peptide-conjugated MPs

The surface charge of MPs with and without peptide conjugates was measured using a Zetasizer Nano ZS (Malvern Instruments, UK). For FTIR measurements, drop-cast films of MPs with and without peptide conjugates were analyzed using an FTIR microscope (Nicolet continuum FTIR microscope (Thermo Scientific). FTIR spectra were collected with a resolution of 4 cm^{-1} and 128 scans of each sample. Conjugation of peptides to MPs was further analyzed through competitive labeling of MPs with 5-carboxytetramethylrhodamine alkyne (TAMRA-alkyne), 5-isomer fluorophore (Lumiprobe). Azide-functionalized MPs were conjugated first with targeting peptides and then labeled with TAMRA-alkyne fluorophore as described before in the conjugation

section. Since the azide groups on the surface of MPs had already interacted with the alkyne group of peptides, they were expected to be non- (or less-) labeled compared to control particles (without peptide conjugates).

5.2.7 *Ex vivo* evaluation of targeting ability of identified peptides

Human lens capsules obtained from XFS patients after washing with BSS buffer were transferred into a solution containing equal volumes of human aqueous humor and BSS irrigating solution. 25 μg of each control MPs (without peptide conjugates), MP-peptide, and scrambled MP-peptide complexes were incubated with lens capsules in that solution in a 0.2 ml tube for 1 hr at 37 °C with gentle shaking. Afterward, the excess particles were washed off with BSS buffer and the lens capsules were mounted on the microscope slide and images were taken using an Axiocam-105 color camera on a stereomicroscope (Stemi-305, Carl Zeiss).

5.2.8 Evaluation of behavior of magnetized XFS materials under magnetic field

Ex vivo evaluation using magnetic pin

Human lens capsules incubated with MP-peptide complexes were laid flat on a microscope slide with the XFS side facing up and 50 μl of BSS buffer was placed on the top of the tissues. A metallic pin which was magnetized by attaching it to the surface of a permanent magnet having field strength at the pole of $\sim$5000 G was used to observe the effect of applied magnetic tool on the XFS materials. Control experiments were carried out on the same tissues using a non-magnetic 23-gauge needle which had almost the same tip size as previously used magnetic pins. Images were taken under the stereomicroscope.

Ex vivo evaluation using rotating magnetic field

The same approach was followed as previously described except for using a rotating magnetic field instead of the static magnetic field applied with a magnetic pin. The lens capsules were first incubated with MP-peptide conjugates and then treated with a rotating Halbach array magnet that produced a ∼5000 G magnetic field across the gap of the magnet (Nickel-plated N48H, Super Magnet Man Inc., Alabama, USA). The tissue samples were incubated at the entrance of the Halbach array gap rotating at 20 Hz for 3 hr and then images were taken under the stereomicroscope. Irrigation and aspiration is used in cataract surgery to remove remaining parts of the lens materials and residual viscoelastic solution from the eye. To mimic the surgery conditions, irrigation of BSS buffer at a rate of 10 ml/min was applied over the processed tissues to observe the effect of buffer irrigation on the removal of the XFS materials after being treated with rotating magnetic field. Control studies were carried out with the same treatment approaches using XFS lens capsules, except for using BSS buffer instead of MP-peptide conjugates.

In order to better evaluate of the effect of rotating magnetic field on removing of XFS materials from the surface of lens capsules, images of lens capsules which were captured before and after treatment with the rotating Halbach array were converted to 16-bit gray-scale images and their intensities analyzed using Adobe Photoshop CC 2015 software (Adobe Systems Inc, San Jose, CA).

5.2.9 Electron microscopy studies

Scanning electron microscopy (SEM)

The monolayer of hTM cells cultured on gelatin-coated glass coverslips in 24-well plates were incubated with 100 μg of MP-peptide complexes for 2 hr at 37 °C. The wells were topped up with the fixative solution (2.5% glutaraldehyde, 4% paraformaldehyde in 0.1 M phosphate buffer, pH 7.4), for 20 min. Upon

serial washing with PBS buffer (pH 7.4), samples were dehydrated with graded ethanol gradually by 20% increments for 30 min each until 100% ethanol. Samples were subsequently treated with hexamethyldisilazane (HMDS) and allowed to dry overnight, then mounted on SEM stubs and sputtered with a gold-palladium film. SEM images were obtained using a Zeiss Sigma FE-SEM scanning electron microscope (Carl Zeiss, Inc., Oberkochen, Germany) at the accelerating voltage of 20 kV.

Transmission electron microscopy (TEM)

Confluent monolayers of hTM cells cultured in 24-well cell culture plates were incubated with MP-peptide complexes as previously described for SEM studies. After washing with Dulbecco's PBS buffer, cells were scraped off the wells and transferred into the microcentrifuge tube. Cells were centrifuged at 1000 rpm for 5 min to form a pellet. The supernatant was removed and the cells pellet was incubated in the fixative solution overnight. Upon washing with 0.1 M phosphate buffer (pH 7.4), samples were post-fixed in 1% osmium tetroxide for 1 hr. Dehydrated pellets were then embedded in Spurr's resin and allowed to polymerize at 70 °C overnight. Ultrathin sections were prepared using an ultramicrotome (Reichert-Jung Ultracut-E, Vienna, Austria) with a diamond knife. The ultrathin sections were stained with 4% uranyl acetate solution and imaged using a Philips–FEI, Morgagni-268 transmission electron microscope (Hillsboro, USA) operating at an acceleration voltage of 80 kV.

5.2.10 Morphology and phenotype of hTM cells

Before biocompatibility studies, the morphology and phenotypic characteristics of cultured hTM cells were studied. Population doubling time of hTM cells was obtained as described elsewhere [24].

5.2.11 Immunohistochemical study

Immunohistochemical assays were employed to identify the expression of characteristic phenotypic markers of trabecular meshwork cells. Confluent monolayers were confirmed using an inverted cell culture microscope (Leica DMi1, Leica Microsystems Inc, Germany). Immunohistochemical labeling was carried out according to the manufacturer's protocol. Rabbit anti-fibronectin (1:200, ab2413, Abcam), rabbit anti-laminin (1:200, ab11575, Abcam) and rabbit anti-myocilin (1:200, ab41552, Abcam) antibodies were used as fluorescently-labeled primary antibodies. Phalloidin-Alexa Fluor 488 (1:40, Molecular Probes) was used to label filamentous actin (F-actin). Upon washing with PBS buffer, grown cells on glass coverslips were fixed with 4% paraformaldehyde in PBS buffer for 10 min at room temperature. Cells were subsequently washed with ice-cold PBS buffer and permeabilized for 5 min with 0.2% Triton X-100. Cells were washed thrice with PBS buffer and incubated with PBS containing 5% goat serum for 1 hr at room temperature to block nonspecific binding sites of the antibodies. Primary antibodies were then added to the wells ad incubated overnight at 4 °C in the dark. Upon washing with PBS buffer, cells were incubated with phalloidin for 20 min. Samples were then covered using fluoroshield mounting medium with DAPI (ab104139, Abcam) and images were taken using an Olympus IX81 inverted fluorescence microscope (Olympus Corporation, Tokyo, Japan).

5.2.12 Biocompatibility studies

MTT cytotoxicity assay

Cytotoxicity of XFS-targeting peptide solutions, as well as MP-peptide conjugates, was tested against hTM cells using MTT assay. Cells were plated in 24-well plates and upon reaching confluency they were treated with different concentrations of peptide solutions and particle-peptide conjugates. Cell pro-

liferation was evaluated 24 hr post-treatment using the Vybrant® MTT cell proliferation assay kit (Molecular Probes).

Live/dead cell viability assay

Cell viability was further assayed using LIVE/DEAD® viability/cytotoxicity kit (Molecular Probes). Monolayers of hTM cells were treated in triplicates with peptides alone in solution (1 mM) and in conjugation with MPs (100 μg). Cell viability was then assessed according to the manufacturer's protocol. The kit is based on calcein AM/ethidium homodimer-1 (EthD-1) system, where calcein AM detects cellular esterase activity of live cells and EthD-1 stains nuclei of dead cells. A similar live/dead assay was used to investigate the effect of MP-peptide conjugates on the viability of hTM cells in the presence of the rotating magnetic field. Cells grown in 24-well plate and treated with MP-peptide conjugates were placed under a rotating magnetic field for 1 hr. The viability of hTM cells was then assessed as described above. A similar live/dead assay was carried out to evaluate the effect of the rotating magnetic field on cultured hTM cells. The plated cells in a 24-well cell culture plate were incubated with 100 μg MP-peptide conjugates. The plate was placed under a rotating magnetic field which was constructed using two attached cuboid-shaped permanent magnet (having a pole field strength of $\sim$5000 G) to provide a larger field over the plate. The cells were treated with the rotating magnetic field for 10 min and then analyzed using live/dead assay as described before. For both MTT and live/dead assays one-way ANOVA test was used to analyse the significance of difference ($p < 0.05$) between the results.

DNA fragmentation analysis

Effect of peptide-particle conjugates and peptide solutions on the induction of apoptotic DNA fragmentation was analyzed in hTM cells. Grown hTM

cells in 24-well plates were incubated with 100 μg of MP-peptide complexes or 0.5 mM peptide solutions for 24 hr at 37 °C. Cells were recovered from wells using a cell scraper. DNA was isolated and purified using DNeasy blood and tissue kit (Qiagen). Extracted DNA molecules from control and treated hTM cells were subjected to 2% agarose gel electrophoresis and visualized by SYBR green staining.

5.3 Results and discussion

5.3.1 *Ex vivo* phage display against XFS materials

Peptide sequences that bind to XFS materials were deduced from the DNA sequences of selected phage clones. Three rounds of biopanning against XFS materials sourced from different patients yielded an enrichment of two peptides: LPSYNLHPHVPP (p-LPS) and IPLLNPGSMQLS (p-IPL) (Appendix 1, Table A1). The high degree of selectivity of these phage towards the XFS materials was aided by: i. removal of phage that bound normal lenses through negative biopanning, and ii. removal of XFS materials from the lens capsules, resulting in specific amplification of phage that only bound to these fibrils. Moreover, the robust nature of the binding was evident as samples came from different patients. Finally, the use of extracted human aqueous humor at 37 °C [25] was vital to these experiments so as to maintain an environment (pH, ionic strength, proteins, osmolarity) that was as close as possible to the physiological environment where the targeting of fibrils would occur.

5.3.2 Evaluating the targeting ability of phage-displayed peptides

Human lens capsules with XFS materials were stained with fluorescently labeled wild-type phages as well as phages displaying the enriched peptides. It is important to note that the conjugated fluorophore (Cy5 NHS ester dye)

molecule did not interfere with phage binding to the XFS materials as it reacts with the primary amino group of lysine, which was not present in the enriched peptides. Both phage-displayed peptides (p-LPS and p-IPL) showed specific binding to XFS materials (Figs. 5.2A, C), where the presence of XFS materials was already confirmed using bright-field microscopy (Figs. 5.2B, D, F). Wild-type phages showed no noticeable interaction with XFS materials on the surface of the lens capsule (Fig. 5.2E). XFS materials do not cover the whole surface of the lens cuspule, meaning that labeled phages had the chance to interact with the non-XFS altered regions of the lens capsule. Phage were observed to bind only to the XFS regions of the lens capsule, further confirming their specificity towards the XFS materials.

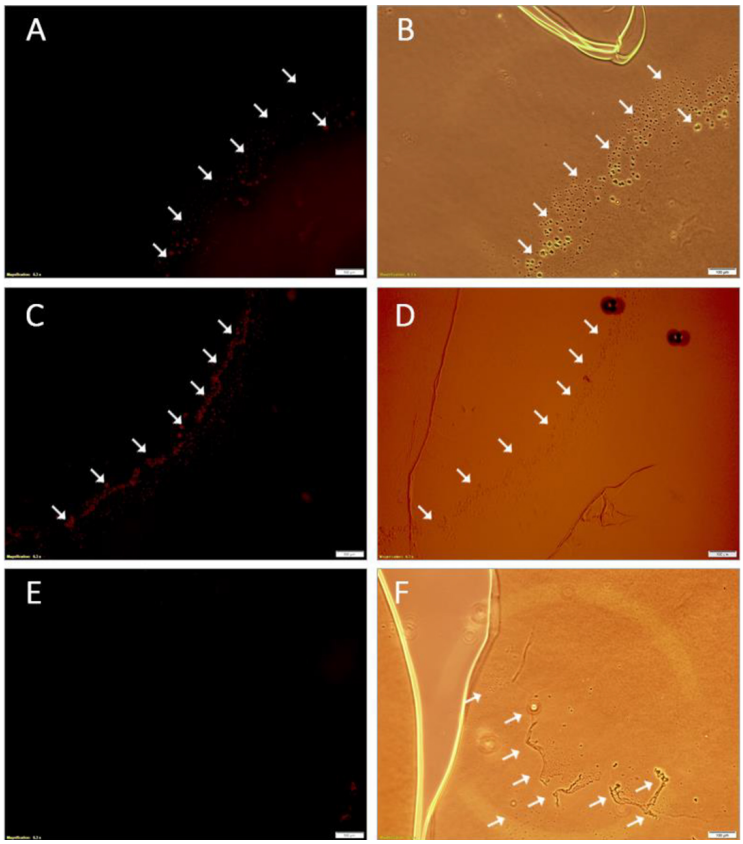

Figure 5.2: Localization of labeled phage-displayed peptides on the human lens capsule having XFS materials. M13 phages with XFS material-targeting peptides displayed on coat protein pIII and wild-type M13 phages were labeled with Cy5 fluorescent dye and incubated with human lens capsule containing XFS materials. Phages with displayed p-LPS (**A**) and p-IPL (**C**) peptides on their surface and labeled with Cy5 dye were selectively bound to the XFS materials on the lens capsule. Wild-type phages labeled with Cy5 dye (control) did not show any specific interaction with XFS materials (**E**). The presence of XFS materials on the lens capsule was confirmed in the bright field mode of the microscope (**B**, **D**, and **F**). Arrows show the exfoliative zones on the human lens capsule. (Scale bars = 100 μm).

5.3.3 Peptide-particle conjugation

Conjugation of alkyne-modified peptides to azide-functionalized MPs (Fig. 5.3A) was confirmed with surface zeta potential measurements, Fourier-transform infrared spectroscopy (FTIR), and a competitive inhibition assay. Peptide tethering through the N-terminal domain was expected to yield an increase in negative charge on the surface of the MPs, as was observed (Fig. 5.3B). FTIR spectrum from MPs before conjugation to peptides showed a transmittance peak around 2071 cm^{-1}, which is due to the asymmetric stretching

vibration of the free azide groups (Figs. 5.3C. a). The free azide group was absent in the spectra of peptide-conjugated MP samples due to the conversion of free azide groups to triazole ring during azide-alkyne cycloaddition (Figs. 5.3C. b, c). The peak observed at 1647 cm^{-1} in p-IPL could represent carbonyl groups of amide bonds of the peptide (Figs. 5.3C. b). The bands at wavelengths between 1400-1650 cm^{-1} correspond to aromatic rings found on p-LPS. (Figs. 5.3C. c).

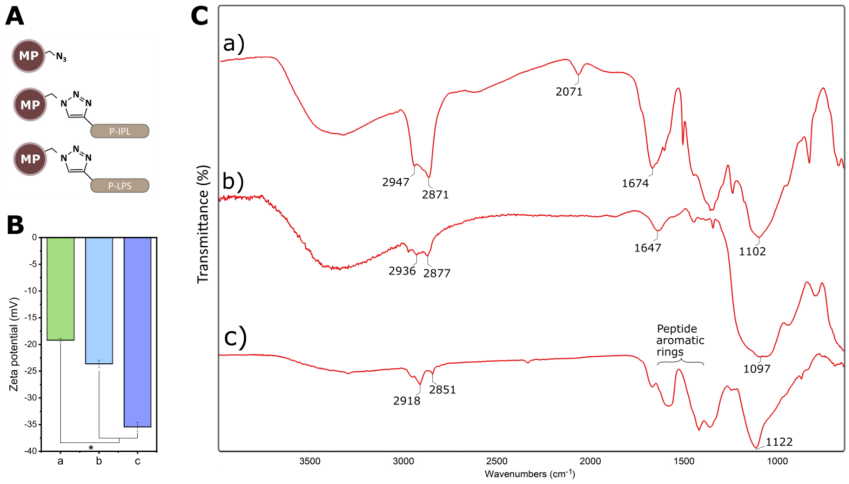

Figure 5.3: Conjugation of peptides to MPs. (**A**) Schematic illustration of MPs with and without peptide conjugates. (**B**) Surface zeta potential measurements and (**C**) FTIR spectra of MPs before and after peptide conjugation to MPs. a) Azide-functionalized MPs without peptide conjugates, b) MP-p-IPL, c) MP-p-LPS. (* represents $p < 0.05$, data represent mean $\pm$ 1 SD, $n \geq 3$).

Conjugation of peptides to MPs was confirmed by labeling particles with or without conjugated peptides with an azide-reactive dye (TAMRA alkyne fluorophore), where subsequent fluorescence indicated that unreacted azides were present on the MP surface (Fig. 5.4). MPs were reacted with p-IPL (Fig. 5.4B) or p-LPS peptides (Fig. 5.4C), those MPs had no fluorescence compared to the control MPs that had no conjugated peptides (Fig. 5.4).

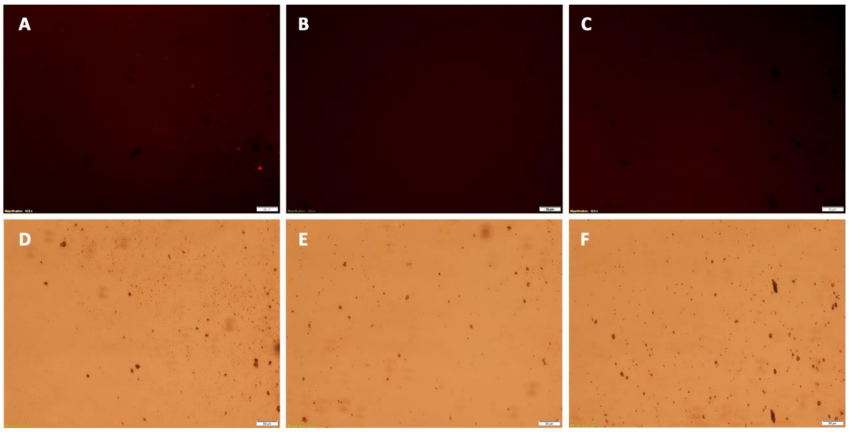

Figure 5.4: Competitive labeling of MPs with TAMRA dye. Peptide-conjugated MPs and azide-functionalized MPs without conjugated peptides were labeled with TAMRA dye. (**A**, **D**) Control particle clumps having free azide groups showed noticeably higher fluorescence under the microscope. MPs conjugated to p-IPL (**B**, **E**) and p-LPS (**C**, **F**) showed almost no fluorescence under the microscope. Top images were taken in the fluorescence mode using TRITC filter and bottom images were taken in the bright field mode to confirm the presence of particles and clumps of particles. (Scale bars = 50 μm).

5.3.4 Targeting capability of MP-peptide conjugates

It is important to note that although there might be patient-to-patient variations in the XFS deposition pattern on the lens capsule, generally it is distributed with a non-XFS intermediate zone that separates exfoliative central and peripheral zones (Fig. 5.5A) [11]. Specific targeting of XFS materials was evaluated through incubating MP-p-IPL, MP-p-LPS, MP-scrambled peptides (control), or unmodified MP (control) with XFS affected lens capsules in equal volume of extracted aqueous humor fluid and BSS irrigating solution at 37 °C. Specific binding of MP-p-IPL and MP-p-LPS to XFS materials was observed (Figs. 5.5B, C). This confirms that MP-peptide conjugates resulted in similar binding patterns as that observed for just fluorescently labeled phage-displayed peptides (Fig. 5.2), whereas scrambled peptide complexes showed a non-specific binding, where the whole surface of the lens capsule having both XFS and non-XFS area was covered with MPs (Fig. 5.5D, E). The other control experiment using virgin MPs resulted in MP being clumped together on the central zone (Fig. 5.5F).

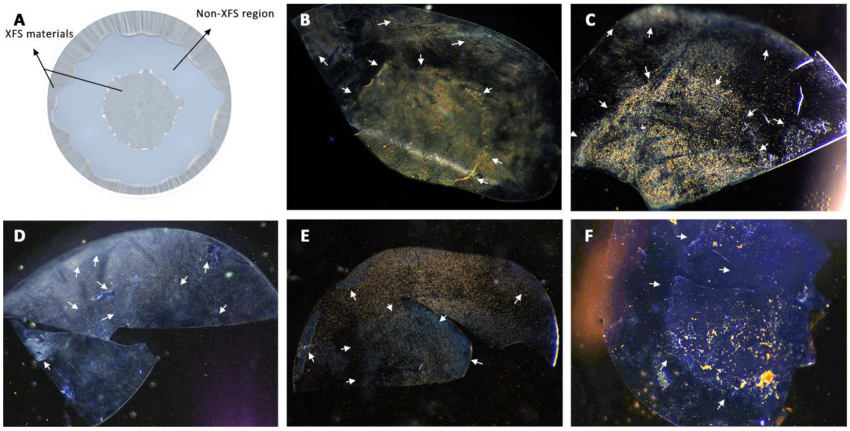

Figure 5.5: Targeting of XFS materials on the surface of the human lens capsule with MP-peptide conjugates. (**A**) Illustration of the anterior lens capsule showing general pattern of XFS deposits on its surface. (**B**) MP-p-IPL showed specific binding to XFS deposits on both central and the peripheral zones of tissue having XFS materials. The non-XFS area of lens capsule (blank spots) showed less or no particles compared to the exfoliated area. (**C**) MP-p-LPS also showed specific targeting of XFS materials on the surface of the lens capsule. (**D**) Scrambled MP-p-IPL interacted non-specifically with both XFS deposits and the area of lens capsule surface without XFS deposits. (**E**) Scrambled MP-p-LPS also showed non-specific interaction with XFS materials. (**F**) MP without peptide conjugates. As shown in the image, there is a high amount of XFS materials on the central part of the human lens capsule, however, there is not enough binding of MPs to the XFS area. Arrows indicate approximate regions of XFS materials in each tissue sample.

5.3.5 Effect of magnetic field on the XFS materials

Micron-sized, iron oxide particles were used as they are the only metal oxide particle clinically approved for biomedical applications, less susceptible to nonspecific cellular uptake or vascular egress, rapidly cleared (< 5 min) by the liver and spleen, and have a high labeling valency that enhances their binding affinity to the molecular targets [21, 26-29]. These particles are biodegradable, where particles (> 150 nm) are captured by phagocytic cells and their coating cleaved by lysosomal enzymes, and the iron oxide core is degraded into iron and oxygen through mechanisms involved in iron metabolism [30, 31].

Magnetic pin test

A metallic pin with a tip size similar to a 23-gauge needle was magnetized by attaching it to the surface of a permanent magnet with a field strength

at the pole of ∼5000 G. This magnetic pin was used to determine if it was possible to remove the MP-bound XFS fibrils via a magnetic field. Although the magnetic force generated at the tip of the pin was not strong enough to remove XFS aggregates, it was strong enough to pull them in the direction of the applied field (Figs. 5.6A-C). This effect was not observed using non-magnetic needles (Figs. 5.6D-F). In some studied lens capsules, it was also observed that magnetic pins were able to start pulling off the XFS materials along the edges of XFS deposits. This pulling force was not strong enough to remove XFS deposits from the surface of the lens capsule, however, it showed that XFS materials were clearly affected in the direction of the applied magnetic field (Figs. 5.6G, H). That said, these results showed that a magnetic pin could be used to collect detached aggregates of XFS materials from the anterior chamber of the eye.

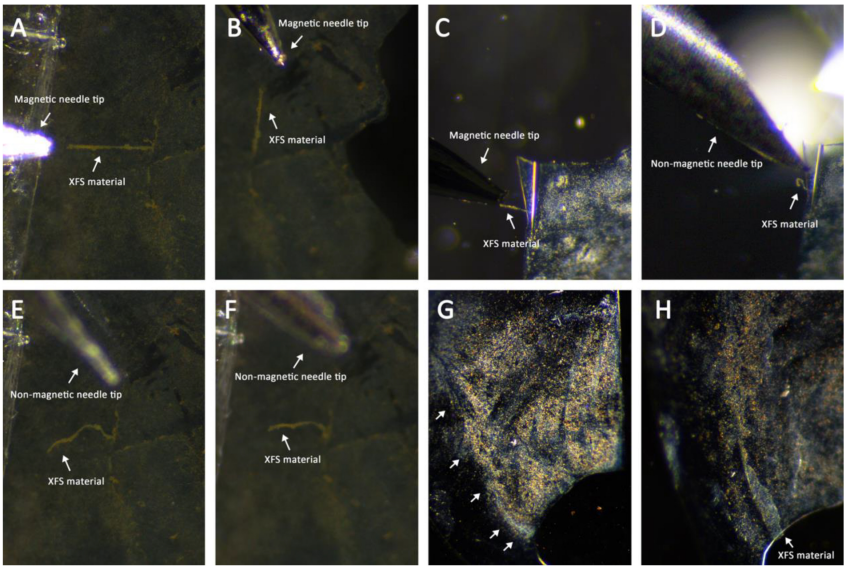

Figure 5.6: Effect of magnetic pins on the magnetized XFS materials. Human lens capsules having XFS materials were incubated with MP-peptide conjugates and subsequently, magnetic behavior of XFS aggregates was studied using magnetic and non-magnetic tools. (**A**, **B**) Large aggregates of XFS materials covered with MP-p-IPL were pulled by magnetic pin in different directions. (**E**, **F**) Control studies with non-magnetic needles showed that XFS materials covered with MP-p-IPL did not react to the non-magnetic tool. (**C**) XFS materials in the center of lens capsule covered with MP-p-LPS were attracted to the magnetic pin. However, in the absence of a magnetic field (i.e. non-magnetic needle) no attraction was observed. (**G**) XFS materials in the center of the human lens capsule covered with MP-peptide conjugates before application of magnetic pin. (**H**) Edges of the same XFS deposits in the central zone of the lens capsule being pulled towards the applied magnetic field through a magnetized pin.

Rotating magnetic field studies

Using the same experimental strategy, a rotating magnetic field was used to determine if it was possible to agitate XFS materials and liberate them from the lens capsule. It has been shown that the oscillation of disk-shaped MPs via low-frequency rotating magnetic fields that produced a uniform 10000 G magnetic field could generate enough destructive force to induce cancer cell death [21]. In this work, *ex vivo* studies were conducted using spherical MPs in combination with a 5000 G uniform magnetic field to generate mechanical force for the removal of XFS deposits. Magnetic field-treated tissues were then irrigated with BSS buffer to observe any possible aid in further removal of XFS materials from the tissues.

Ex vivo studies using a Halbach array showed that the mechanical force generated using MPs under the rotating magnetic field was strong enough to agitate and remove most of the XFS materials from the surface of the lens capsule (Fig. 5.7). Subsequent irrigation further aided in the removal of some remaining XFS materials from the surface of the tissue. As an example, a lens capsule with central zone deposits that was bound to MP-p-IPL particles (Fig. 5.7D) showed a large amount of XFS removal upon applying the rotating magnetic field (Fig. 5.7DII). Another tissue having XFS deposits on both central and peripheral zones (Fig. 5.7E), bound with MP-p-IPL particles, showed that the application of the rotating magnetic field removed aggregates from both zones of the tissue (Fig. 5.7EII). MP-p-IPL bound materials on a lens capsule with XFS deposits on the central zone had all large XFS aggregates removed only through the magnetic field (Fig. 5.7F). However, this tissue had a dense amount of cataractous materials on the posterior side of the lens capsule, which caused the attachment of MPs to those materials making the evaluation difficult. Therefore, although not as visually effective as the previous tissues, the rotating magnetic field was still actually effective in the removal of the large XFS aggregates form the surface of that lens capsule (Fig. 5.7FII). Lens capsules shown in (Figs. 5.7G and H) were exposed to MP-p-LPS conjugates and treated with the rotating magnetic field. The central zone of one sample (Fig. 5.7G) was lost due to surgery, however, XFS materials on the lens surface were mostly removed after applying the rotating magnetic field (Fig. 5.7GII). The rotating field was also effective in removing some of XFS aggregates from the other tissue (Fig. 5.7H) incubated with MP-p-LPS. In this case, the peripheral zone of the tissue was mostly cut out of the images due to the coverslips used for holding the tissue in place during irrigation. Irrigation of BSS buffer over the tissue was shown to be effective in removing some XFS aggregates from the surface of the lens capsule (Figs. 5.7D-H). The

control tissues that were treated with the rotating magnetic field showed almost no removal of XFS materials (Figs. 5.7A-C). Due to the tissue handing difficulties, we could not do BSS irrigation on one of the control tissues (Fig. 5.7C). XFS materials being partially lost in the control lens capsule shown in (Fig. 5.7BIII) was not due to the effect of magnetic field and sample handing led to that. The control lens capsule shown in (Fig. 5.7A) showed a very little removal of XFS aggregates during BSS irrigation and no effect was observed after treating with rotating magnetic field (Fig. 5.7AIII).

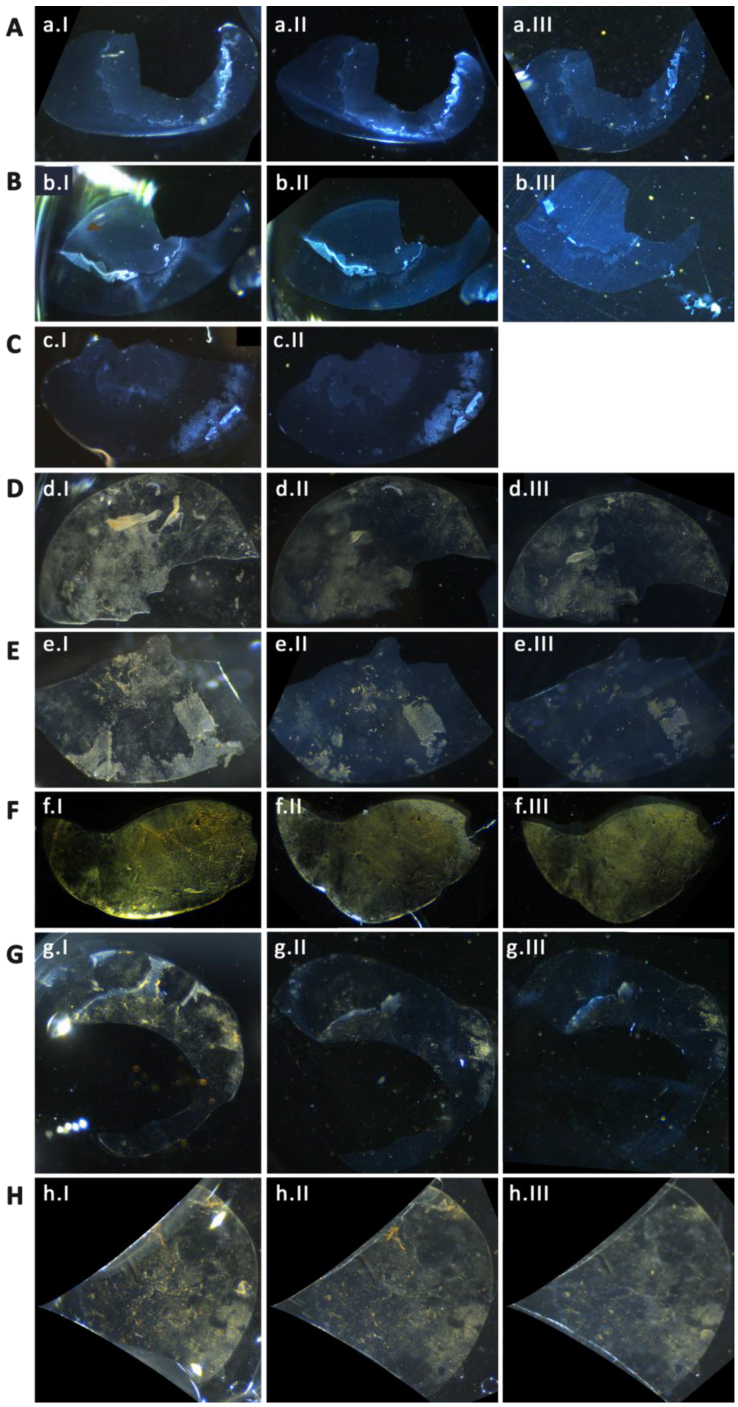

Figure 5.7: Effect of rotating magnetic field on XFS materials. (**A**-**C**) Control XFS lens capsules treated with rotating magnetic field without MPs. (**D**-**F**) XFS lens capsules interacted with MP-p-IPL. (**G**, **H**) XFS lens capsules interacted with MP-p-LPS. In each raw, images numbered as "I" represent tissues before treated with rotating magnetic field, images numbered as "II" represent XFS lens capsule after 3 hr treatment with rotating magnetic field, and images numbered as "III" represent lens capsules after buffer irrigation over the tissue.

To better evaluate the effectiveness of the observed rotating magnetic field, images of tissues before and after applied magnetic field and irrigation (Fig. 5.7), were analyzed based on the intensity of the lens capsule surface before and after each test (Fig. 5.8).

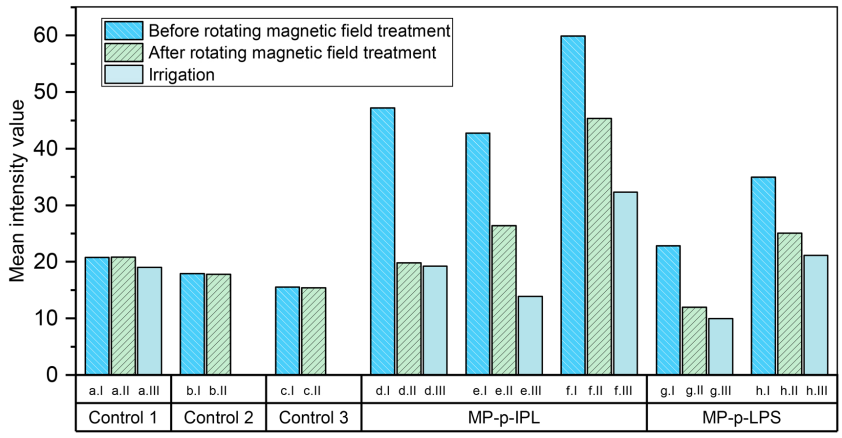

Figure 5.8: Mean intensity measurements of XFS lens capsules incubated with MP-peptide conjugates. (**Control 1-Control 3**) Control tissues incubated with BSS and treated with rotating magnetic field. (**MP-p-IPL**) Representative mean intensity values measured using images of XFS lens capsules interacted with MP-p-IPL. (**MP-p-LPS**) Mean intensity values of different lens capsules interacted with MP-p-LPS. Both groups of graphs related to test samples showed that intensities were decreased due to the removal of XFS materials from the surface of lens capsules. In each graph, column "I" represents intensity value of the images of the surface of lens capsule before treating with rotating magnetic field, column "II" represents values after 3 hr treatment with the rotating magnet, and column "III" represents intensities after applying BSS irrigation over the control XFS lens capsules. In all images, intensity values have been reported after background subtraction.

5.3.6 Cytotoxicity studies of MP-peptide conjugates

Prior to toxicity studies, the common phenotypic features of cultured hTM cells were assessed using immunohistochemical studies (Appendix 1, Fig. A3). The *in vitro* cytotoxicity of peptides in free and MP-conjugated form was evaluated against obtained hTM cells using live/dead cell viability assay, MTT assay, and DNA cleavage. All *in vitro* cell assays showed that both free peptide and MP-peptide particles were not toxic in the concentrations studied, as detailed below.

Live/Dead cell viability assay performed on hTM monolayers

XFS-specific peptides in both solution free or MP bound form were incubated with hTM cells and their cytotoxic effects assessed. It was found that both MP-p-IPL and MP-p-LPS constructs were not toxic in the concentrations studied. Green represents live cells and red represents dead cells in (Fig. 5.9). Confluent cultured cells were incubated with 50 μg and 100 μg of MP-p-IPL or MP-p-LPS (Figs. 5.9B-E). hTM monolayers were also incubated with 1 mM of p-IPL or p-LPS peptide solutions, and their viability was analyzed in a similar way as the MP-peptide constructs. As seen in the case of MP-peptide conjugates, free peptides were not toxic in used concentrations (Figs. 5.9K, N, and Table 5.1). Live/dead assay of hTM cells treated with rotating magnetic field also showed that cells incubated with MP-peptide conjugates did not show significant loss compared to control cells incubated with water (Table 5.2). Because of the sensitivity of hTM cells, it was not possible to treat cells with a rotating magnetic field outside of a CO_2 regulated atmosphere for longer than 10 min. That said, even control cells showed significant loss upon removal from the CO_2 incubator, thus, an optimal 10 min exposure to the magnetic field was chosen to evaluate the viability of cells in the presence of rotating magnetic field (Table 5.2).

MP-peptide conjugates		Free peptide solution	
Sample	% of live cells	Sample	% of live cells
Control	99.01 ± 0.51	Control	99.36 ± 0.36
MP-p-IPL (50 μg)	99.60 ± 0.18	1 mM p-IPL	99.00 ± 0.37
MP-p-IPL (100 μg)	99.66 ± 0.07	1 mM p-LPS	99.12 ± 0.94
MP-p-LPS (50 μg)	99.58 ± 0.20		
MP-p-LPS (100 μg)	98.47 ± 1.46		

Table 5.1: Live/dead assay performed on hTM monolayers treated with MP-peptide conjugates and free peptide solution. No statistical significant difference ($P < 0.05$) was found between studied groups. (Data represent mean ± 1 SD, $n \geq 3$).

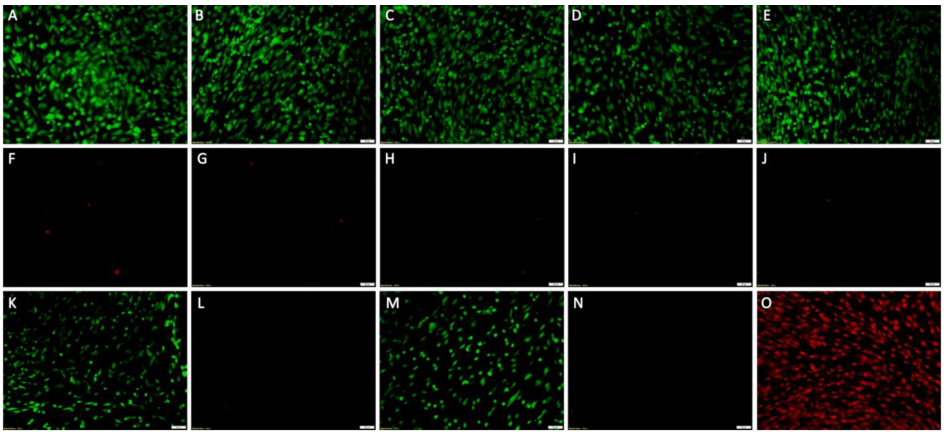

Figure 5.9: Cell viability (live/dead) assay of hTM cells incubated with free peptide and MP-peptide constructs. Calcein AM (CAM)/ EthD-1 system: Calcein AM detects cellular esterase activity of live cells, EthD-1 stains nuclei of dead cells. The green cells are live (CAM) and red cells are dead cells (EthD-1). (**A**, **F**) Control cells treated with water (without MPs). (**B**, **G**) hTM cells incubated with 50 μg MP-p-IPL for 24 hr. (**C**, **H**) hTM cells incubated with 100 μg MP-p-IPL for 24 hr. (**D**, **I**) hTM cells incubated with 50 μg MP-p-LPS for 24 hr. (**E**, **J**) hTM cells incubated with 100 μg MP-p-IPL for 24 hr. (**K**, **L**) hTM cells treated with 1 mM free p-IPL peptide solution (without MPs). (**M**, **N**) hTM cells treated with 1 mM free p-LPS peptide solution (without MPs). (**O**) All cells dead (methanol treated). Each treatment included three biological and three technical replicates. (Scales bars = 50 μm).

MP-peptide conjugates	
Sample	% of live cells
Control	98.74 ± 0.45
MP-p-IPL (100 μg)	98.53 ± 1.10
MP-p-LPS (100 μg)	98.88 ± 0.51

Table 5.2: Live/dead assay performed on hTM monolayers incubated with MP-peptide conjugates and treated under 10 min rotating magnetic field. No statistical significant difference ($P < 0.05$) was found between studied groups. (Data represent mean ± 1 SD, $n \geq 3$).

MTT cell proliferation assay

hTM cell proliferation in the presence of solution free and MP bound peptides was conducted using the MTT colorimetric assay. A one-way ANOVA test showed that no significant difference ($p < 0.05$) was observed between the absorbance of hTM cells treated with MP-peptide conjugates or solution free peptides compared to control cells treated with water (Fig. 5.10). The results confirmed that both sets of test samples did not suppress the proliferation of hTM cells.

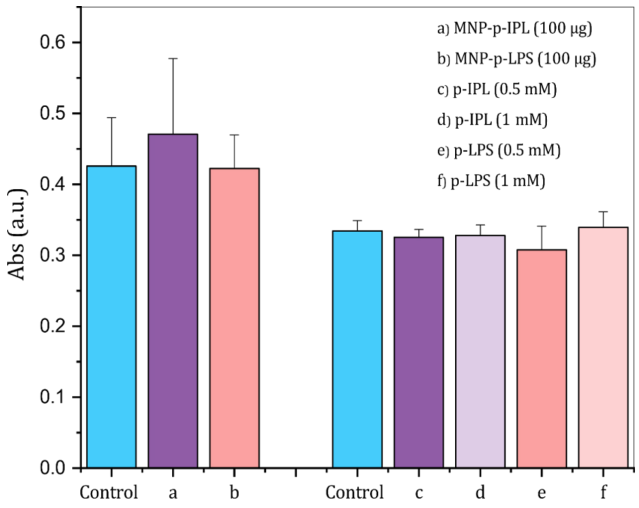

Figure 5.10: MTT colorimetric assay of viable hTM cells in the presence of XFS-specific peptides in free and conjugated form. (Left) MTT assay conducted using peptide-conjugated MPs. (Right) MTT assay results after incubation of hTM cells for 24 hr with 0.5 mM and 1 mM free peptide solutions. The optical density was measured at 570 nm after 24 hr incubation of hTM cells with each test sample. (Data represent mean $\pm$ 1 SD, $n \geq 3$, no statistical difference was observed between the means).

DNA fragmentation

Effect of free and conjugated XFS-targeting peptides on the induction of apoptosis was investigated *via* chromosomal DNA fragmentation analysis: DNA fragments indicate apoptosis induction. MP-peptide constructs, as well as solution free peptides, did not initiate apoptosis for hTM cells; chromosomal DNA remained intact after 24 hr incubation with MP-p-IPL, MP-p-LPS, p-LPS, or p-IPL solutions (Fig. 5.11).

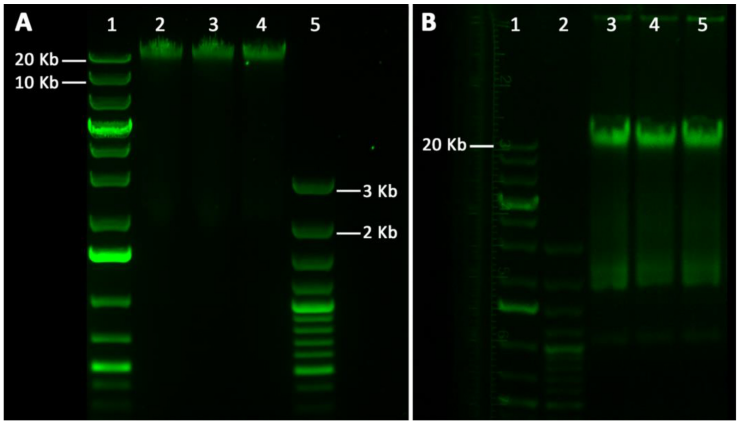

Figure 5.11: Electrophoretic analyses of the apoptotic chromosomal DNA fragmentation of hTM cells. (**A**) Isolated DNA from hTM cells after being incubated with MP-peptide conjugates for 24 hr. lane 1: 1 Kb plus DNA ladder, lane 2: Control, hTM cells treated with water, lane 3: Extracted DNA of hTM cells incubated with 100 μg MP-p-IPL for 24 hr, lane 4: Extracted DNA of hTM cells incubated with 100 μg MP-p-LPS for 24 hr, lane 5: 100 bp plus DNA ladder. (**B**) Isolated DNA from hTM cells incubated with free XFS-targeting peptide solutions. Lane 1: 1 Kb plus DNA ladder, lane 2: 100 bp plus DNA ladder, lane 3: Control, hTM cells treated with water, lane 4: hTM cells incubated with 1mM MP-p-IPL for 24 hr, lane 4: hTM cells incubated with 1mM MP-p-LPS for 24 hr.

Cell uptake studies using electron microscopy

One of the key functions of trabecular cells is the phagocytosis of foreign materials and extracellular debris [32], a cellular function also observed *in vitro* [33]. The internalization of MP-peptide constructs into hTM cells may lead to cell death if exposed to an oscillating magnetic field. Thus, hTM cells were incubated for 2 hr with 100 μg of each of MP-p-IPL or MP-p-LPS and TEM micrographs showed that individual particles were taken up by hTM cells (Fig. 5.12B), and some particles were engulfed by hTM cells (Figs. 5.12E, F). Aggregates of both MP-p-IPL and MP-p-LPS particles were observed outside of cultured hTM cells as well (Figs. 5.12C, D). Individual particles, as well as aggregated MPs, were also observed in SEM micrographs of regions surrounding cultured hTM cells (Figs. 5.12G, H). It seems that MPs in large aggregates have less propensity to enter the cultured cells. It has been previously shown that intravitreal or anterior chamber injection of magnetic nano- and microparticles had almost no signs of effect on retinal morphology,

photoreceptor function or IOP in the anterior chamber of animal models [34]. Regardless, according to different cell viability assays conducted in this study, no statistical difference was observed for cell mortality upon incubation with MPs in cultured hTM cells.

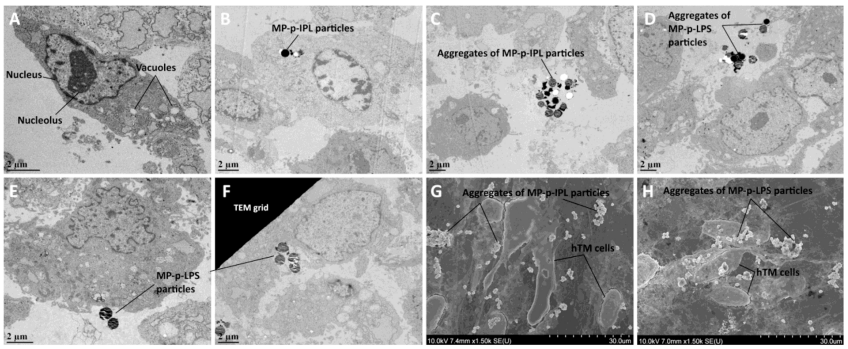

Figure 5.12: Electron micrographs of hTM cells incubated with MP-peptide conjugates. (**A**-**F**) TEM micrographs. (**G**, **H**) SEM micrographs. hTM cells were incubated with 100 μg of MP- peptide conjugates for 2 hr. (**A**) Control hTM cells incubated with water. (**B**) MP-p-IPL particles located inside the hTM cells. (**C**) Aggregates of MP-p-IPL particles located outside of the cells. (**D**, **E**) Aggregates of MP-p-LPS particles located outside of hTM cells. (**F**) MP-p-LPS particles being engulfed by the hTM cell. Black dirt between particles could be trapped dye molecules. (**G**) SEM micrograph showing aggregates of MP-p-IPL particles around hTM cells. (**H**) SEM micrograph of MP-p-LPS particles located around the hTM cells.

5.4 Conclusions

This study set out to identify small peptides having a selective affinity to XFS materials in the human eye. An *ex vivo* panning procedure was developed to explore targeting peptides for the XFS materials using the phage display technique. The selective affinity of phage-displayed peptides was confirmed through ex vivo studies using human lens capsule and fluorescently labeled phages. XFS-targeting peptides were successfully conjugated to MPs using azide-alkyne cycloaddition click chemistry. FTIR analysis and zeta potential measurements were used to confirm the conjugation of peptides to MPs. Competitive labeling of MPs using alkyne-modified fluorophore was also used to confirm the attachment of peptides to the particles. Targeting capability of

MP-peptide complexes to XFS materials was studied ex vivo in the same experimental conditions that phage panning was conducted. Compared to the scrambled peptide sequences, the identified XFS-targeting peptide conjugates showed selective and high affinity to XFS materials on the human lens capsule. Although XFS materials have been clinically characterized with a general deposition pattern on the lens capsule, there are variations from patient to patient, considering those variations, results of the ex vivo experiments showed that the identified peptides had acceptable selective binding to XFS materials in most of the lens capsule areas associated with XFS materials. The effect of the magnetic pin and rotating magnetic field on the behavior of magnetized XFS materials was observed under the stereomicroscope. A low frequency rotating magnetic field which was producing a uniform magnetic field across the designed system provided suitable conditions to remove most of the XFS aggregates form the surface of lens capsules. Biocompatibility of free peptides and corresponding MP conjugates was confirmed using MTT cell toxicity assay and live/dead cell proliferation assay. DNA fragmentation studies also showed that either MP-peptide conjugates or free peptide solutions did not induce apoptotic cellular death in hTM cells. Electron microscopy studies showed that compared to the particles being in aggregated form, individual particles were more likely to be uptaken by the cultured hTM cells. Considering targeting evaluation findings and biocompatibility studies results, MP-peptide conjugates having specific affinity to XFS materials could provide a useful tool in the development of a therapeutic system for XFS. Where, removal of large deposits of XFS aggregates from the anterior chamber of affected eyes might help in long term management of exfoliation glaucoma.

5.5 Acknowledgements

We gratefully thank Dr. Andrew Crichton, Dr. Anne MacDonald, and Dr. Rehan Riyaz for providing human lens capsule tissue samples for this study. We also gratefully thank all staff and nurses in the operating room of the Royal Alexandra Hospital (Edmonton, AB, Canada) as well as at the Rockyview Hospital (Calgary, AB, Canada) for their assistance in sample collection. We are also grateful to all patients who consented to participate in the study.

5.6 References

[1] R. Ritch, "Exfoliation syndrome-the most common identifiable cause of open-angle glaucoma.," *J. Glaucoma*, vol. 3, no. 2, pp. 176–177, 1994.

[2] M. Davanger, "The pseudo-exfoliation syndrome. A scanning electron microscopic study. I. The anterior lens surface.," *Acta Ophthalmol.*, vol. 53, no. 6, pp. 809–820, Dec. 1975.

[3] M. Ghosh and J. S. Speakman, "The ciliary body in senile exfoliation of the lens.," *Can. J. Ophthalmol.*, vol. 8, no. 3, pp. 394–403, Jul. 1973.

[4] J. P. Harnisch, "Exfoliation material in different sections of the eye.," *Albrecht Von Graefes Arch. Klin. Exp. Ophthalmol.*, vol. 203, no. 3–4, pp. 181–190, Sep. 1977.

[5] U. Schlötzer-Schrehardt, M. Küchle, and G. O. Naumann, "Electron-microscopic identification of pseudoexfoliation material in extrabulbar tissue.," *Arch. Ophthalmol.*, vol. 109, no. 4, pp. 565–570, 1991.

[6] B. W. Streeten, S. A. Gibson, and A. J. Dark, "Pseudoexfoliative material contains an elastic microfibrillar-associated glycoprotein.," *Trans. Am. Ophthalmol. Soc.*, vol. 84, pp. 304–320, 1986.

[7] R. Ritch, U. Schlötzer-Schrehardt, and A. G. P. Konstas, "Why is glaucoma associated with exfoliation syndrome?," *Prog. Retin. Eye Res.*, vol. 22, no. 3, pp. 253–275, 2003.

[8] G. Hollo, A. Katsanos, and A. G. Konstas, "Management of exfoliative glaucoma: challenges and solutions.," *Clin. Ophthalmol.*, vol. 9, pp. 907–919, 2015.

[9] I. F. Aboobakar, W. M. Johnson, W. D. Stamer, M. A. Hauser, and R. R. Allingham, "Major review: Exfoliation syndrome; advances in disease ge-

netics, molecular biology, and epidemiology," *Exp. Eye Res.*, vol. 154, pp. 88–103, 2017.

[10] R. Ritch, "Ocular and systemic manifestations of exfoliation syndrome," *J. Glaucoma*, vol. 23, no. 8, pp. S1–S8, 2014.

[11] R. Ritch and U. Schlötzer-Schrehardt, "Exfoliation syndrome," *Surv. Ophthalmol.*, vol. 45, no. 4, pp. 265–315, 2001.

[12] E. Elhawy, G. Kamthan, C. Q. Dong, and J. Danias, "Pseudoexfoliation syndrome, a systemic disorder with ocular manifestations.," *Hum. Genomics*, vol. 6, p. 22, Oct. 2012.

[13] M. Citirik, G. Acaroglu, C. Batman, L. Yildiran, and O. Zilelioglu, "A possible link between the pseudoexfoliation syndrome and coronary artery disease.," *Eye (Lond).*, vol. 21, no. 1, pp. 11–15, Jan. 2007.

[14] K. A. Gonen, T. Gonen, and B. Gumus, "Renal artery stenosis and abdominal aorta aneurysm in patients with pseudoexfoliation syndrome.," *Eye (Lond).*, vol. 27, no. 6, pp. 735–741, Jun. 2013.

[15] Z. Ma et al., "Phage display-derived oligopeptide-functionalized probes for in vivo specific photoacoustic imaging of osteosarcoma.," *Nanomedicine*, vol. 13, no. 1, pp. 111–121, Jan. 2017.

[16] A. K. Sato, M. Viswanathan, R. B. Kent, and C. R. Wood, "Therapeutic peptides: technological advances driving peptides into development.," *Curr. Opin. Biotechnol.*, vol. 17, no. 6, pp. 638–642, Dec. 2006.

[17] C. K. Kang, V. Jayasinha, and P. T. Martin, "Identification of peptides that specifically bind Abeta1-40 amyloid in vitro and amyloid plaques in Alzheimer's disease brain using phage display.," *Neurobiol. Dis.*, vol. 14, no. 1, pp. 146–156, Oct. 2003.

[18] B. P. Orner, L. Liu, R. M. Murphy, and L. L. Kiessling, "Phage display af-

fords peptides that modulate beta-amyloid aggregation," *J. Am. Chem. Soc.*, vol. 128, no. 36, pp. 11882–11889, 2006.

[19] U. R. Chowdhury, B. J. Madden, M. C. Charlesworth, and M. P. Fautsch, "Proteome analysis of human aqueous humor.," *Invest. Ophthalmol. Vis. Sci.*, vol. 51, no. 10, pp. 4921–4931, Oct. 2010.

[20] C. Sun, J. S. H. Lee, and M. Zhang, "Magnetic nanoparticles in MR imaging and drug delivery.," *Adv. Drug Deliv. Rev.*, vol. 60, no. 11, pp. 1252–1265, Aug. 2008.

[21] Y. Cheng et al., "Rotating magnetic field induced oscillation of magnetic particles for in vivo mechanical destruction of malignant glioma.," *J. Control. Release*, vol. 223, pp. 75–84, Feb. 2016.

[22] K. A. Kelly, P. Waterman, and R. Weissleder, "In vivo imaging of molecularly targeted phage.," *Neoplasia*, vol. 8, no. 12, pp. 1011–1018, Dec. 2006.

[23] S. I. Presolski, V. P. Hong, and M. G. Finn, "Copper-Catalyzed Azide–Alkyne Click Chemistry for Bioconjugation.," *Curr. Protoc. Chem. Biol.*, vol. 3, no. 4, pp. 153–162, 2011.

[24] W. M. Saltzman, Tissue engineering: engineering principles for the design of replacement organs and tissues. *Oxford University Press*, 2004.

[25] J. J. Heys and V. H. Barocas, "A boussinesq model of natural convection in the human eye and the formation of Krukenberg's spindle.," *Ann. Biomed. Eng.*, vol. 30, no. 3, pp. 392–401, Mar. 2002.

[26] A. K. Hauser, R. J. Wydra, N. A. Stocke, K. W. Anderson, and J. Z. Hilt, "Magnetic nanoparticles and nanocomposites for remote controlled therapies," *J. Control. Release*, vol. 219, pp. 76–94, 2015.

[27] M. Chirita, M. L. Kiss, and C. Savii, "Magnetite, Properties and Modern Biomedical Applications," in Magnetite: Synthesis, Uses and Biological Oc-

currences, *J. Ward, Ed. Nova Science Publishers, Inc.*, 2014, pp. 119–181.

[28] N. Zarghami et al., "Optimization of molecularly targeted MRI in the brain: empirical comparison of sequences and particles.," *Int. J. Nanomedicine*, vol. 13, pp. 4345–4359, 2018.

[29] N. Singh, G. J. S. Jenkins, R. Asadi, and S. H. Doak, "Potential toxicity of superparamagnetic iron oxide nanoparticles (SPION)," *Nano Rev.*, vol. 1, p. 10.3402/nano.v1i0.5358, 2010.

[30] L. H. Reddy, J. L. Arias, J. Nicolas, and P. Couvreur, "Magnetic nanoparticles: design and characterization, toxicity and biocompatibility, pharmaceutical and biomedical applications.," *Chem. Rev.*, vol. 112, no. 11, pp. 5818–5878, Nov. 2012.

[31] H. E. Daldrup-Link, "Ten things you might not know about iron oxide nanoparticles," *Radiology*, vol. 284, no. 3, pp. 616–629, 2017.

[32] W. D. Stamer and A. F. Clark, "The many faces of the trabecular meshwork cell.," *Exp. Eye Res.*, vol. 158, pp. 112–123, May 2017.

[33] J. R. Polansky, I. S. Wood, M. T. Maglio, and J. A. Alvarado, "Trabecular meshwork cell culture in glaucoma research: evaluation of biological activity and structural properties of human trabecular cells in vitro.," *Ophthalmology*, vol. 91, no. 6, pp. 580–595, Jun. 1984.

[34] H. B. Raju, Y. Hu, A. Vedula, S. R. Dubovy, and J. L. Goldberg, "Evaluation of magnetic micro- and nanoparticle toxicity to ocular tissues.," *PLoS One*, vol. 6, no. 5, p. e17452, 2011.

Chapter 6

Concluding remarks and perspectives

6.1 Major Conclusions

This research aimed to use oligopeptide-based targeting strategies to investigate their applicability for the development of non- or less-invasive treatment approaches for cataracts and XFS. To our knowledge, this is the first report of screening phage-displayed random peptide libraries to isolate targeting peptides for cataract and exfoliation syndrome.

Recombinantly expressed human βB2-crystallin protein was used to form model cataract aggregates under acidic denaturing conditions. Electron microscopy studies showed that formed protein aggregates had fibrillar structure. It has been previously shown that crystallin proteins extracted from bovine lens, formed amyloid-like structures *in vitro*, which exhibited structural patterns similar to amyloid fibrils [1]. Moreover, it has been shown that cataractous material excised from the human lens, contained amyloid β-sheet secondary structures [2]. In our work, amyloid dye-binding assays showed positive results, suggesting similarities between βB2-crystallin fibrillar aggregates and amyloid fibrils. Further analysis with XRFD showed that fibrils of βB2-crystallin followed the common core structural pattern of amyloid fibrils. Given the evidence that fibrillar aggregates are associated with cataract de-

velopment, we used phage display technique to identify targeting peptides for fibrils of βB2-crystallin, a major β-crystallin in the lens. The binding ability of identified phage displayed-peptides was investigated using the ELISA method. Further studies using synthesized peptides and competitive binding inhibition ELISA confirmed their high affinity to βB2-crystallin fibrils. It is thought that the identification of targeting peptides could offer treatment options for cataract through non-invasive techniques.

A similar objective was approached in the case of XFS, however, all experiments were conducted using human tissue samples including human lens capsule and aqueous humor. This allowed us to develop an *ex vivo* phage display approach to identify targeting peptides for XFS materials. All evaluation studies were also carried out using human tissue samples which confirmed the high specificity of identified targeting peptides.

In the first part of XFS research, two targeting peptides were identified after three rounds of *ex vivo* phage display. The binding ability of phage-displayed peptides was confirmed using fluorescently labeled phage particles where compared to wild-type M13 phages (i.e. without peptide inserts in their coat protein), a significant difference in binding to XFS materials on the surface of lens capsule was observed under the fluorescence microscope.

In the second part of the XFS study, we aimed to combine the targeting ability of identified peptides with unique properties of magnetic particles to develop a potential therapeutic system for removal of XFS fibrils from the human eye. Peptides were conjugated to magnetic particles *via* click reaction which is highly selective and can be carried out in the presence of various solvents over a wide range of pH and temperature [3]. FTIR analysis and surface zeta potential measurements confirmed the conjugation of peptides to magnetic particles. Conjugation was further evaluated using competitive labeling assay. Upon incubation with XFS lens capsules in a solution containing aque-

ous humor and same irrigation solution used during surgery, specific binding of MP-peptide conjugates was confirmed where both original MP-peptide conjugates were shown to be mostly bound to XFS deposits, however all studies conducted by controls (scrambled peptides) showed non-specific coverage of both XFS and non-XFS areas.

The behavior of magnetized XFS materials was studied using both static and rotating magnetic fields. It was shown that XFS materials interacted with targeting agents (MP-peptide conjugates) were pulled in different parts of the lens capsule towards magnetized pins. Further studies using a Halbach array magnet showed that the low-frequency rotating uniform magnetic field could provide enough mechanical force to remove most of the XFS deposits from the surface of the lens capsule.

In the third part of XFS research, we evaluated the biocompatibility of constructed peptide-particle conjugates as well as free peptides in solution using hTM cells. MTT cell proliferation and live/dead cell viability assays showed that identified peptides at both free and conjugated forms did not exhibit any cytotoxicity against cultured cells. DNA fragmentation studies also showed that targeting agents and peptide solutions did not induce apoptosis in trabecular meshwork cells. We also conducted electron microscopy studies over cells incubated with MP-peptide constructs to evaluate their possible internalization into the cells. It was shown that particles in aggregated form had less propensity to enter the cells, however, individual particles could be uptaken by cultured hTM cells. Given the fact that XFS is a progressive condition that accumulation of its aggregates could block the normal drainage of aqueous humor and induce XFG, findings of this study suggest that the designed peptide-based targeting approach could potentially provide a low cost and less-invasive therapy to remove the XFS aggregates form the anterior chamber of the eye. This could provide better long-term management over

IOP in XFS and XFG eyes. Besides, the removal of XFS aggregates from different surfaces of the anterior chamber of the affected eyes might help to better control other ocular complications associated with XFS.

In the fourth part of XFS related research, we aimed to study any possible structural polymorphism in the fibrillar aggregates associated with this disease. A non-destructive method was pursued to remove the XFS materials from the anterior side of the lens capsules obtained from different patients being at different stages of XFS. Electron microscopy studies showed structural polymorphism in XFS fibrils in different patients. Given the importance of structural diversity of disease-associated amyloid fibrils in understanding biological factors underlying the aggregation process, it is thought that this observation could lead to higher resolution studies on the physical properties of XFS fibrils which might help to better understand pathomechanism of this systemic disorder.

6.2 Future outlook

6.2.1 βB2-crystallin fibrils and cataract

The findings of *in vitro* model for cataract, suggest the possible role of identified targeting cyclic peptides to deliver therapeutic molecules into the lens. The binding ability of identified peptides could be evaluated using cataractous material excised from the human lens. It has been suggested that some small molecules or peptides might be able to block the fibrillation process [4], thus *in vitro* studies using these peptides and lens crystallin proteins under denaturing conditions might reveal their possible role in the inhibition of aggregation. It has been recently shown that mature human lenses with no diagnosable signs of cataract might contain amyloid fibrils, indicating that the fibrillation process starts before diagnoses [2]. Thus peptides of this sort having targeting

ability might be used for early diagnosis of cataract development. Moreover, targeting peptides might be able to bind to those very early formed fibrils and sequester them from further aggregation. Moreover, drug delivery into the lens is an emerging field of investigation to prevent cataract [5], further studies using these targeting peptides could improve targeted drug delivery into the lens. In the case of any therapeutic or diagnostic applications, cytotoxicity of these peptides should be evaluated.

6.2.2 Targeting of XFS fibrils

Although the cytotoxicity studies showed positive results using hTM cell lines, it will be essential to further investigate their possible risks and adverse effect on the other types of ocular cells such as corneal endothelium. It is also important to note that nano-particle based systems may not cause obvious cellular damage but result in changes in cellular function, thus before introducing this therapeutic approach as a viable candidate for clinical testing, any possible changes in cellular function should be further investigated [6, 7].

Due to the complexity of XFS and XFG, one of the major problems associated with studying these ocular conditions is the lack of animal models. However, there are some recent successes in generation animal models for XFS [8, 9]. Our engineered peptides could be applied in animal models for further investigations. Although it has been previously shown that magnetic micro- and nanoparticles could be safely used in the eye [10], ocular safety of designed particle-peptide conjugates could be further investigated using animal models. Furthermore, one of the important structures of the anterior chamber that its function is affected by XFS materials is the zonular apparatus [11]. Thus, given the possible zonular instability associated with XFS, this is of high importance to study the effect of our designed system on the stability of zonular fibers in XFS eyes. Study on zonular fibers needs using animal models

or autopsy eyes.

6.2.3 Structural diversity of XFS fibrils

It is thought that high-resolution insight into XFS fibrils could help to better understand different aspects of this systemic disease. Except for a few reports of using amyloid binding dyes on XFS tissues, the core structure of XFS fibrils is still unknown. To study the structural properties of XFS fibrils, the X-Ray microdiffraction technique, which has been previously used to study characteristics of fibrillar aggregates in different human tissue sections could be a useful technique [12, 13]. This technique might be useful to reveal information about the *in situ* architecture of fibrillar aggregates in XFS tissues. These studies could also be extended using two-dimensional infrared spectroscopy, which has been used successfully to identify amyloid β-sheet secondary structure in postmortem human lenses diagnosed with cataract [2].

6.3 References

[1] S. Meehan, Y. Berry, B. Luisi, C. M. Dobson, J. A. Carver, and C. E. MacPhee, "Amyloid Fibril Formation by Lens Crystallin Proteins and Its Implications for Cataract Formation," *J. Biol. Chem.*, vol. 279, no. 5, pp. 3413–3419, 2004.

[2] A. M. Alperstein, J. S. Ostrander, T. O. Zhang, and M. T. Zanni, "Amyloid found in human cataracts with two-dimensional infrared spectroscopy," *Proc. Natl. Acad. Sci.* U. S. A., vol. 116, no. 14, pp. 6602–6607, 2019.

[3] A. A. H. Ahmad Fuaad, F. Azmi, M. Skwarczynski, and I. Toth, "Peptide conjugation via CuAAC 'click' chemistry.," *Molecules*, vol. 18, no. 11, pp. 13148–13174, Oct. 2013.

[4] T. Hard and C. Lendel, "Inhibition of amyloid formation.," *J. Mol. Biol.*, vol. 421, no. 4–5, pp. 441–465, Aug. 2012.

[5] T. R. Thrimawithana, I. D. Rupenthal, S. S. Rasch, J. C. Lim, J. D. Morton, and C. R. Bunt, "Drug delivery to the lens for the management of cataracts.," *Adv. Drug Deliv. Rev.*, vol. 126, pp. 185–194, Feb. 2018.

[6] N. J. Kim et al., "Nanotechnology and glaucoma: a review of the potential implications of glaucoma nanomedicine.," *Br. J. Ophthalmol.*, vol. 98, no. 4, pp. 427–431, Apr. 2014.

[7] N. Lewinski, V. Colvin, and R. Drezek, "Cytotoxicity of nanoparticles.," *Small*, vol. 4, no. 1, pp. 26–49, Jan. 2008.

[8] S. W. M. John, J. M. Harder, J. H. Fingert, and M. G. Anderson, "Animal models of exfoliation syndrome, now and future.," *J. Glaucoma*, vol. 23, no. 8 Suppl 1, pp. S68-72, 2014.

[9] M. G. Anderson, K. J. Meyer, A. Hedberg-Buenz, and J. H. Fingert, "Up-

date on Animal Models of Exfoliation Syndrome.," *J. Glaucoma*, vol. 27 Suppl 1, pp. S78–S82, Jul. 2018.

[10] H. B. Raju, Y. Hu, A. Vedula, S. R. Dubovy, and J. L. Goldberg, "Evaluation of magnetic micro- and nanoparticle toxicity to ocular tissues.," *PLoS One*, vol. 6, no. 5, p. e17452, 2011.

[11] G. O. Naumann, U. Schlotzer-Schrehardt, and M. Kuchle, "Pseudoexfoliation syndrome for the comprehensive ophthalmologist. Intraocular and systemic manifestations.," *Ophthalmology*, vol. 105, no. 6, pp. 951–968, Jun. 1998.

[12] J. Liu et al., "Amyloid structure exhibits polymorphism on multiple length scales in human brain tissue.," *Sci. Rep.*, vol. 6, p. 33079, Sep. 2016.

[13] F. Briki et al., "Synchrotron x-ray microdiffraction reveals intrinsic structural features of amyloid deposits in situ.," *Biophys. J.*, vol. 101, no. 2, pp. 486–493, Jul. 2011.

References

Chapter 1

[1] G. A. Stevens et al., "Global prevalence of vision impairment and blindness: magnitude and temporal trends, 1990-2010.," *Ophthalmology*, vol. 120, no. 12, pp. 2377–2384, Dec. 2013.

[2] World Health Organization. "VISION2020: The Right to Sight. Global Initiative for the Elimination of Avoidable Blindness: *Action Plan* 2006–2011". 2007;1–97. World Health Organization Geneva, Switzerland.

[3] R. R. A. Bourne et al., "Magnitude, temporal trends, and projections of the global prevalence of blindness and distance and near vision impairment: a systematic review and meta-analysis," *Lancet. Glob. Heal.*, vol. 5, no. 9, pp. e888–e897, 2017.

[4] D. Pascolini and S. P. Mariotti, "Global estimates of visual impairment: 2010.," *Br. J. Ophthalmol.*, vol. 96, no. 5, pp. 614–618, 2012.

[5] World Health Organization. "Blindness and vision impairment," [Online]. Available: https://www.who.int/news-room/fact-sheets/detail/blindness-and-visual-impairment.

[6] G. W. Belovay, D. K. Varma, and I. I. K. Ahmed, "Cataract surgery in pseudoexfoliation syndrome.," *Curr. Opin. Ophthalmol.*, vol. 21, no. 1, pp. 25–34, Jan. 2010.

[7] R. Ritch, U. Schlötzer-Schrehardt, and A. G. P. Konstas, "Why is glau-

coma associated with exfoliation syndrome?," *Prog. Retin. Eye Res.*, vol. 22, no. 3, pp. 253–275, 2003.

[8] R. W. Nickells, G. R. Howell, I. Soto, and S. W. M. John, "Under pressure: cellular and molecular responses during glaucoma, a common neurodegeneration with axonopathy.," *Annu. Rev. Neurosci.*, vol. 35, pp. 153–179, 2012.

[9] H. A. Quigley and A. T. Broman, "The number of people with glaucoma worldwide in 2010 and 2020.," *Br. J. Ophthalmol.*, vol. 90, no. 3, pp. 262–267, Mar. 2006.

[10] Y. C. Tham, X. Li, T. Y. Wong, H. A. Quigley, T. Aung, and C.-Y. Cheng, "Global prevalence of glaucoma and projections of glaucoma burden through 2040: a systematic review and meta-analysis.," *Ophthalmology*, vol. 121, no. 11, pp. 2081–2090, Nov. 2014.

[11] World Health Organization. "Global data on visual impairments 2010.," 2010.

[12] E. Chan, O. A. R. Mahroo, and D. J. Spalton, "Complications of cataract surgery.," *Clin. Exp. Optom.*, vol. 93, no. 6, pp. 379–389, Nov. 2010.

[13] N. M. N. Haddad, J. K. Sun, S. Abujaber, D. K. Schlossman, and P. S. Silva, "Cataract surgery and its complications in diabetic patients.," *Semin. Ophthalmol.*, vol. 29, no. 5–6, pp. 329–337, 2014.

[14] T. W. Blackstad, O. A. Sunde, and J. Trœtteberg, "On the ultrastructure of the deposits of busacca in eyes with glaucoma simplex and so-called senile exfoliation of the anterior lens capsule1).," *Acta Ophthalmol.*, vol. 38, no. 5, pp. 587–598, Oct. 1960.

[15] N. Ashton, M. Shakib, R. Collyer, and R. Blach, "Electron Microscopic Study of Pseudo-Exfoliation of the Lens Capsule. I. Lens Capsule and Zonular Fibers.," *Invest. Ophthalmol.*, vol. 4, no. 2, pp. 141–153, 1965.

[16] A. J. Dark, B. W. Streeten, and C. C. Cornwall, "Pseudoexfoliative disease of the lens: a study in electron microscopy and histochemistry.," *Br. J. Ophthalmol.*, vol. 61, no. 7, pp. 462–472, Jul. 1977.

[17] S. Meehan, Y. Berry, B. Luisi, C. M. Dobson, J. A. Carver, and C. E. MacPhee, "Amyloid fibril formation by lens crystallin proteins and its implications for cataract formation," *J. Biol. Chem.*, vol. 279, no. 5, pp. 3413–3419, 2004.

[18] K. Papanikolopoulou et al., "Formation of amyloid fibrils in vitro by human γD-crystallin and its isolated domains," *Mol. Vis.*, vol. 14, p. 81, 2008.

[19] Y. Wang et al., "Formation of amyloid fibrils in vitro from partially unfolded intermediates of human γC-crystallin," *Invest. Ophthalmol. Vis. Sci.*, vol. 51, no. 2, pp. 672–678, 2010.

[20] A. M. Alperstein, J. S. Ostrander, T. O. Zhang, and M. T. Zanni, "Amyloid found in human cataracts with two-dimensional infrared spectroscopy," *Proc. Natl. Acad. Sci. U. S. A.*, vol. 116, no. 14, pp. 6602–6607, 2019.

[21] P. M. Bettelheim FA, "Light scattering of normal human lens I. Application of random density and orientation fluctuation theory.," *Biophys. J.*, vol. 26, no. 1, pp. 85–99, 1979.

[22] H. J. K. Wilfried W. de Jong, Nicolette H. Lubsen, "Molecular evolution of the eye lens.," *Prog. Retin. Eye Res.*, vol. 13, no. 2, pp. 391–442, 1994.

[23] H. Bloemendal, W. De Jong, R. Jaenicke, N. H. Lubsen, C. Slingsby, and A. Tardieu, "Ageing and vision: Structure, stability and function of lens crystallins.," *Prog. Biophys. Mol. Biol.*, vol. 86, no. 3, pp. 407–485, 2004.

[24] M. Delaye and A. Tardieu, "Short-range order of crystallin proteins accounts for eye lens transparency.," *Nature*, vol. 302, no. 5907, pp. 415–417, 1983.

[25] G. Dvorak-Theobald, "Pseudo-exfoliation of the lens capsule: relation to true exfoliation of the lens capsule as reported in the literature and role in the production of glaucoma capsulocuticulare.," *Am. J. Ophthalmol.*, vol. 37, no. 1, pp. 1–12, 1954.

[26] C. L. Karp, J. R. Fazio, W. W. Culbertson, and W. R. Green, "True Exfoliation of the Lens Capsule," *Arch. Ophthalmol.*, vol. 117, no. 8, pp. 1078–1080, Aug. 1999.

[27] S. Ashok Vardhan et al., "Association of pseudoexfoliation with systemic vascular diseases in a South Indian population," *JAMA Ophthalmol.*, vol. 135, no. 4, pp. 348–354, 2017.

[28] G. E. Erkayhan and S. Dogan, "Cataract Surgery and Possible Complications in Patients with Pseudoexfoliation Syndrome.," *Eurasian J. Med.*, vol. 49, no. 1, pp. 22–25, Feb. 2017.

[29] A. Kurt and T. Yaşar, "Complications of Phacoemulsification and Extracapsular Cataract Extraction Surgery in Eyes with Pseudoexfoliation Syndrome," *Ophthalmol. Res. An Int. J.*, vol. 8, no. 2, pp. 1–8, 2018.

[30] L. Ilveskoski, C. Taipale, E. J. Holmström, and R. Tuuminen, "Macular edema after cataract surgery in eyes with and without pseudoexfoliation syndrome," *Eur. J. Ophthalmol.*, pp. 1–6, 2018.

[31] M. P. Fautsch et al., "Aqueous humor outflow: What do we know? Where will it lead us?," *Investig. Ophthalmol. Vis. Sci.*, vol. 47, no. 10, pp. 4181–4187, 2006.

[32] W. D. Stamer and A. F. Clark, "The many faces of the trabecular meshwork cell.," *Exp. Eye Res.*, vol. 158, pp. 112–123, May 2017.

[33] M. M. Civan and A. D. C. Macknight, "The ins and outs of aqueous humour secretion.," *Exp. Eye Res.*, vol. 78, no. 3, pp. 625–631, Mar. 2004.

[34] "Glaucoma now second leading cause of blindness," *Bull. World Health Organ.*, vol. 82, pp. 844–951, 2004.

[35] R. Ritch, "Exfoliation syndrome-the most common identifiable cause of open-angle glaucoma.," *J. Glaucoma*, vol. 3, no. 2, pp. 176–177, 1994.

[36] E. Vesti and T. Kivela, "Exfoliation syndrome and exfoliation glaucoma.," *Prog. Retin. Eye Res.*, vol. 19, no. 3, pp. 345–368, May 2000.

[37] U. Schlotzer-Schrehardt and G. O. H. Naumann, "Ocular and systemic pseudoexfoliation syndrome.," *Am. J. Ophthalmol.*, vol. 141, no. 5, pp. 921–937, 2006

[38] M. A. Desai and R. K. Lee, "The medical and surgical management of pseudoexfoliation glaucoma.," *Int. Ophthalmol. Clin.*, vol. 48, no. 4, pp. 95–113, 2008.

[39] R. M. Conway, U. Schlotzer-Schrehardt, M. Kuchle, and G. O. H. Naumann, "Pseudoexfoliation syndrome: pathological manifestations of relevance to intraocular surgery.," *Clin. Experiment. Ophthalmol.*, vol. 32, no. 2, pp. 199–210, Apr. 2004.

[40] B. K. Derham and J. J. Harding, "Alpha-crystallin as a molecular chaperone.," *Prog. Retin. Eye Res.*, vol. 18, no. 4, pp. 463–509, 1999.

[41] W. W. de Jong, W. Hendriks, J. W. M. Mulders, and H. Bloemendal, "Evolution of eye lens crystallins: the stress connection," *Trends Biochem. Sci.*, vol. 14, no. 9, pp. 365–368, 1989.

[42] P. V. Rao, Q. ling Huang, J. Horwitz, and J. S. Zigler, "Evidence that α-crystallin prevents non-specific protein aggregation in the intact eye lens," *BBA - Gen. Subj.*, vol. 1245, no. 3, pp. 439–447, 1995.

[43] C. Slingsby and N. J. Clout, "Structure of the crystallins.," *Eye*, vol. 13, pp. 395–402, 1999.

[44] K. L. Moreau and J. A. King, "Protein misfolding and aggregation in cataract disease and prospects for prevention.," *Trends Mol. Med.*, vol. 18, no. 5, pp. 273–282, 2012.

[45] H. Ecroyd and J. A. Carver, "Crystallin proteins and amyloid fibrils.," *Cell. Mol. Life Sci.*, vol. 66, no. 1, pp. 62–81, Jan. 2009.

[46] S. D. Moran, T. O. Zhang, S. M. Decatur, and M. T. Zanni, "Amyloid fiber formation in human γd-crystallin induced by UV-B photodamage.," *Biochemistry*, vol. 52, no. 36, pp. 6169–6181, 2013.

[47] B. Ovodenko et al., "Proteomic analysis of exfoliation deposits," *Investig. Ophthalmol. Vis. Sci.*, vol. 48, no. 4, pp. 1447–1457, 2007.

[48] M. Zenkel, P. Lewczuk, A. Jünemann, F. E. Kruse, G. O. H. Naumann, and U. Schlötzer-Schrehardt, "Proinflammatory cytokines are involved in the initiation of the abnormal matrix process in pseudoexfoliation syndrome/glaucoma," *Am. J. Pathol.*, vol. 176, no. 6, pp. 2868–2879, 2010.

[49] U. S.-S. Robert Ritch, "Exfoliation syndrome," *Surv. Ophthalmol.*, vol. 45, no. 4, pp. 265–315, 2001.

[50] M. Zenkel and U. Schlötzer-Schrehardt, "The composition of exfoliation material and the cells involved in its production," *J. Glaucoma*, vol. 23, no. 8, pp. S12–S14, 2014.

[51] A. Henninot, J. C. Collins, and J. M. Nuss, "The Current State of Peptide Drug Discovery: Back to the Future?," *J. Med. Chem.*, vol. 61, no. 4, pp. 1382–1414, Feb. 2018.

[52] Z. Jiang, J. Guan, J. Qian, and C. Zhan, "Peptide ligand-mediated targeted drug delivery of nanomedicines.," *Biomater. Sci.*, vol. 7, no. 2, pp. 461–471, Jan. 2019.

[53] R. C. Ladner, A. K. Sato, J. Gorzelany, and M. de Souza, "Phage display-

derived peptides as therapeutic alternatives to antibodies.," *Drug Discov. Today*, vol. 9, no. 12, pp. 525–529, Jun. 2004.

[54] J. L. Lau and M. K. Dunn, "Therapeutic peptides: Historical perspectives, current development trends, and future directions," *Bioorganic Med. Chem.*, vol. 26, no. 10, pp. 2700–2707, 2018.

[55] J. Pande, M. M. Szewczyk, and A. K. Grover, "Phage display: Concept, innovations, applications and future.," *Biotechnol. Adv.*, vol. 28, no. 6, pp. 849–858, 2010.

[56] G. P. Smith and V. A. Petrenko, "Phage display," *Chem. Rev.*, vol. 97, no. 2, pp. 391–410, 1997.

[57] S. S. Sidhu, H. B. Lowman, B. C. Cunningham, and J. A. Wells, "Phage display for selection of novel binding peptides.," *Methods Enzymol.*, vol. 328, pp. 333–363, 2000.

[58] C. K. Kang, V. Jayasinha, and P. T. Martin, "Identification of peptides that specifically bind Abeta1-40 amyloid in vitro and amyloid plaques in Alzheimer's disease brain using phage display.," *Neurobiol. Dis.*, vol. 14, no. 1, pp. 146–156, Oct. 2003.

[59] B. Bohrmann et al., "Gantenerumab: a novel human anti-Abeta antibody demonstrates sustained cerebral amyloid-beta binding and elicits cell-mediated removal of human amyloid-beta.," *J. Alzheimers. Dis.*, vol. 28, no. 1, pp. 49–69, 2012.

[60] I. Ercan, K. U. Tufekci, E. Karaca, S. Genc, and K. Genc, "Peptide Derivatives of Erythropoietin in the Treatment of Neuroinflammation and Neurodegeneration.," *Adv. Protein Chem. Struct.* Biol., vol. 112, pp. 309–357, 2018.

[61] J. Lubkowski, F. Hennecke, A. Pluckthun, and A. Wlodawer, "Filamentous phage infection: crystal structure of g3p in complex with its coreceptor,

the C-terminal domain of TolA.," *Structure*, vol. 7, no. 6, pp. 711–722, Jun. 1999.

[62] K. McNamara and S. A. M. Tofail, "Nanoparticles in biomedical applications," *Adv. Phys. X*, vol. 2, no. 1, pp. 54–88, 2017.

[63] S. Parveen, R. Misra, and S. K. Sahoo, "Nanoparticles: a boon to drug delivery, therapeutics, diagnostics and imaging.," *Nanomedicine nanotechnology, Biol. Med.*, vol. 8, no. 2, pp. 147–166, Feb. 2012.

[64] J. Dobson, "Magnetic micro- and nano-particle-based targeting for drug and gene delivery.," *Nanomedicine (Lond).*, vol. 1, no. 1, pp. 31–37, Jun. 2006.

[65] J. Gao, H. Gu, and B. Xu, "Multifunctional magnetic nanoparticles: design, synthesis, and biomedical applications.," *Acc. Chem. Res.*, vol. 42, no. 8, pp. 1097–1107, Aug. 2009.

[66] M. K. Yu, J. Park, and S. Jon, "Targeting strategies for multifunctional nanoparticles in cancer imaging and therapy," *Theranostics*, vol. 2, no. 1, pp. 3–44, 2012.

[67] C. P. Moerland, L. J. van IJzendoorn, and M. W. J. Prins, "Rotating magnetic particles for lab-on-chip applications - a comprehensive review," *Lab Chip*, vol. 19, no. 6, pp. 919–933, Mar. 2019.

[68] F. Mosconi, J. F. Allemand, and V. Croquette, "Soft magnetic tweezers: a proof of principle.," *Rev. Sci. Instrum.*, vol. 82, no. 3, p. 34302, Mar. 2011.

[69] S. Forth, M. Y. Sheinin, J. Inman, and M. D. Wang, "Torque measurement at the single-molecule level.," *Annu. Rev. Biophys.*, vol. 42, pp. 583–604, 2013.

[70] Y. Cheng et al., "Rotating magnetic field induced oscillation of magnetic particles for in vivo mechanical destruction of malignant glioma.," *J. Control.*

Release, vol. 223, pp. 75–84, Feb. 2016.

[71] Y. Gao, A. van Reenen, M. A. Hulsen, A. M. De Jong, M. W. J. Prins, and J. M. J. Den Toonder, "Chaotic fluid mixing by alternating microparticle topologies to enhance biochemical reactions," *Microfluid. Nanofluidics*, vol. 16, no. 1–2, pp. 265–274, 2014.

[72] T. Franke, L. Schmid, D. A. Weitz, and A. Wixforth, "Magneto-mechanical mixing and manipulation of picoliter volumes in vesicles," *Lab Chip*, vol. 9, no. 19, pp. 2831–2835, 2009.

[73] M. Chen et al., "Remote Control of Mechanical Forces via Mitochondrial-Targeted Magnetic Nanospinners for Efficient Cancer Treatment," *Small*, vol. 16, no. 3, pp. e1905424–e1905424, Jan. 2020.

[74] A. Elbourne et al., "Antibacterial Liquid Metals: Biofilm Treatment via Magnetic Activation," *ACS Nano*, vol. 14, no. 1, pp. 802–817, Jan. 2020.

[75] Y. I. Golovin et al., "Towards nanomedicines of the future: Remote magneto-mechanical actuation of nanomedicines by alternating magnetic fields," *J. Control. Release*, vol. 219, pp. 43–60, Dec. 2015.

[76] "WHO. Draft action plan for the prevention of avoidable blindness and visual impairment 2014–2019. Universal eye health: a global action plan 2014–2019. Geneva: *World Health Organization*, 2013."

[77] C. Sabanayagam and C.-Y. Cheng, "Global causes of vision loss in 2015: are we on track to achieve the Vision 2020 target?," *Lancet. Glob. Heal.*, vol. 5, no. 12, pp. e1164–e1165, Dec. 2017.

[78] J. Ramke and C. E. Gilbert, "Universal eye health: are we getting closer?," *Lancet. Glob. Heal.*, vol. 5, no. 9, pp. e843–e844, Sep. 2017.

[79] P. Puska and A. Tarkkanen, "Exfoliation syndrome as a risk factor for cataract development: five-year follow-up of lens opacities in exfoliation syn-

drome.," *J. Cataract Refract. Surg.*, vol. 27, no. 12, pp. 1992–1998, Dec. 2001.

[80] P. Challa, "Genetics of pseudoexfoliation syndrome.," *Curr. Opin. Ophthalmol.*, vol. 20, no. 2, pp. 88–91, Mar. 2009.

[81] G. Hollo, A. Katsanos, and A. G. Konstas, "Management of exfoliative glaucoma: challenges and solutions.," *Clin. Ophthalmol.*, vol. 9, pp. 907–919, 2015.

[82] S. Nazarali, F. Damji, and K. F. Damji, "What have we learned about exfoliation syndrome since its discovery by John Lindberg 100 years ago?," *Br. J. Ophthalmol.*, vol. 102, no. 10, pp. 1342–1350, Oct. 2018.

[83] S. A. Funke and D. Willbold, "Peptides for therapy and diagnosis of Alzheimer's disease.," *Curr. Pharm. Des.*, vol. 18, no. 6, pp. 755–767, 2012.

[84] Y. Nagai et al., "Inhibition of polyglutamine protein aggregation and cell death by novel peptides identified by phage display screening.," *J. Biol. Chem.*, vol. 275, no. 14, pp. 10437–10442, Apr. 2000.

[85] C. Zhang et al., "Dual-functional nanoparticles targeting amyloid plaques in the brains of Alzheimer's disease mice.," *Biomaterials*, vol. 35, no. 1, pp. 456–465, Jan. 2014.

Chapter 2

[1] A. Tarkkanen and T. Kivelä, "John G. Lindberg and the discovery of exfoliation syndrome.," *Acta Ophthalmol. Scand.*, vol. 80, no. 2, pp. 151–154, 2002.

[2] G. Dvorak-Theobald, "Pseudo-exfoliation of the lens capsule: relation to true exfoliation of the lens capsule as reported in the literature and role in the production of glaucoma capsulocuticulare.," *Am. J. Ophthalmol.*, vol. 37, no.

1, pp. 1–12, 1954.

[3] Davanger M, "The pseudo-exfoliation syndrome. A scanning electron microscopic study. I. The anterior lens surface. *Acta Ophthalmol* 53: 809–820, 1975.

[4] M. Ghosh and J. S. Speakman, "The ciliary body in senile exfoliation of the lens.," *Can. J. Ophthalmol.*, vol. 8, no. 3, pp. 394–403, Jul. 1973.

[5] J. P. Harnisch, "Exfoliation material in different sections of the eye.," *Albrecht Von Graefes Arch. Klin. Exp. Ophthalmol.*, vol. 203, no. 3–4, pp. 181–190, Sep. 1977.

[6] Ringvold A, Electron microscopy of the wall of iris vessels in eyes with and without exfoliation syndrome (pseudoexfoliation of the lens capsule). *Virchows Arch A, Pathol Pathol Anat* 348: 328–341, 1969.

[7] A. Ringvold and T. Vegge, "Electron microscopy of the trabecular meshwork in eyes with exfoliation syndrome. (Pseudoexfoliation of the lens capsule).," *Virchows Arch. A, Pathol. Pathol. Anat.*, vol. 353, no. 2, pp. 110–127, 1971.

[8] M. Shakib, N. Ashton, and R. Blach, "Electron Microscopic Study of Pseudo-exfoliation of the Lens Capsule II. Iris and Ciliary Body," *Invest. Ophthalmol.*, vol. 4, pp. 154–161, Apr. 1965.

[9] R. Ritch and U. Schlotzer-Schrehardt, "Exfoliation syndrome.," *Surv. Ophthalmol.*, vol. 45, no. 4, pp. 265–315, 2001.

[10] U. M. Schl and M. R. Koca, "Pseudoexfoliation Syndrome Ocular Manifestation of a Systemic Disorder?," *Arch, vol.* 110, pp. 1752–2756, 1992.

[11] T. W. Blackstad, O. A. Sunde, and J. Trœtteberg, "On the ultrastructure of the deposits of busacca in eyes with glaucoma simplex and so-called senile exfoliation of the anterior lens capsule1).," *Acta Ophthalmol.*, vol. 38, no. 5,

pp. 587–598, Oct. 1960.

[12] B. Ovodenko et al., "Proteomic analysis of exfoliation deposits," *Investig. Ophthalmol. Vis. Sci.*, vol. 48, no. 4, pp. 1447–1457, 2007.

[13] M. Zenkel, P. Lewczuk, A. Jünemann, F. E. Kruse, G. O. H. Naumann, and U. Schlötzer-Schrehardt, "Proinflammatory cytokines are involved in the initiation of the abnormal matrix process in pseudoexfoliation syndrome/glaucoma," *Am. J. Pathol.*, vol. 176, no. 6, pp. 2868–2879, 2010.

[14] P. Challa and W. M. Johnson, "Composition of Exfoliation Material.," *Glaucoma*, vol. 27, no. 7, pp. 29–31, 2018.

[15] M. Zenkel, A. Krysta, F. Pasutto, A. Juenemann, F. E. Kruse, and U. Schlötzer-Schrehardt, "Regulation of Lysyl Oxidase-like 1 (LOXL1) and elastin-related genes by pathogenic factors associated with pseudoexfoliation syndrome.," *Investig. Ophthalmol. Vis. Sci.*, vol. 52, no. 11, pp. 8488–8495, 2011.

[16] D. Chiras, G. Kitsos, M. B. Petersen, I. Skalidakis, and C. Kroupis, "Oxidative stress in dry age-related macular degeneration and exfoliation syndrome.," *Critical Reviews in Clinical Laboratory Sciences*, vol. 52, no. 1. Informa Healthcare USA, Inc., pp. 12–27, 2015.

[17] U. Schlotzer-Schrehardt, "New pathogenetic insights into pseudoexfoliation syndrome/glaucoma. Therapeutically relevant?," *Ophthalmologe*, vol. 109, no. 10, pp. 944–951, Oct. 2012.

[18] N. Ashton, M. Shakib, R. Collyer, and R. Blach, "Electron Microscopic Study of Pseudo-Exfoliation of the Lens Capsule. I. Lens Capsule and Zonular Fibers.," *Invest. Ophthalmol.*, vol. 4, pp. 141–153, 1965.

[19] M. Zenkel and U. Schlötzer-Schrehardt, "The composition of exfoliation material and the cells involved in its production.," *J. Glaucoma*, vol. 23, no.

8 Suppl 1, pp. S12-4, 2014.

[20] S. Ashok Vardhan et al., "Association of pseudoexfoliation with systemic vascular diseases in a South Indian population," *JAMA Ophthalmol.*, vol. 135, no. 4, pp. 348–354, 2017.

[21] G. Egemen Erkayhan and S. Dogan, "Cataract Surgery and Possible Complications in Patients with Pseudoexfoliation Syndrome," *Eurasian J. Med.*, vol. 49, no. 1, pp. 22–25, 2016.

[22] L. Ilveskoski, C. Taipale, E. J. Holmström, and R. Tuuminen, "Macular edema after cataract surgery in eyes with and without pseudoexfoliation syndrome," *Eur. J. Ophthalmol.*, pp. 1–6, 2018.

[23] A. Kurt and T. Yaşar, "Complications of Phacoemulsification and Extracapsular Cataract Extraction Surgery in Eyes with Pseudoexfoliation Syndrome," *Ophthalmol. Res. An Int. J.*, vol. 8, no. 2, pp. 1–8, 2018.

[24] K. Grødum, A. Heijl, and B. Bengtsson, "Glaucoma and mortality," *Graefe's Arch. Clin. Exp. Ophthalmol.*, vol. 242, no. 5, pp. 397–401, 2004.

[25] A. Ringvold, S. Blika, and L. Sandvik, "Pseudo-exfoliation and mortality," *Acta Ophthalmol. Scand.*, vol. 75, no. 3, pp. 255–256, 2009.

[26] K. R. Shrum, M. G. Hattenhauer, and D. Hodge, "Cardiovascular and cerebrovascular mortality associated with ocular pseudoexfoliation," *Am. J. Ophthalmol.*, vol. 129, no. 1, pp. 83–86, 2000.

[27] J. K. Slettedal, L. Sandvik, and A. Ringvold, "Ocular pseudoexfoliation syndrome and life span.," *EBioMedicine*, vol. 2, no. 7, pp. 765–769, Jul. 2015.

[28] R. Svensson and C. Ekstrom, "Pseudoexfoliation and mortality: a population-based 30-year follow-up study.," *Acta Ophthalmol.*, vol. 93, no. 2, pp. 162–164, Mar. 2015.

[29] R. F. Brubaker, "Flow of aqueous humor in humans [The Friedenwald

Lecture].," *Invest. Ophthalmol. Vis. Sci.*, vol. 32, no. 13, pp. 3145–3166, Dec. 1991.

[30] M. Goel, R. G. Picciani, R. K. Lee, and S. K. Bhattacharya, "Aqueous Humor Dynamics: A Review," *Open Ophthalmol. J.*, vol. 4, pp. 52–59, 2010.

[31] M. P. Fautsch et al., "Aqueous humor outflow: What do we know? Where will it lead us?," *Investig. Ophthalmol. Vis. Sci.*, vol. 47, no. 10, pp. 4181–4187, 2006.

[32] W. D. Stamer and A. F. Clark, "The many faces of the trabecular meshwork cell," *Exp. Eye Res.*, vol. 158, pp. 112–123, 2017.

[33] M. M. Civan and A. D. C. Macknight, "The ins and outs of aqueous humour secretion.," *Exp. Eye Res.*, vol. 78, no. 3, pp. 625–631, Mar. 2004.

[34] Y.-C. Tham, X. Li, T. Y. Wong, H. A. Quigley, T. Aung, and C.-Y. Cheng, "Global prevalence of glaucoma and projections of glaucoma burden through 2040: a systematic review and meta-analysis.," *Ophthalmology*, vol. 121, no. 11, pp. 2081–2090, Nov. 2014.

[35] U. Schlotzer-Schrehardt and G. O. Naumann, "Trabecular meshwork in pseudoexfoliation syndrome with and without open-angle glaucoma. A morphometric, ultrastructural study.," *Invest. Ophthalmol. Vis. Sci.*, vol. 36, no. 9, pp. 1750–1764, Aug. 1995.

[36] R. Ritch, "Exfoliation syndrome-the most common identifiable cause of open-angle glaucoma.," *J. Glaucoma*, vol. 3, no. 2, pp. 176–177, 1994.

[37] S. F. Nilsson, "The uveoscleral outflow routes.," *Eye (Lond).*, vol. 11 (Pt 2), pp. 149–154, 1997.

[38] A. Alm and S. F. E. Nilsson, "Uveoscleral outflow-a review.," *Exp. Eye Res.*, vol. 88, no. 4, pp. 760–768, Apr. 2009.

[39] T. V Johnson, S. Fan, C. B. Camras, and C. B. Toris, "Aqueous humor

dynamics in exfoliation syndrome.," *Arch. Ophthalmol.* (Chicago, Ill. 1960), vol. 126, no. 7, pp. 914–920, Jul. 2008.

[40] U. Schlötzer-schrehardt and G. O. H. Naumann, "Trabecular Mechanisms of Intraocular Pressure Elevation Pseudoexfoliation Syndrome," in Mechanisms of the Glaucomas: Disease Processes and Therapeutic Modalities, *Humana press*, 2008, pp. 117–138.

[41] E. Vesti and T. Kivela, "Exfoliation syndrome and exfoliation glaucoma.," *Prog. Retin. Eye Res.*, vol. 19, no. 3, pp. 345–368, May 2000.

[42] I. F. Aboobakar, W. M. Johnson, W. D. Stamer, M. A. Hauser, and R. R. Allingham, "Major review: Exfoliation syndrome; advances in disease genetics, molecular biology, and epidemiology," *Exp. Eye Res.*, vol. 154, pp. 88–103, 2017.

[43] R. M. Conway, U. Schlötzer-Schrehardt, M. Küchle, and G. O. H. Naumann, "Pseudoexfoliation syndrome: Pathological manifestations of relevance to intraocular surgery," *Clin. Exp. Ophthalmol.*, vol. 32, no. 2, pp. 199–210, 2004.

[44] M. A. Desai and R. K. Lee, "The medical and surgical management of pseudoexfoliation glaucoma.," *Int. Ophthalmol. Clin.*, vol. 48, no. 4, pp. 95–113, 2008.

[45] R. Ritch, "Ocular and systemic manifestations of exfoliation syndrome," *J. Glaucoma*, vol. 23, no. 8, pp. S1–S8, 2014.

[46] H. Chung, S. Arora, K. F. Damji, and E. Weis, "Association of pseudoexfoliation syndrome with cardiovascular and cerebrovascular disease: a systematic review and meta-analysis," *Can. J. Ophthalmol.*, vol. 53, no. 4, pp. 365–372, 2018.

[47] P. Oltulu and R. Oltulu, "The Association of Cataract and Lens Epithe-

lial Cell Apoptosis in Patients with Pseudoexfoliation Syndrome," *Curr. Eye Res.*, vol. 43, no. 3, pp. 300–303, 2018.

[48] R. Ritch, "Systemic Associations of Exfoliation Syndrome.," *Asia-Pacific J. Ophthalmol.* (Philadelphia, Pa.), vol. 5, no. 1, pp. 45–50, 2016.

[49] G. Thorleifsson et al., "Common sequence variants in the LOXL1 gene confer susceptibility to exfoliation glaucoma.," *Science*, vol. 317, no. 5843, pp. 1397–1400, Sep. 2007.

[50] X. Liu et al., "Elastic fiber homeostasis requires lysyl oxidase-like 1 protein," *Nat. Genet.*, vol. 36, no. 2, pp. 178–182, 2004.

[51] K. S. Midwood and J. E. Schwarzbauer, "Elastic Fibers: Building Bridges Between Cells and Their Matrix.," *Curr Biol.*, vol. 12, no. 02, pp. 279–281, 2002.

[52] L. I. Smith-Mungo and H. M. Kagan, "Lysyl oxidase: Properties, regulation and multiple functions in biology," *Matrix Biol.*, vol. 16, no. 7, pp. 387–398, 1998.

[53] S. E. I. Williams et al., "Major LOXL1 risk allele is reversed in exfoliation glaucoma in a black South African population," *Mol. Vis.*, vol. 16, pp. 705–712, Apr. 2010.

[54] S. Kim and Y. Kim, "Variations in LOXL1 associated with exfoliation glaucoma do not affect amine oxidase activity," *Mol. Vis.*, vol. 18, pp. 265–270, 2012.

[55] T. Aung et al., "A common variant mapping to CACNA1A is associated with susceptibility to exfoliation syndrome," *Nat. Genet.*, vol. 47, no. 4, pp. 387–392, 2015.

[56] I. F. Aboobakar and R. R. Allingham, "Genetics of exfoliation syndrome and glaucoma.," *Int. Ophthalmol. Clin.*, vol. 54, no. 4, pp. 43–56, 2014.

[57] M. Zenkel and U. Schlötzer-Schrehardt, "Expression and regulation of LOXL1 and elastin-related genes in eyes with exfoliation syndrome," *J. Glaucoma*, vol. 23, no. 8, pp. S62–S63, 2014.

[58] U. Schlötzer-Schrehardt et al., "Genotype-correlated expression of lysyl oxidase-like 1 in ocular tissues of patients with pseudoexfoliation syndrome/glaucoma and normal patients," *Am. J. Pathol.*, vol. 173, no. 6, pp. 1724–1735, 2008.

[59] F. Pasutto et al., "Pseudoexfoliation syndrome-associated genetic variants affect transcription factor binding and alternative splicing of LOXL1," *Nat. Commun.*, vol. 8, no. May, 2017.

[60] D. Berner et al., "Posttranscriptional regulation of LOXL1 expression *via* alternative splicing and nonsense-mediated mRNA decay as an adaptive stress response," *Investig. Ophthalmol. Vis. Sci.*, vol. 58, no. 13, pp. 5930–5940, 2017.

[61] D. Berner et al., "The protective variant rs7173049 at LOXL1 locus impacts on retinoic acid signaling pathway in pseudoexfoliation syndrome.," *Hum. Mol. Genet.*, vol. 28, pp. 2531–2548, Apr. 2019.

[62] T. Aung et al., "Genetic association study of exfoliation syndrome identifies a protective rare variant at LOXL1 and five new susceptibility loci," *Nat. Genet.*, vol. 49, no. 7, pp. 993–1004, 2017.

[63] T. Aung, A. S. Chan, and C.-C. Khor, "Genetics of Exfoliation Syndrome.," *J. Glaucoma*, vol. 27 Suppl 1, pp. S12–S14, Jul. 2018.

[64] D. Pietrobon, "CAv2.1 channelopathies," *Pflugers Arch. Eur. J. Physiol.*, vol. 460, no. 2, pp. 374–393, 2010.

[65] U. Schlötzer-Schrehardt, M. Zenkel, M. Küchle, L. Y. Sakai, and G. O. H. Naumann, "Role of Transforming Growth Factor-β1 and its Latent Form

Binding Protein in Pseudoexfoliation Syndrome," *Exp. Eye Res.*, vol. 73, no. 6, pp. 765–780, 2001.

[66] U. Schlötzer-Schrehardt, "Molecular Biology of Exfoliation Syndrome," *J. Glaucoma*, vol. 27, no. 7, pp. S32–S37, 2018.

[67] M. Zenkel, F. E. Kruse, A. G. Jünemann, G. O. H. Naumann, and U. Schlötzer-Schrehardt, "Clusterin deficiency in eyes with pseudoexfoliation syndrome may be implicated in the aggregation and deposition of pseudoexfoliative material," *Investig. Ophthalmol. Vis. Sci.*, vol. 47, no. 5, pp. 1982–1990, 2006.

[68] S. E. Jones and C. Jomary, "Clusterin.," *Int. J. Biochem. Cell Biol.*, vol. 34, no. 5, pp. 427–431, May 2002.

[69] A. M. Rodríguez-Piñeiro, M. P. de la Cadena, Á. López-Saco, and F. J. Rodríguez-Berrocal, "Differential Expression of Serum Clusterin Isoforms in Colorectal Cancer," *Mol. Cell. Proteomics*, vol. 5, no. 9, pp. 1647–1657, 2006.

[70] M. E. Rosenberg and J. Silkensen, "Clusterin: Physiologic and pathophysiologic considerations," *Int. J. Biochem. Cell Biol.*, vol. 27, no. 7, pp. 633–645, 1995.

[71] M. E. Fini, A. Bauskar, S. Jeong, and M. R. Wilson, "Clusterin in the eye: An old dog with new tricks at the ocular surface," *Exp. Eye Res.*, vol. 147, pp. 57–71, 2016.

[72] S. Poon, T. M. Treweek, M. R. Wilson, S. B. Easterbrook-Smith, and J. A. Carver, "Clusterin is an extracellular chaperone that specifically interacts with slowly aggregating proteins on their off-folding pathway," *FEBS Lett.*, vol. 513, no. 2–3, pp. 259–266, 2002.

[73] M. Calero, A. Rostagno, E. Matsubara, B. Zlokovic, B. Frangione, and J.

Ghiso, "Apolipoprotein J (clusterin) and Alzheimer's disease," *Microsc. Res. Tech.*, vol. 50, no. 4, pp. 305–315, 2000.

[74] I. Doudevski, A. Rostagno, M. Cowman, J. Liebmann, R. Ritch, and J. Ghiso, "Clusterin and complement activation in exfoliation glaucoma," *Investig. Ophthalmol. Vis. Sci.*, vol. 55, no. 4, pp. 2491–2499, 2014.

[75] R. Creasey et al., "Detecting protein aggregates on untreated human tissue samples by atomic force microscopy recognition imaging," *Biophys. J.*, vol. 99, no. 5, pp. 1660–1667, 2010.

[76] J. Stafiej et al., "Immunohistochemical analysis of microsomal glutathione S-transferase 1 and clusterin expression in lens epithelial cells of patients with pseudoexfoliation syndrome," *Exp. Ther. Med.*, vol. 13, no. 3, pp. 1057–1063, 2017.

[77] B. J. Fan, L. R. Pasquale, J. H. Kang, H. Levkovitch-Verbin, J. L. Haines, and J. L. Wiggs, "Association of clusterin (CLU) variants and exfoliation syndrome: An analysis in two Caucasian studies and a meta-analysis," *Exp. Eye Res.*, vol. 139, pp. 115–122, 2015.

[78] B. Padhy, G. G. Nanda, M. Chowdhury, D. Padhi, A. Rao, and D. P. Alone, "Role of an extracellular chaperone, Clusterin in the pathogenesis of Pseudoexfoliation Syndrome and Pseudoexfoliation Glaucoma," *Exp. Eye Res.*, vol. 127, pp. 69–76, 2014.

[79] J. Magalhães and M. J. Saraiva, "Clusterin overexpression and its possible protective role in transthyretin deposition in familial amyloidotic polyneuropathy," *J. Neuropathol. Exp. Neurol.*, vol. 70, no. 12, pp. 1097–1106, 2011.

[80] K. P. Burdon et al., "Genetic analysis of the clusterin gene in pseudoexfoliation syndrome.," *Mol. Vis.*, vol. 14, pp. 1727–1736, Sep. 2008.

[81] M. Krumbiegel et al., "Exploring functional candidate genes for genetic

association in german patients with pseudoexfoliation syndrome and pseudoexfoliation glaucoma.," *Invest. Ophthalmol. Vis. Sci.*, vol. 50, no. 6, pp. 2796–2801, Jun. 2009.

[82] S. K. Dubey, J. F. Hejtmancik, S. R. Krishnadas, R. Sharmila, A. Haripriya, and P. Sundaresan, "Evaluation of genetic polymorphisms in clusterin and tumor necrosis factor-alpha genes in South Indian individuals with pseudoexfoliation syndrome.," *Curr. Eye Res.*, vol. 40, no. 12, pp. 1218–1224, 2015.

[83] H. Lesiewska, K. Linkowska, J. Stafiej, T. Grzybowski, J. Swobodziński, and G. Malukiewicz, "CLU polymorphisms in patients with pseudoexfoliation syndrome in polish population," *J. Ophthalmol.*, vol. 2019, 2019.

[84] J. L. Wiggs, J. H. Kang, B. Fan, H. Levkovitch-Verbin, and L. R. Pasquale, "A Role for Clusterin in Exfoliation Syndrome and Exfoliation Glaucoma?," *J. Glaucoma*, vol. 27 Suppl 1, pp. S61–S66, Jul. 2018.

[85] K. Zagajewska et al., "GWAS links variants in neuronal development and actin remodeling related loci with pseudoexfoliation syndrome without glaucoma," *Exp. Eye Res.*, vol. 168, no. June 2017, pp. 138–148, 2018.

[86] Y. N. Ma, T. Y. Xie, and X. Y. Chen, "Multiple Gene Polymorphisms Associated with Exfoliation Syndrome in the Uygur Population," *J. Ophthalmol.*, vol. 2019, 2019.

[87] M. Nakano et al., "Novel common variants and susceptible haplotype for exfoliation glaucoma specific to Asian population," *Sci. Rep.*, vol. 4, pp. 1–6, 2014.

[88] M. Krumbiegel et al., "Genome-wide association study with DNA pooling identifies variants at CNTNAP2 associated with pseudoexfoliation syndrome," *Eur. J. Hum. Genet.*, vol. 19, no. 2, pp. 186–193, 2011.

[89] J. L. Wiggs et al., "Common variants at 9p21 and 8q22 are associated

with increased susceptibility to optic nerve degeneration in glaucoma," *PLoS Genet.*, vol. 8, no. 4, pp. 1–12, 2012.

[90] V. F. Oliver, K. A. van Bysterveldt, and S. L. Merbs, "Chapter 22-Epigenetics in Ocular Medicine," TOBT-ME Tollefsbol, (ed.). Medical Epigenetics. Boston: *Academic Press*, 2016, pp. 391–412.

[91] W. M. Johnson, L. K. Finnegan, M. A. Hauser, and W. D. Stamer, "LncRNAs, DNA Methylation, and the Pathobiology of Exfoliation Glaucoma," *J. Glaucoma*, vol. 27, no. 3, pp. 202–209, 2018.

[92] A. W. Hewitt, J. J. Wang, H. Liang, and J. E. Craig, "Epigenetic effects on eye diseases," *Expert Rev. Ophthalmol.*, vol. 7, no. 2, pp. 127–134, 2014.

[93] H. A. Alkozi, R. Franco, and J. J. Pintor, "Epigenetics in the eye: An overview of the most relevant ocular diseases," *Front. Genet.*, vol. 8, no. 144, pp. 1–7, 2017.

[94] H. Ye et al., "LOXL1 hypermethylation in pseudoexfoliation syndrome in the uighur population," *Investig. Ophthalmol. Vis. Sci.*, vol. 56, no. 10, pp. 5838–5843, 2015.

[95] J. Cao, "The functional role of long non-coding RNAs and epigenetics," *Biol. Proced. Online*, vol. 16, no. 11, pp. 1–13, 2014.

[96] T. R. Mercer, M. E. Dinger, and J. S. Mattick, "Long non-coding RNAs: insights Into Functions," *Nat. Rev. Genet.*, vol. 10, pp. 155–159, 2009.

[97] P. Wan, W. Su, and Y. Zhuo, "The Role of Long Noncoding RNAs in Neurodegenerative Diseases," *Mol. Neurobiol.*, vol. 54, pp. 2012–2021, 2017.

[98] M. A. Hauser et al., "Genetic variants and cellular stressors associated with exfoliation syndrome modulate promoter activity of a lncRNA within the LOXL1 locus," *Hum. Mol. Genet.*, vol. 24, no. 22, pp. 6552–6563, 2015.

[99] G. Arun, S. D. Diermeier, and D. L. Spector, "Therapeutic Targeting of

Long Non-Coding RNAs in Cancer," *Trends Mol. Med.*, vol. 24, no. 3, pp. 257–277, 2018.

[100] T. Wu and Y. Du, "LncRNAs: From Basic Research to Medical Application," *Int. J. Biol. Sci.*, vol. 13, pp. 295–307, 2017.

[101] V. Ambros, "The functions of animal microRNAs," *Nature*, vol. 431, no. 7006, pp. 350–355, 2004.

[102] P. Gonzalez, G. Li, J. Qiu, J. Wu, and C. Luna, "Role of microRNAs in the trabecular meshwork.," *J. Ocul. Pharmacol. Ther.*, vol. 30, no. 2–3, pp. 128–137, 2014.

[103] C. Luna, G. Li, J. Qiu, D. L. Epstein, and P. Gonzalez, "Cross-talk between miR-29 and transforming growth factor-betas in trabecular meshwork cells," Investig. *Ophthalmol. Vis. Sci.*, vol. 52, no. 6, pp. 3567–3572, 2011.

[104] C. Luna, G. Li, J. Qiu, D. L. Epstein, and P. Gonzalez, "Role of miR-29b on the regulation of the extracellular matrix in human trabecular meshwork cells under chronic oxidative stress.," *Mol. Vis.*, vol. 15, pp. 2488–2497, Nov. 2009.

[105] J. J. Dunmire, E. Lagorous, R. A. Bouhenni, M. Jones, and D. P. Edward, "MicroRNA in aqueous humor from patients with cataract," *Exp. Eye Res.*, vol. 108, pp. 68–71, 2013.

[106] Y. Tanaka et al., "Profiles of extracellular miRNAs in the aqueous humor of glaucoma patients assessed with a microarray system," *Sci. Rep.*, vol. 4, pp. 1–7, 2014.

[107] M. D. Drewry et al., "Differentially expressed microRNAs in the aqueous humor of patients with exfoliation glaucoma or primary open-angle glaucoma," *Hum. Mol. Genet.*, vol. 27, no. 7, pp. 1263–1275, 2018.

[108] A. Chatzikyriakidou et al., "MicroRNA-related polymorphisms in pseu-

doexfoliation syndrome, pseudoexfoliative glaucoma, and primary open-angle glaucoma," *Ophthalmic Genet.*, vol. 39, no. 5, pp. 603–609, 2018.

[109] A. G. Hindle et al., "Identification of candidate miRNA biomarkers for glaucoma," *Investig. Ophthalmol. Vis. Sci.*, vol. 60, no. 1, pp. 134–146, 2019.

[110] C. H. Johnson, J. Ivanisevic, and G. Siuzdak, "Metabolomics: Beyond biomarkers and towards mechanisms," *Nat. Rev. Mol. Cell Biol.*, vol. 17, no. 7, pp. 451–459, 2016.

[111] M. S. Monteiro, M. Carvalho, M. L. Bastos, and P. Guedes de Pinho, "Metabolomics Analysis for Biomarker Discovery: Advances and Challenges," *Curr. Med. Chem.*, vol. 20, no. 2, pp. 257–271, 2013.

[112] S. McNally and C. J. O'Brien, "Metabolomics/proteomics strategies used to identify biomarkers for exfoliation glaucoma," *J. Glaucoma*, vol. 23, no. 8, pp. S51–S54, 2014.

[113] S. Leruez et al., "A Plasma Metabolomic Signature of the Exfoliation Syndrome Involves Amino Acids, Acylcarnitines, and Polyamines.," *Invest. Ophthalmol. Vis. Sci.*, vol. 59, no. 2, pp. 1025–1032, Feb. 2018.

[114] I. Dikic, "Proteasomal and Autophagic Degradation Systems," *Annu. Rev. Biochem.*, vol. 86, no. 1, pp. 193–224, 2017.

[115] L. de Juan-Marcos, F. A. Escudero-Dominguez, E. Hernandez-Galilea, F. Cruz-Gonzalez, I. Follana-Neira, and R. Gonzalez-Sarmiento, "Investigation of Association between Autophagy-Related Gene Polymorphisms and Pseudoexfoliation Syndrome and Pseudoexfoliation Glaucoma in a Spanish Population.," *Semin. Ophthalmol.*, vol. 33, no. 3, pp. 361–366, 2018.

[116] A. Want et al., "Autophagy and mitochondrial dysfunction in tenon fibroblasts from exfoliation glaucoma patients," *PLoS One*, vol. 11, no. 7, pp.

1–21, 2016.

[117] J. M. Wolosin, R. Ritch, and A. M. Bernstein, "Is Autophagy Dysfunction a Key to Exfoliation Glaucoma?," *J. Glaucoma*, vol. 27, no. 3, pp. 197–201, 2018.

[118] A. M. Bernstein, R. Ritch, and J. M. Wolosin, "Exfoliation syndrome: A disease of autophagy and LOXL1 proteopathy.," *J. Glaucoma*, vol. 27, no. 7, pp. S44–S53, 2018.

[119] M. Audano, A. Schneider, and N. Mitro, "Mitochondria, lysosomes, and dysfunction: their meaning in neurodegeneration," *J. Neurochem.*, vol. 147, no. 3, pp. 291–309, 2018.

[120] A. M. Leidal, B. Levine, and J. Debnath, "Autophagy and the cell biology of age-related disease," *Nat. Cell Biol.*, vol. 20, no. 12, pp. 1338–1348, 2018.

[121] L. Galluzzi, J. M. Bravo-San Pedro, B. Levine, D. R. Green, and G. Kroemer, "Pharmacological modulation of autophagy: therapeutic potential and persisting obstacles," *Nat. Rev. Drug Discov.*, vol. 16, pp. 487–511, 2017.

[122] B. Levine and G. Kroemer, "Biological Functions of Autophagy Genes: A Disease Perspective," *Cell*, vol. 176, no. 1–2, pp. 11–42, 2019.

Chapter 3

[1] O. Okoye, B. I. Eze, and C. M. Chuka-Okosa, "Eliminating the barriers to uptake of cataract surgery in a resource-poor setting: A focus on direct surgical cost," *Niger. J. Clin. Pract.*, vol. 18, no. 3, pp. 333–336, 2015.

[2] M. S. Kosinski-Collins and J. King, "*In vitro* unfolding, refolding, and polymerization of human gamma D crystallin, a protein involved in cataract formation.," *Protein Sci.*, vol. 12, no. 3, pp. 480–90, 2003.

[3] A. Surguchev and A. Surguchov, "Conformational diseases: looking into the eyes," *Brain Res. Bull.*, vol. 81, no. 1, pp. 12–24, 2010.

[4] H. Ecroyd and J. A. Carver, "Crystallin proteins and amyloid fibrils," *Cell. Mol. Life Sci.*, vol. 66, no. 1, pp. 62–81, 2009.

[5] K. L. Moreau and J. A. King, "Protein misfolding and aggregation in cataract disease and prospects for prevention," *Trends Mol. Med.*, vol. 18, no. 5, pp. 273–282, 2012.

[6] J. Liao et al., "Meta-analysis of genome-wide association studies in multi-ethnic Asians identifies two loci for age-related nuclear cataract," *Hum. Mol. Genet.*, vol. 23, no. 22, pp. 6119–6128, 2014.

[7] T. Härd and C. Lendel, "Inhibition of amyloid formation," *J. Mol. Biol.*, vol. 421, no. 4–5, pp. 441–465, 2012.

[8] Y. S. Eisele et al., "Targeting protein aggregation for the treatment of degenerative diseases," *Nat. Rev. Drug Discov.*, vol. 14, no. 11, p. 759, 2015.

[9] K. L. Sciarretta, D. J. Gordon, and S. C. Meredith, "Peptide-based inhibitors of amyloid assembly," *Methods Enzymol.*, vol. 413, pp. 273–312, 2006.

[10] M. Hamzeh-Mivehroud, A. A. Alizadeh, M. B. Morris, W. B. Church, and S. Dastmalchi, "Phage display as a technology delivering on the promise of peptide drug discovery," *Drug Discov. Today*, vol. 18, no. 23–24, pp. 1144–1157, 2013.

[11] B. P. Orner, L. Liu, R. M. Murphy, and L. L. Kiessling, "Phage display affords peptides that modulate beta-amyloid aggregation," *J. Am. Chem. Soc.*, vol. 128, no. 36, pp. 11882–11889, 2006.

[12] W. D. Marcus, H. Wang, S. M. Lindsay, and M. R. Sierks, "Characterization of an antibody scFv that recognizes fibrillar insulin and beta-amyloid

using atomic force microscopy.," *Nanomedicine*, vol. 4, no. 1, pp. 1–7, Mar. 2008.

[13] C. K. Kang, V. Jayasinha, and P. T. Martin, "Identification of peptides that specifically bind Abeta1-40 amyloid *in vitro* and amyloid plaques in Alzheimer's disease brain using phage display.," *Neurobiol. Dis.*, vol. 14, no. 1, pp. 146–156, Oct. 2003.

[14] K. Srivastava, J. M. Chaves, O. P. Srivastava, and M. Kirk, "Multicrystallin complexes exist in the water-soluble high molecular weight protein fractions of aging normal and cataractous human lenses," *Exp. Eye Res.*, vol. 87, no. 4, pp. 356–366, 2008.

[15] W. W. de Jong, N. H. Lubsen, and H. J. Kraft, "Molecular evolution of the eye lens," *Prog. Retin. Eye Res.*, vol. 13, no. 2, pp. 391–442, 1994.

[16] C. M. Dobson, "Protein-misfolding diseases: Getting out of shape," *Nature*, vol. 418, no. 6899, p. 729, 2002.

[17] H. Ecroyd, M. Garvey, D. C. Thorn, J. A. Gerrard, and J. A. Carver, "Amyloid fibrils from readily available sources: milk casein and lens crystallin proteins," in *Protein Nanotechnology*, Springer, 2013, pp. 103–117.

[18] S. Meehan, Y. Berry, B. Luisi, C. M. Dobson, J. A. Carver, and C. E. MacPhee, "Amyloid fibril formation by lens crystallin proteins and its implications for cataract formation," *J. Biol. Chem.*, vol. 279, no. 5, pp. 3413–3419, 2004.

[19] Y. Wang et al., "Formation of amyloid fibrils *in vitro* from partially unfolded intermediates of human γC-crystallin," *Invest. Ophthalmol. Vis. Sci.*, vol. 51, no. 2, pp. 672–678, 2010.

[20] K. Papanikolopoulou et al., "Formation of amyloid fibrils *in vitro* by human γD-crystallin and its isolated domains," *Mol. Vis.*, vol. 14, p. 81, 2008.

[21] T. O. Zhang, A. M. Alperstein, and M. T. Zanni, "Amyloid β-Sheet Secondary Structure Identified in UV-Induced Cataracts of Porcine Lenses using 2D IR Spectroscopy," *J. Mol. Biol.*, vol. 429, no. 11, pp. 1705–1721, 2017.

[22] K. J. Lampi, P. A. Wilmarth, M. R. Murray, and L. L. David, "Lens β-crystallins: the role of deamidation and related modifications in aging and cataract," *Prog. Biophys. Mol. Biol.*, vol. 115, no. 1, pp. 21–31, 2014.

[23] B. G. Mohr, C. M. Dobson, S. C. Garman, and M. Muthukumar, "Electrostatic origin of *in vitro* aggregation of human γ-crystallin," *J. Chem. Phys.*, vol. 139, no. 12, p. 09B614¬1, 2013.

[24] J. I. Clark, "Self-assembly of protein aggregates in ageing disorders: the lens and cataract model," *Philos. Trans. R. Soc. B Biol. Sci.*, vol. 368, no. 1617, p. 20120104, 2013.

[25] K. J. Lampi, K. K. Amyx, P. Ahmann, and E. A. Steel, "Deamidation in human lens betaB2-crystallin destabilizes the dimer.," *Biochemistry*, vol. 45, no. 10, pp. 3146–3153, Mar. 2006.

[26] J. F. Hejtmancik, P. T. Wingfield, and Y. V Sergeev, "β¬Crystallin association," *Exp. Eye Res.*, vol. 79, no. 3, pp. 377¬383, 2004.

[27] M. A. Smith, O. A. Bateman, R. Jaenicke, and C. Slingsby, "Mutation of interfaces in domain-swapped human betaB2-crystallin.," *Protein Sci.*, vol. 16, no. 4, pp. 615–625, Apr. 2007.

[28] M. Michiel et al., "Aggregation of deamidated human betaB2-crystallin and incomplete rescue by alpha-crystallin chaperone.," *Exp. Eye Res.*, vol. 90, no. 6, pp. 688–698, Jun. 2010.

[29] P. Marinelli, V. Castillo, and S. Ventura, "Trifluoroethanol modulates amyloid formation by the all α-helical URN1 FF domain," *Int. J. Mol. Sci.*, vol. 14, no. 9, pp. 17830–17844, 2013.

[30] S. Srisailam et al., "Amyloid-like Fibril Formation in an All β-Barrel Protein partially structured intermediate state (s) is a precursor for fibril formation," *J. Biol. Chem.*, vol. 278, no. 20, pp. 17701–17709, 2003.

[31] S. Cetinel, L. Unsworth, and C. Montemagno, "Peptide-based treatment strategies for cataract," *J. Glaucoma*, vol. 23, pp. S73–S76, 2014.

[32] A. Hawe, M. Sutter, and W. Jiskoot, "Extrinsic fluorescent dyes as tools for protein characterization," *Pharm. Res.*, vol. 25, no. 7, pp. 1487–1499, 2008.

[33] T. P. J. Knowles, M. Vendruscolo, and C. M. Dobson, "The amyloid state and its association with protein misfolding diseases," *Nat. Rev. Mol. cell Biol.*, vol. 15, no. 6, p. 384, 2014.

[34] M. Sunde, L. C. Serpell, M. Bartlam, P. E. Fraser, M. B. Pepys, and C. C. F. Blake, "Common core structure of amyloid fibrils by synchrotron X-ray diffraction," *J. Mol. Biol.*, vol. 273, no. 3, pp. 729–739, 1997.

[35] E. D. Eanes and G. G. Glenner, "X-ray diffraction studies on amyloid filaments," *J. Histochem. Cytochem.*, vol. 16, no. 11, pp. 673–677, 1968.

[36] B. A. Vernaglia, J. I. A. Huang, and E. D. Clark, "Guanidine hydrochloride can induce amyloid fibril formation from hen egg-white lysozyme," *Biomacromolecules*, vol. 5, no. 4, pp. 1362–1370, 2004.

[37] M. Vodnik, U. Zager, B. Strukelj, and M. Lunder, "Phage display: selecting straws instead of a needle from a haystack," *Molecules*, vol. 16, no. 1, pp. 790–817, 2011.

[38] M. Vodnik, B. Štrukelj, and M. Lunder, "HWGMWSY, an unanticipated polystyrene binding peptide from random phage display libraries," *Anal. Biochem.*, vol. 424, no. 2, pp. 83–86, 2012.

[39] J. Huang, B. Ru, S. Li, H. Lin, and F.-B. Guo, "SAROTUP: scanner and

reporter of target-unrelated peptides," *Biomed Res. Int.*, vol. 2010, 2010.

[40] J. Huang et al., "MimoDB 2.0: a mimotope database and beyond," *Nucleic Acids Res.*, vol. 40, no. D1, pp. D271–D277, 2011.

[41] B. Moores et al., "Effect of surfaces on amyloid fibril formation," *PLoS One*, vol. 6, no. 10, p. e25954, 2011.

Chapter 4

[1] M. Küchle, U. Schlötzer-Schrehardt, and G. O. Naumann, "Occurrence of pseudoexfoliative material in parabulbar structures in pseudoexfoliation syndrome.," *Acta Ophthalmol.*, vol. 69, no. 1, pp. 124–130, Feb. 1991.

[2] J. C. Morrison and W. R. Green, "Light microscopy of the exfoliation syndrome.," *Acta Ophthalmol. Suppl. (Oxf.).*, vol. 184, pp. 5–27, 1988.

[3] U. Schlotzer-Schrehardt and G. O. H. Naumann, "Ocular and systemic pseudoexfoliation syndrome.," *Am. J. Ophthalmol.*, vol. 141, no. 5, pp. 921–937, May 2006.

[4] R. Ritch and U. Schlötzer-Schrehardt, "Exfoliation syndrome," *Surv. Ophthalmol.*, vol. 45, no. 4, pp. 265–315, 2001.

[5] R. Ritch, "Exfoliation syndrome-the most common identifiable cause of open-angle glaucoma.," *J. Glaucoma*, vol. 3, no. 2, pp. 176–178, 1994.

[6] T. W. Blackstad, O. A. Sunde, and J. Trœtteberg, "On the ultrastructure of the deposits of busacca in eyes with glaucoma simplex and so-called senile exfoliation of the anterior lens capsule," *Acta Ophthalmol.*, vol. 38, no. 5, pp. 587–598, 1960.

[7] A. Ringvold and G. Husby, "Pseudo-exfoliation material-an amyloid-like substance.," *Exp. Eye Res.*, vol. 17, no. 3, pp. 289–299, Nov. 1973.

[8] J. Meretoja and A. Tarkkanen, "Occurrence of Amyloid in Eyes with

Pseudo-exfoliation," *Ophthalmic Res.*, vol. 9, no. 2, pp. 80–91, 1977.

[9] L. P. Repo, A. Naukkarinen, L. Paljärvi, and M. E. Teräsvirta, "Pseudoexfoliation syndrome with poorly dilating pupil: A light and electron microscopic study of the sphincter area," *Graefe's Arch. Clin. Exp. Ophthalmol.*, vol. 234, no. 3, pp. 171–176, 1996.

[10] A. J. Dark, B. W. Streeten, and C. C. Cornwall, "Pseudoexfoliative disease of the lens: a study in electron microscopy and histochemistry.," *Br. J. Ophthalmol.*, vol. 61, no. 7, pp. 462–472, Jul. 1977.

[11] C. G. Clement and L. D. Truong, "An evaluation of Congo red fluorescence for the diagnosis of amyloidosis," *Hum. Pathol.*, vol. 45, no. 8, pp. 1766–1772, 2014.

[12] R. P. Linke, H. V. Gartner, and H. Michels, "High-sensitivity diagnosis of AA amyloidosis using Congo red and immunohistochemistry detects missed amyloid deposits," *J. Histochem. Cytochem.*, vol. 43, no. 9, pp. 863–869, 1995.

[13] M. Davanger and O. O. Pedersen, "Pseudo-exfoliation material on the anterior lens surface. Demonstration and examination of an interfibrillar ground substance," *Acta Ophthalmol*, vol. 53, no. 1, pp. 3–18, 1975.

[14] J. Berlau et al., "Analysis of aqueous humour proteins of eyes with and without pseudoexfoliation syndrome.," *Graefes Arch. Clin. Exp. Ophthalmol.*, vol. 239, no. 10, pp. 743–746, 2001.

[15] R. Tycko, "Amyloid polymorphism: structural basis and neurobiological relevance.," *Neuron*, vol. 86, no. 3, pp. 632–645, May 2015.

[16] W. Qiang, W. M. Yau, J.-X. Lu, J. Collinge, and R. Tycko, "Structural variation in amyloid-beta fibrils from Alzheimer's disease clinical subtypes.," *Nature*, vol. 541, no. 7636, pp. 217–221, Jan. 2017.

[17] R. Ritch, "Systemic associations of exfoliation syndrome," *Asia-Pacific J. Ophthalmol.*, vol. 5, no. 1, pp. 45–50, 2016.

[18] C. M. Dobson, "Protein aggregation and its consequences for human disease.," *Protein Pept. Lett.*, vol. 13, no. 3, pp. 219–227, 2006.

[19] M. Stefani and C. M. Dobson, "Protein aggregation and aggregate toxicity: new insights into protein folding, misfolding diseases and biological evolution.," *J. Mol. Med. (Berl).*, vol. 81, no. 11, pp. 678–699, Nov. 2003.

[20] M. Zenkel and U. Schlötzer-Schrehardt, "The composition of exfoliation material and the cells involved in its production.," *J. Glaucoma*, vol. 23, no. 8 Suppl 1, pp. S12-4, 2014.

[21] B. H. Toyama and J. S. Weissman, "Amyloid structure: conformational diversity and consequences.," *Annu. Rev. Biochem.*, vol. 80, pp. 557–585, 2011.

[22] S. J. Ludtke, P. R. Baldwin, and W. Chiu, "EMAN: semiautomated software for high-resolution single-particle reconstructions.," *J. Struct. Biol.*, vol. 128, no. 1, pp. 82–97, Dec. 1999.

[23] J. L. Jiménez, G. Tennent, M. Pepys, and H. R. Saibil, "Structural diversity of *ex vivo* amyloid fibrils studied by cryo-electron microscopy," *J. Mol. Biol.*, vol. 311, no. 2, pp. 241–247, 2001.

[24] M. Davanger, "A method of isolating and collecting pseudo-exfoliation material from extracted cataractous lenses.," *Acta Ophthalmol.*, vol. 55, no. 4, pp. 634–640, Aug. 1977.

[25] U. Schlötzer-Schrehardt, M. Küchle, and G. O. Naumann, "Electron-microscopic identification of pseudoexfoliation material in extrabulbar tissue.," *Arch. Ophthalmol.*, vol. 109, no. 4, pp. 565–570, 1991.

[26] W. J. Tromans, R. W. Horne, G. A. Gresham, and A. J. Bailey, "Electron

microscope studies on the structure of collagen fibrils by negative staining.," *Z. Zellforsch. Mikrosk. Anat.*, vol. 58, pp. 798–802, 1963.

[27] D. Schwartz and A. Veis, "Structure of bovine anterior lens capsule basement membrane collagen molecules from electron microscopy.," *Biopolymers*, vol. 18, no. 9, pp. 2363–2367, Sep. 1979.

[28] M. Davanger, "The pseudo-exfoliation syndrome. A scanning electron microscopic study. I. The anterior lens surface.," *Acta Ophthalmol.*, vol. 53, no. 6, pp. 809–820, Dec. 1975.

[29] M. Davanger, "On the ultrastructure and the formation of pseudo-exfoliation material.," *Acta Ophthalmol.*, vol. 58, no. 4, pp. 520–527, Aug. 1980.

[30] M. D. Shoulders and R. T. Raines, "Collagen structure and stability.," *Annu. Rev. Biochem.*, vol. 78, pp. 929–958, 2009.

[31] G. O. Naumann, U. Schlotzer-Schrehardt, and M. Kuchle, "Pseudoexfoliation syndrome for the comprehensive ophthalmologist. Intraocular and systemic manifestations.," *Ophthalmology*, vol. 105, no. 6, pp. 951–968, Jun. 1998.

[32] T. I. Bertelsen, P. A. Drabloes, and P. R. Flood, "The socalled senile exfoliation (pseudoexfoliation) of the anterior lens capsule, a product of the lens epithelium. Fibrillopathia epitheliocapsularis. A microscopic, histochemic and electron microscopic investigation.," *Acta Ophthalmol.*, vol. 42, pp. 1096–1113, 1964.

[33] L. R. Volpatti, M. Vendruscolo, C. M. Dobson, and T. P. J. Knowles, "A clear view of polymorphism, twist, and chirality in amyloid fibril formation.," *ACS Nano, vol.* 7, no. 12, pp. 10443–10448, Dec. 2013.

[34] A. Aggeli et al., "Hierarchical self-assembly of chiral rod-like molecules as a model for peptide beta-sheet tapes, ribbons, fibrils, and fibers.," *Proc. Natl.*

Acad. Sci. U. S. A., vol. 98, no. 21, pp. 11857–11862, Oct. 2001.

[35] J. X. Lu, W. Qiang, W. M. Yau, C. D. Schwieters, S. C. Meredith, and R. Tycko, "Molecular structure of beta-amyloid fibrils in Alzheimer's disease brain tissue.," *Cell*, vol. 154, no. 6, pp. 1257–1268, Sep. 2013.

[36] B. W. Street and A. J. D. En, "Pseudoexfoliation syndrome," in A. Gamer, G.K. Klintworth (Eds.), *Pathobiology of Ocular Disease, Part A*, Marcel Dekker, New York, 1994, pp. 591–629.

[37] M. Fandrich, J. Meinhardt, and N. Grigorieff, "Structural polymorphism of Alzheimer Abeta and other amyloid fibrils.," *Prion*, vol. 3, no. 2, pp. 89–93, 2009.

[38] K. Annamalai et al., "Polymorphism of Amyloid Fibrils *In Vivo*," *Angew. Chem. Int. Ed. Engl.*, vol. 55, no. 15, pp. 4822–4825, Apr. 2016.

[39] E. Vazquez-Fernandez et al., "The Structural Architecture of an Infectious Mammalian Prion Using Electron Cryomicroscopy.," *PLoS Pathog.*, vol. 12, no. 9, p. e1005835, Sep. 2016.

Chapter 5

[1] R. Ritch, "Exfoliation syndrome-the most common identifiable cause of open-angle glaucoma.," *J. Glaucoma*, vol. 3, no. 2, pp. 176–177, 1994.

[2] M. Davanger, "The pseudo-exfoliation syndrome. A scanning electron microscopic study. I. The anterior lens surface.," *Acta Ophthalmol.*, vol. 53, no. 6, pp. 809–820, Dec. 1975.

[3] M. Ghosh and J. S. Speakman, "The ciliary body in senile exfoliation of the lens.," *Can. J. Ophthalmol.*, vol. 8, no. 3, pp. 394–403, Jul. 1973.

[4] J. P. Harnisch, "Exfoliation material in different sections of the eye.," *Albrecht Von Graefes Arch. Klin. Exp. Ophthalmol.*, vol. 203, no. 3–4, pp.

181–190, Sep. 1977.

[5] U. Schlötzer-Schrehardt, M. Küchle, and G. O. Naumann, "Electron-microscopic identification of pseudoexfoliation material in extrabulbar tissue.," *Arch. Ophthalmol.*, vol. 109, no. 4, pp. 565–570, 1991.

[6] B. W. Streeten, S. A. Gibson, and A. J. Dark, "Pseudoexfoliative material contains an elastic microfibrillar-associated glycoprotein.," *Trans. Am. Ophthalmol. Soc.*, vol. 84, pp. 304–320, 1986.

[7] R. Ritch, U. Schlötzer-Schrehardt, and A. G. P. Konstas, "Why is glaucoma associated with exfoliation syndrome?," *Prog. Retin. Eye Res.*, vol. 22, no. 3, pp. 253–275, 2003.

[8] G. Hollo, A. Katsanos, and A. G. Konstas, "Management of exfoliative glaucoma: challenges and solutions.," *Clin. Ophthalmol.*, vol. 9, pp. 907–919, 2015.

[9] I. F. Aboobakar, W. M. Johnson, W. D. Stamer, M. A. Hauser, and R. R. Allingham, "Major review: Exfoliation syndrome; advances in disease genetics, molecular biology, and epidemiology," *Exp. Eye Res.*, vol. 154, pp. 88–103, 2017.

[10] R. Ritch, "Ocular and systemic manifestations of exfoliation syndrome," *J. Glaucoma*, vol. 23, no. 8, pp. S1–S8, 2014.

[11] R. Ritch and U. Schlötzer-Schrehardt, "Exfoliation syndrome," *Surv. Ophthalmol.*, vol. 45, no. 4, pp. 265–315, 2001.

[12] E. Elhawy, G. Kamthan, C. Q. Dong, and J. Danias, "Pseudoexfoliation syndrome, a systemic disorder with ocular manifestations.," *Hum. Genomics*, vol. 6, p. 22, Oct. 2012.

[13] M. Citirik, G. Acaroglu, C. Batman, L. Yildiran, and O. Zilelioglu, "A possible link between the pseudoexfoliation syndrome and coronary artery dis-

ease.," *Eye (Lond).*, vol. 21, no. 1, pp. 11–15, Jan. 2007.

[14] K. A. Gonen, T. Gonen, and B. Gumus, "Renal artery stenosis and abdominal aorta aneurysm in patients with pseudoexfoliation syndrome.," *Eye (Lond).*, vol. 27, no. 6, pp. 735–741, Jun. 2013.

[15] Z. Ma et al., "Phage display-derived oligopeptide-functionalized probes for in vivo specific photoacoustic imaging of osteosarcoma.," *Nanomedicine*, vol. 13, no. 1, pp. 111–121, Jan. 2017.

[16] A. K. Sato, M. Viswanathan, R. B. Kent, and C. R. Wood, "Therapeutic peptides: technological advances driving peptides into development.," *Curr. Opin. Biotechnol.*, vol. 17, no. 6, pp. 638–642, Dec. 2006.

[17] C. K. Kang, V. Jayasinha, and P. T. Martin, "Identification of peptides that specifically bind Abeta1-40 amyloid in vitro and amyloid plaques in Alzheimer's disease brain using phage display.," *Neurobiol. Dis.*, vol. 14, no. 1, pp. 146–156, Oct. 2003.

[18] B. P. Orner, L. Liu, R. M. Murphy, and L. L. Kiessling, "Phage display affords peptides that modulate beta-amyloid aggregation," *J. Am. Chem. Soc.*, vol. 128, no. 36, pp. 11882–11889, 2006.

[19] U. R. Chowdhury, B. J. Madden, M. C. Charlesworth, and M. P. Fautsch, "Proteome analysis of human aqueous humor.," *Invest. Ophthalmol. Vis. Sci.*, vol. 51, no. 10, pp. 4921–4931, Oct. 2010.

[20] C. Sun, J. S. H. Lee, and M. Zhang, "Magnetic nanoparticles in MR imaging and drug delivery.," *Adv. Drug Deliv. Rev.*, vol. 60, no. 11, pp. 1252–1265, Aug. 2008.

[21] Y. Cheng et al., "Rotating magnetic field induced oscillation of magnetic particles for in vivo mechanical destruction of malignant glioma.," *J. Control. Release*, vol. 223, pp. 75–84, Feb. 2016.

[22] K. A. Kelly, P. Waterman, and R. Weissleder, "In vivo imaging of molecularly targeted phage.," *Neoplasia*, vol. 8, no. 12, pp. 1011–1018, Dec. 2006.

[23] S. I. Presolski, V. P. Hong, and M. G. Finn, "Copper-Catalyzed Azide–Alkyne Click Chemistry for Bioconjugation.," *Curr. Protoc. Chem. Biol.*, vol. 3, no. 4, pp. 153–162, 2011.

[24] W. M. Saltzman, Tissue engineering: engineering principles for the design of replacement organs and tissues. *Oxford University Press*, 2004.

[25] J. J. Heys and V. H. Barocas, "A boussinesq model of natural convection in the human eye and the formation of Krukenberg's spindle.," *Ann. Biomed. Eng.*, vol. 30, no. 3, pp. 392–401, Mar. 2002.

[26] A. K. Hauser, R. J. Wydra, N. A. Stocke, K. W. Anderson, and J. Z. Hilt, "Magnetic nanoparticles and nanocomposites for remote controlled therapies," *J. Control. Release*, vol. 219, pp. 76–94, 2015.

[27] M. Chirita, M. L. Kiss, and C. Savii, "Magnetite, Properties and Modern Biomedical Applications," in Magnetite: Synthesis, Uses and Biological Occurrences, *J. Ward, Ed. Nova Science Publishers, Inc.*, 2014, pp. 119–181.

[28] N. Zarghami et al., "Optimization of molecularly targeted MRI in the brain: empirical comparison of sequences and particles.," *Int. J. Nanomedicine*, vol. 13, pp. 4345–4359, 2018.

[29] N. Singh, G. J. S. Jenkins, R. Asadi, and S. H. Doak, "Potential toxicity of superparamagnetic iron oxide nanoparticles (SPION)," *Nano Rev.*, vol. 1, p. 10.3402/nano.v1i0.5358, 2010.

[30] L. H. Reddy, J. L. Arias, J. Nicolas, and P. Couvreur, "Magnetic nanoparticles: design and characterization, toxicity and biocompatibility, pharmaceutical and biomedical applications.," *Chem. Rev.*, vol. 112, no. 11, pp. 5818–5878, Nov. 2012.

[31] H. E. Daldrup-Link, "Ten things you might not know about iron oxide nanoparticles," *Radiology*, vol. 284, no. 3, pp. 616–629, 2017.

[32] W. D. Stamer and A. F. Clark, "The many faces of the trabecular meshwork cell.," *Exp. Eye Res.*, vol. 158, pp. 112–123, May 2017.

[33] J. R. Polansky, I. S. Wood, M. T. Maglio, and J. A. Alvarado, "Trabecular meshwork cell culture in glaucoma research: evaluation of biological activity and structural properties of human trabecular cells in vitro.," *Ophthalmology*, vol. 91, no. 6, pp. 580–595, Jun. 1984.

[34] H. B. Raju, Y. Hu, A. Vedula, S. R. Dubovy, and J. L. Goldberg, "Evaluation of magnetic micro- and nanoparticle toxicity to ocular tissues.," *PLoS One*, vol. 6, no. 5, p. e17452, 2011.

Conclusions

[1] S. Meehan, Y. Berry, B. Luisi, C. M. Dobson, J. A. Carver, and C. E. MacPhee, "Amyloid Fibril Formation by Lens Crystallin Proteins and Its Implications for Cataract Formation," *J. Biol. Chem.*, vol. 279, no. 5, pp. 3413–3419, 2004.

[2] A. M. Alperstein, J. S. Ostrander, T. O. Zhang, and M. T. Zanni, "Amyloid found in human cataracts with two-dimensional infrared spectroscopy," *Proc. Natl. Acad. Sci.* U. S. A., vol. 116, no. 14, pp. 6602–6607, 2019.

[3] A. A. H. Ahmad Fuaad, F. Azmi, M. Skwarczynski, and I. Toth, "Peptide conjugation via CuAAC 'click' chemistry.," *Molecules*, vol. 18, no. 11, pp. 13148–13174, Oct. 2013.

[4] T. Hard and C. Lendel, "Inhibition of amyloid formation.," *J. Mol. Biol.*, vol. 421, no. 4–5, pp. 441–465, Aug. 2012.

[5] T. R. Thrimawithana, I. D. Rupenthal, S. S. Rasch, J. C. Lim, J. D.

Morton, and C. R. Bunt, "Drug delivery to the lens for the management of cataracts.," *Adv. Drug Deliv. Rev.*, vol. 126, pp. 185–194, Feb. 2018.

[6] N. J. Kim et al., "Nanotechnology and glaucoma: a review of the potential implications of glaucoma nanomedicine.," *Br. J. Ophthalmol.*, vol. 98, no. 4, pp. 427–431, Apr. 2014.

[7] N. Lewinski, V. Colvin, and R. Drezek, "Cytotoxicity of nanoparticles.," *Small*, vol. 4, no. 1, pp. 26–49, Jan. 2008.

[8] S. W. M. John, J. M. Harder, J. H. Fingert, and M. G. Anderson, "Animal models of exfoliation syndrome, now and future.," *J. Glaucoma*, vol. 23, no. 8 Suppl 1, pp. S68-72, 2014.

[9] M. G. Anderson, K. J. Meyer, A. Hedberg-Buenz, and J. H. Fingert, "Update on Animal Models of Exfoliation Syndrome.," *J. Glaucoma*, vol. 27 Suppl 1, pp. S78–S82, Jul. 2018.

[10] H. B. Raju, Y. Hu, A. Vedula, S. R. Dubovy, and J. L. Goldberg, "Evaluation of magnetic micro- and nanoparticle toxicity to ocular tissues.," *PLoS One*, vol. 6, no. 5, p. e17452, 2011.

[11] G. O. Naumann, U. Schlotzer-Schrehardt, and M. Kuchle, "Pseudoexfoliation syndrome for the comprehensive ophthalmologist. Intraocular and systemic manifestations.," *Ophthalmology*, vol. 105, no. 6, pp. 951–968, Jun. 1998.

[12] J. Liu et al., "Amyloid structure exhibits polymorphism on multiple length scales in human brain tissue.," *Sci. Rep.*, vol. 6, p. 33079, Sep. 2016.

[13] F. Briki et al., "Synchrotron x-ray microdiffraction reveals intrinsic structural features of amyloid deposits in situ.," *Biophys. J.*, vol. 101, no. 2, pp. 486–493, Jul. 2011.

Appendix

Supplementary figures of chapter 3

TEM of βB2-crystallin fibrills

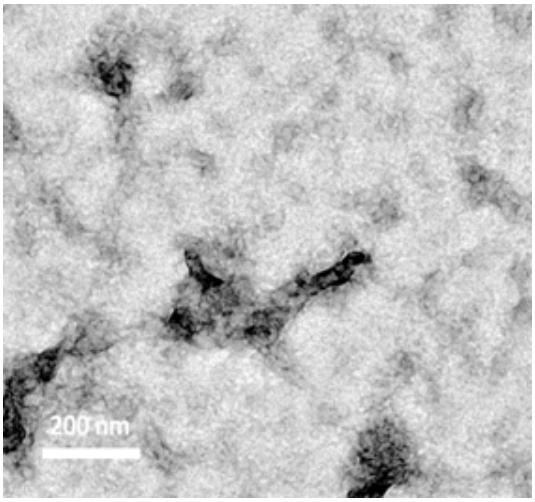

Figure A1: Transmission electron micrograph of βB2-crystallin incubated in 10% (v/v) TFE, pH 2.0 at 60 °C for 24 hr.

X-ray fiber diffraction (XRFD) pattern of βB2-crystallin fibrils

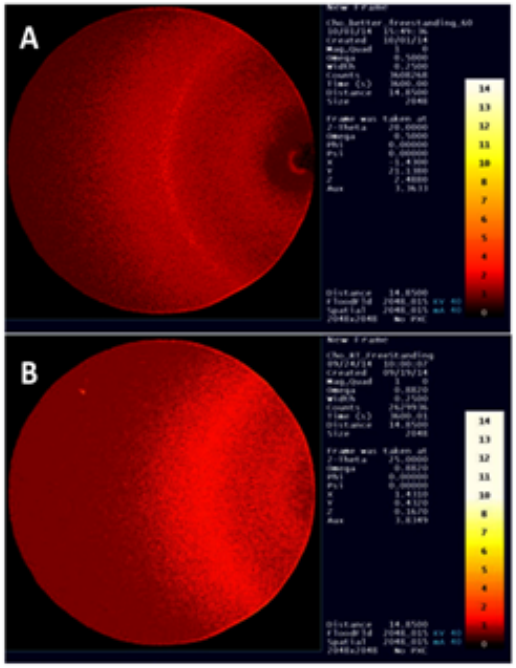

Figure A2: Diffraction pattern of βB2-crystallin fibrils formed in in 10% (v/v) TFE, pH 2.0 at (A) 60 °C and (B) RT.

Supplementary figures of chapter 5

Peptide enrichment during *ex vivo* biopanning against exfoliated lens capsules

Biopanning	Peptide	Copies	% of sequences	Lens capsule type
Negative panning (Subtraction)	---	---	---	without XFS materials
Round 1	---	---	---	with XFS materials
Round 2	p-LPS	3/12	25	with XFS materials
	p-IPL	4/12	33	
Round 3	p-LPS	11/52	21	with XFS materials
	p-IPL	37/52	71	

Table A1: Peptide enrichment during *ex vivo* biopanning against human lens capsules.

Immunohistochemical analyses of hTM cells

The population doubling time for obtained hTM cells was determined to be 11.3 ± 2.1 hours, which is typical for fetal hTM cells [1]. Immunohistochemical analyses of hTM cells included evaluation of expression of fibronectin, myocilin, laminin, and actin. Is has been shown that actin microfilaments are mainly aligned parallel to the longitudinal axis of cultured hTM cells [2], which was also observed for our cells when stained with phalloidin dye (Fig. A3. B). Expression of fibronectin protein was also confirmed in the cultured hTM cells (Fig. A3. E). This proteins is one of the major extracellular matrix glycoproteins of hTM cells which is secreted as loosely aligned filaments on the cultured hTM cells surface or large bundles at the periphery of individual cells [3] Myocilin protein (or trabecular meshwork–inducible glucocorticoid response protein) is an highly expressed glycoprotein in the trabecular meshwork, and has been found within the cytoplasm of hTM cells when in association with extracellular matrix components [4, 5]. The expression of myocilin is a key phenotypic characteristic of hTM cells and was observed in our cell culture (Fig. A3. H). Expression of laminin is a marker to characterize cultured hTM cells [6], and was observed in immunohistochemical studies (Fig. A3. K). The common morphology of hTM cells is the spindle-like shape which was also observed in monolayers of cultured hTM cells (Fig. A3. M).

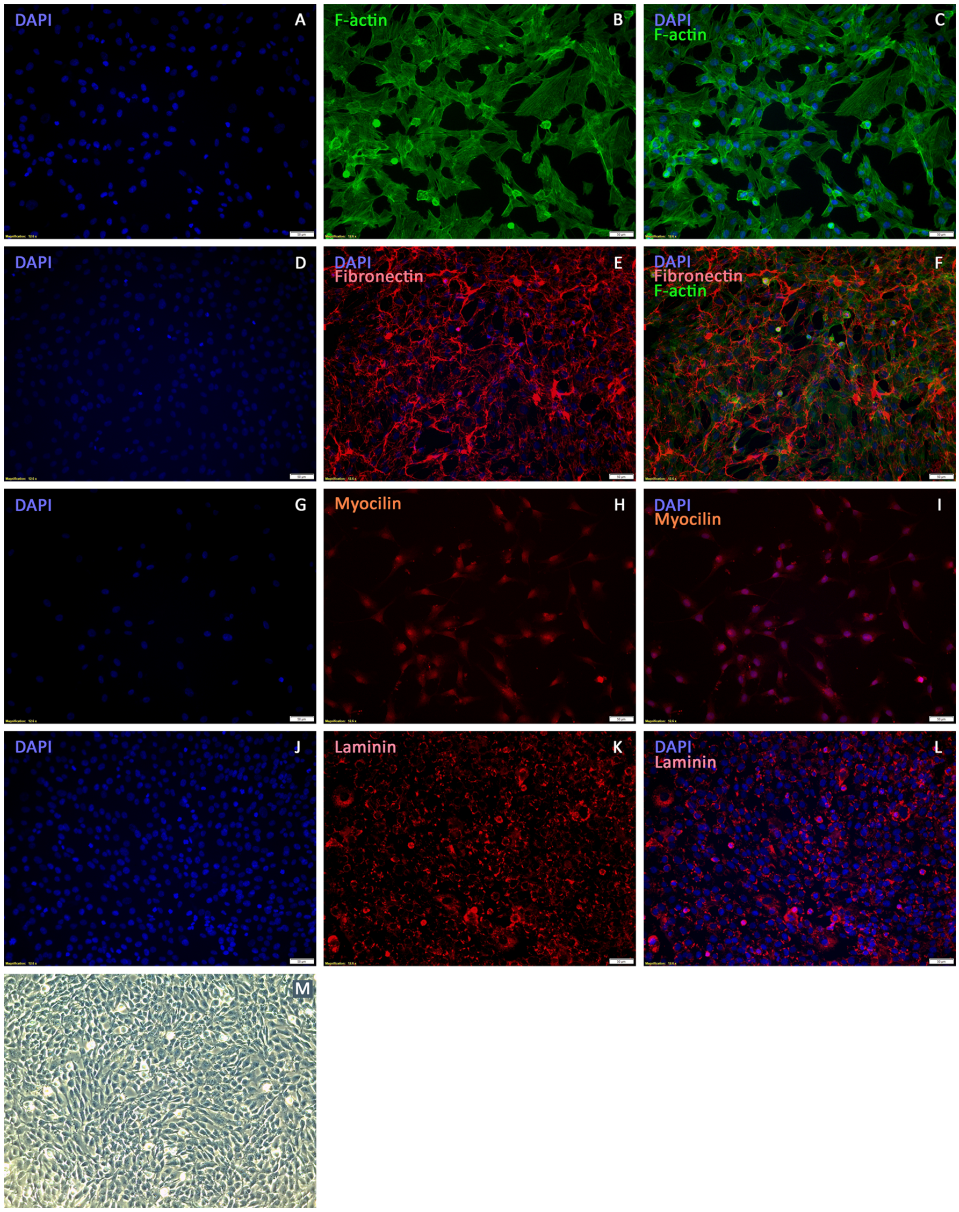

Figure A3: Morphological analysis and immunofluorescence labeling of hTM Cells. (**A**-**C**) F-actin stained semi-confluent monolayer of cultured hTM cells. (**D**-**F**) hTM cells normally secreted fibronectin when grown on coverslips. (**G**-**L**) Grown cells expressed myocilin protein and laminin protein as a sign of normal phenotype. (**M**) Confluent monolayer of cultured cells showed contact inhibition having spindle-like shape, a typical characteristic of cultured hTM cells. (Sale bars = 50 μm).

References

[1] S. Lin, O.-T. Lee, P. Minasi, and J. Wong, "Isolation, culture, and characterization of human fetal trabecular meshwork cells.," *Curr. Eye Res.*, vol. 32, no. 1, pp. 43–50, Jan. 2007.

[2] A. F. Clark et al., "Dexamethasone alters F-actin architecture and promotes cross-linked actin network formation in human trabecular meshwork tissue.," *Cell Motil. Cytoskeleton*, vol. 60, no. 2, pp. 83–95, Feb. 2005.

[3] H. T. Steely, S. L. Browder, M. B. Julian, S. T. Miggans, K. L. Wilson, and A. F. Clark, "The effects of dexamethasone on fibronectin expression in cultured human trabecular meshwork cells.," *Invest. Ophthalmol. Vis. Sci.*, vol. 33, no. 7, pp. 2242–2250, Jun. 1992.

[4] J. R. Polansky et al., "Cellular pharmacology and molecular biology of the trabecular meshwork inducible glucocorticoid response gene product.," *Ophthalmologica*, vol. 211, no. 3, pp. 126–139, 1997.

[5] E. R. Tamm, "Myocilin and glaucoma: facts and ideas.," *Prog. Retin. Eye Res.*, vol. 21, no. 4, pp. 395–428, Jul. 2002.

[6] M. R. Hernandez, B. I. Weinstein, J. Schwartz, R. Ritch, G. G. Gordon, and A. L. Southren, "Human trabecular meshwork cells in culture: morphology and extracellular matrix components.," *Invest. Ophthalmol. Vis. Sci.*, vol. 28, no. 10, pp. 1655–1660, Oct. 1987.